2022

CONCEPT EVALUATION AND DEVELOPMENT OF A NOVEL APPROACH FOR INTEGRATION OF TURBOGENERATION, ELECTRIFICATION AND SUPERCHARGING ON HEAVY DUTY ENGINES

Satyum Joshi
Michigan Technological University, satyumj@mtu.edu

CONCEPT EVALUATION AND DEVELOPMENT OF A NOVEL APPROACH FOR INTEGRATION OF TURBOGENERATION, ELECTRIFICATION AND SUPERCHARGING ON HEAVY DUTY ENGINES

By

Satyum Joshi

A DISSERTATION

Submitted in partial fulfillment of the requirements for the degree of

DOCTOR OF PHILOSOPHY

In Mechanical Engineering-Engineering Mechanics

MICHIGAN TECHNOLOGICAL UNIVERSITY

2022

This dissertation has been approved in partial fulfillment of the requirements for the Degree of DOCTOR OF PHILOSOPHY in Mechanical Engineering-Engineering Mechanics.

Department of Mechanical Engineering-Engineering Mechanics

Dissertation Advisor:	*Dr. Jeffrey D. Naber*
Committee Member:	*Dr. Bo Chen*
Committee Member:	*Dr. Darrell Robinette*
Committee Member:	*Dr. Mufaddel Dahodwala*
Department Chair:	*Dr. Jason Blough*

Dedication

I dedicate this dissertation to my family, especially my father Ret. Col. Shivdarshan Joshi, my mother Bharati Joshi, my wife Tejaswi Worlikar, my brother Saiyam Joshi and my pets – Simba and Mowgli. I would not have been able to complete this work without their love and support.

Table of Contents

List of Figures

List of Tables

Author Contribution Statement

I would like to acknowledge the contribution of my colleagues Erik Koehler, Mufaddel Dahodwala and Michael Franke in writing and reviewing the portions of SAE paper 2018-01-0887 and 2020-01-0847, which are part of this dissertation. I would also like to thank the other co-authors and all FEV North America, Inc. colleagues who took the time to review the multiple SAE papers published on this topic (SAE 2018-01-0887, SAE 2019-01-0229, ASME ICEF2018-9703) and provided valuable feedback.

Acknowledgements

I am extremely grateful to my advisor Dr. Jeffrey Naber for providing me the opportunity, valuable guidance and tremendous support to pursue this research. I would like to sincerely thank him for the thorough reviews and key inputs which significantly improved the quality of this research. I would not have been able to complete this research without his supervision and mentoring. I would also like to thank Dr. Mufaddel Dahodwala, Dr. Bo Chen and Dr. Darrell Robinette for being part of my research committee.

I would like to thank FEV North America, Inc. management, especially Dean Tomazic and Michael Franke, for encouraging this research and providing the resources necessary to accomplish its goals. I would like to express my deepest appreciation to Erik Koehler and Dr. Mufaddel Dahodwala of FEV North America, Inc. for their support and guidance throughout the research process. I would also like to thank Nirmal Sabu Ettuparayil, Abhijit Warale, Joern Baumann, Greg Kolwich and Marc Pomerleau of FEV North America, Inc. for their support in 1D modeling, CAD modeling, geartrain analysis and cost analysis.

A special mention goes out to my professor Dr. Huei Peng at University of Michigan, Ann Arbor where I completed my master's degree in mechanical engineering. Dr. Peng's research inspired me to apply power-split hybrid vehicle concepts to engine air handling systems, which developed the foundation of this research.

Finally, I would like to thank my family members and friends for their continuous support and encouragement.

List of Abbreviations

ACT	Advanced Clean Trucks
ARB	Air Resources Board
BEV	Battery Electric Vehicle
BMEP	Brake Mean Effective Pressure
BR	Band Brake
BSFC	Brake Specific Fuel Consumption
BTE	Brake Thermal Efficiency
CAC	Charge Air Cooler
CAFE	Corporate Average Fuel Economy
CAN	Controller Area Network
CFR	Code of Federal Regulations
CL	Dog Clutch
CNG	Compressed Natural Gas
CO_2	Carbon Dioxide
CVT	Continuously Variable Transmission
DC	Direct Current
DOD	Depth of Discharge
DOE	Department of Energy
DoE	Design of Experiments
DOT	Department of Transportation
E-booster	Electrically Assisted Compressor
ECMS	Equivalent Consumption Minimization Strategy
ECU	Electronic Control Unit
eCVT	Electronic Continuously Variable Transmission
EGR	Exhaust Gas Recirculation
EOL	End of Life
EPA	Environmental Protection Agency
EV	Electric Vehicle
FC	Fuel Cell
FRM	Fast Running Model
FTP	Federal Test Procedure
GEM	Greenhouse Gas Emissions Model
GHG	Greenhouse Gas
GR	Gear Ratio
GT	Gamma Technologies
GT-ISE	Gamma Technologies – Integrated Simulation Environment
GVW	Gross Vehicle Weight
GVWR	Gross Vehicle Weight Rating
H2-ICE	Hydrogen Internal Combustion Engine

HDFTP	Heavy Duty Federal Test Procedure
HDUDDS	Heavy Duty Urban Dynamometer Driving Schedule
HHD/HD	Heavy Heavy Duty
HHDDT	Heavy Heavy-Duty Diesel Truck
HPPC	Hybrid Power Pulse Characterization
HVAC	Heating, Ventilation and Air Conditioning
ICE	Internal Combustion Engine
ITES	Integrated Turbogeneration, Electrification and Supercharging
LCO	Lithium Cobalt Oxide
LFP	Lithium Iron Phosphate
LTO	Lithium Titanate Oxide
MG	Motor Generator Unit
MHD	Medium Heavy-Duty
MHD/MD	Medium Heavy-Duty
MHEV	Mild Hybrid Electric Vehicle
MPG	Miles per Gallon
MPGe	Miles per Gallon Equivalent
NHTSA	National Highway Traffic Safety Administration
NMC	Nickel Manganese Cobalt Oxide Li Ion Battery
NOx	Nitrous Oxide
NREL	National Renewable Energy Laboratory
NTE	Not to Exceed
NZEV	Near-Zero Emission Vehicle
OCV	Open Circuit Voltage
ORC	Organic Rankine Cycle
PEM	Proton Exchange Membrane
PGS	Planetary Gear Set
PHEV	Plug-in Hybrid Electric Vehicle
SOC	State of Charge
WHR	Waste Heat Recovery
WHTC	World Harmonized Transient Cycle
ZEV	Zero Emission Vehicle
1RC	Equivalent Single Resistance and Single Capacitance Model

Abstract

While many technologies such as electrically assisted turbocharging, exhaust energy recovery and mild hybridization have already proven to significantly increase heavy-duty engine efficiency, the key challenge to their widespread adoption has been their cost effectiveness and packaging. This research specifically addresses these challenges through evaluation and development of a novel technology concept termed as the Integrated Turbogeneration, Electrification and Supercharging (ITES) system. The concept integrates a secondary compressor, a turbocompound/expander turbine and an electric motor through a planetary gearset into the engine cranktrain. The approach enables a reduced system cost and space-claim, while maximizing the efficiency benefits of independent technologies.

First, an assessment of design alternatives for integration of the identified key engine technologies on a heavy-duty engine was conducted. Once the ITES concept was down selected, the research then focused on model-based optimization and evaluation of the ITES system for a downsized medium heavy-duty diesel engine applied in Class 6-7 urban vocational application. As an outcome of the evaluation, a 1D simulation based sizing methodology of ITES system components was proposed. Furthermore, a novel control strategy for the ITES system was developed that combines equivalent consumption based steady-state offline optimization with functional controls for transient operation and smooth mode switching. The offline optimization method was also extended to evaluate the potential of ITES system in increasing aftertreatment temperature, which is critical for meeting future ultra-low NOx emission standards. Lastly, using 1D simulation of validated models, the efficiency benefit of ITES system on engine certification and vehicle drive cycles was predicted for the Class 6-7 urban vocational application. In comparison to baseline engine, the downsized engine with ITES system predicted an 8.5% reduction in engine fuel consumption on HDFTP cycle, 19.3% increase in fuel economy on ARB Transient cycle and 23.7% increase in fuel economy on a real-world drive cycle.

1 Introduction

Since its invention in 1859, the internal combustion engine (ICE) has been one of the revolutionary and irreplaceable technologies for power. The technology has realized significant advancements in transportation, power generation, agriculture, industrial and marine applications throughout the world. At the same time, the combustion of fossil fuels within the ICE has contributed to the sharp increase in greenhouse gas emissions, leading to global warming and its adverse climate change impact. In recent years, the advancements in battery electric and fuel cell technologies have led to replacement of ICE based powertrains in various light-duty applications. The long-term goal is to eventually transition to a renewable energy-based power grid and significantly reduce greenhouse gas emissions. However, due to higher energy density and higher durability requirements of heavy-duty applications, ICE based powertrains will continue to dominate for years to come. Furthermore, hybrid-electric powertrains and use of low carbon and sustainable fuels in ICEs can enable a faster reduction in greenhouse gas emissions without major industry disruption. Therefore, continued research to increase ICE engine efficiency is essential for addressing the adverse impacts of climate change.

1.1 Motivation

In 2014, EPA introduced Phase 1 greenhouse gas emission standards that regulated CO_2 emissions from medium and heavy-duty engines and vehicles [1]. The rule was followed by a Phase 2 standard in 2017, which will be phased in from MY2021 to MY2027 [2]. The standards are applied at engine as well as vehicle level and require up to 5.2% reduction in fuel consumption on engines and up to 27% reduction on vehicle fuel consumption depending on application [2]. While many technology solutions exist to reduce fuel consumption, the challenge lies in keeping the cost of technology addition low. **Figure 1** shows the potential in fuel consumption reduction of different technologies and their cost effectiveness for MD and HD applications. The technologies that stand out are engine downsizing, downspeeding, friction reduction and mild hybridization. Other technologies that have high potential in fuel consumption reduction are waste heat recovery technologies such as turbocompounding and organic rankine cycle. These technologies are similar to those identified by EPA as enablers to meet greenhouse gas emission targets [3].

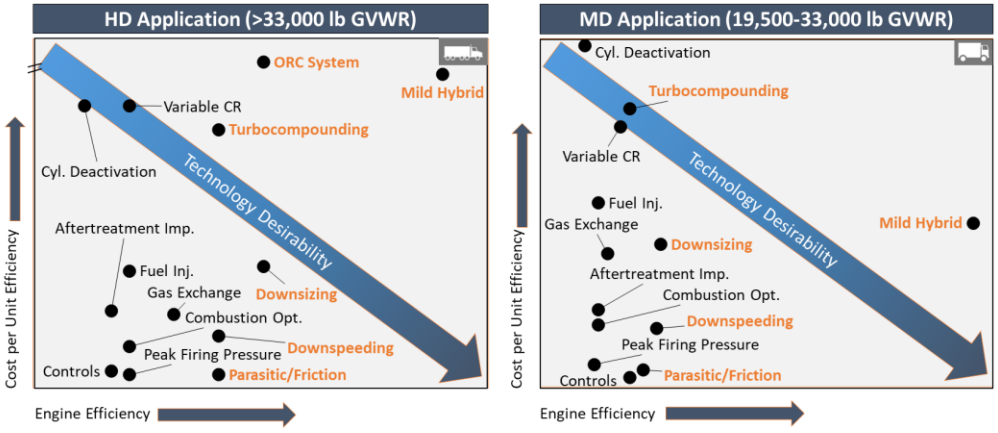

Figure 1 Potential of different engines technologies and their cost effectiveness.

The goal of this research is to explore a system for integration of waste heat recovery, low voltage electrification and secondary boosting on medium and heavy-duty engines, that maximizes the efficiency benefit of each technology while minimizing integration cost and package size.

1.2 Research Focus

A combined approach incorporating the three main technology areas of turbogeneration, electrification and supercharging has the potential to reduce fuel consumption by at least 10-15% [3]. However, the associated component cost and packaging makes their integration and implementation a formidable challenge. While the previous integration approaches described in Chapter 2 have investigated integration of two out of the three technology areas, this research investigates concepts for integration of all three areas (electrification, advanced boosting, and waste heat recovery) while achieving reduced cost, reduced space claim and increased efficiency, in comparison to the independent integration of each of these technologies. The research then explores a method for component sizing and optimization for this integration concept through system modeling and simulation. Another novel aspect of this research is to explore a robust and optimal control strategy for this highly integrated system. This control strategy would need to simultaneously address requirements of the engine air system and mild-hybrid system, which has not been explored so far in the literature. The research also aims to explore the potential of this integrated concept in improving thermal management of the aftertreatment system. Overall, this research will contribute towards model-based optimization, controls development and trade-off assessment of highly-integrated engine air and mild-hybrid systems.

Specifically, the research aims to:

- Examine design alternatives for integration of turbogeneration, electrification, and supercharging (ITES) on medium and heavy-duty engines
- Model the concept and integrate with engine/vehicle models for verification of intended operation
- Develop a method for optimizing the size of the novel integrated system
- Develop an optimal control strategy for the novel integrated system
- Evaluate the potential of the integrated system in reducing engine fuel consumption, exhaust emissions and aftertreatment warmup time for a medium-heavy-duty application using 1D simulation

1.3 Dissertation Outline

The outline of this dissertation has been summarized in **Figure 2**. The dissertation starts with Chapter 2 that provides a review of the past research and prior art to identify the gaps in the existing methodology for technology integration. The chapter also describes a novel concept that has been proposed to address the limitations identified in the state-of-the-art concepts. Thereafter, Chapter 3 focuses on sizing and optimization of the concept for a medium heavy-duty diesel application through 1D engine simulation. The chapter

describes the modeling methodology, sizing of components and the optimization process. Chapter 4 focuses on development and optimization of a novel control strategy for this integrated concept. Offline optimization using equivalent consumption minimization method has been proposed for steady state operation while rule-based strategies have been proposed for transient control of the integrated concept. Lastly, the chapter applies the optimized supervisory and component level control strategy for the integrated concept, that was evaluated through vehicle simulation.

After the development of control strategy, Chapters 5 and 6 evaluate the integration concept through 1D engine and vehicle simulation. While Chapter 5 evaluates the potential of the integration concept during steady state engine operation, engine certification cycle and aftertreatment warmup, Chapter 6 evaluates the performance and the efficiency impact of the integration concept on certification and real-world drive cycles. Finally, the key conclusions from this research work and the potential future investigations have been summarized in Chapter 7. The dissertation also includes two appendix sections that document the validation of the baseline engine and vehicle models.

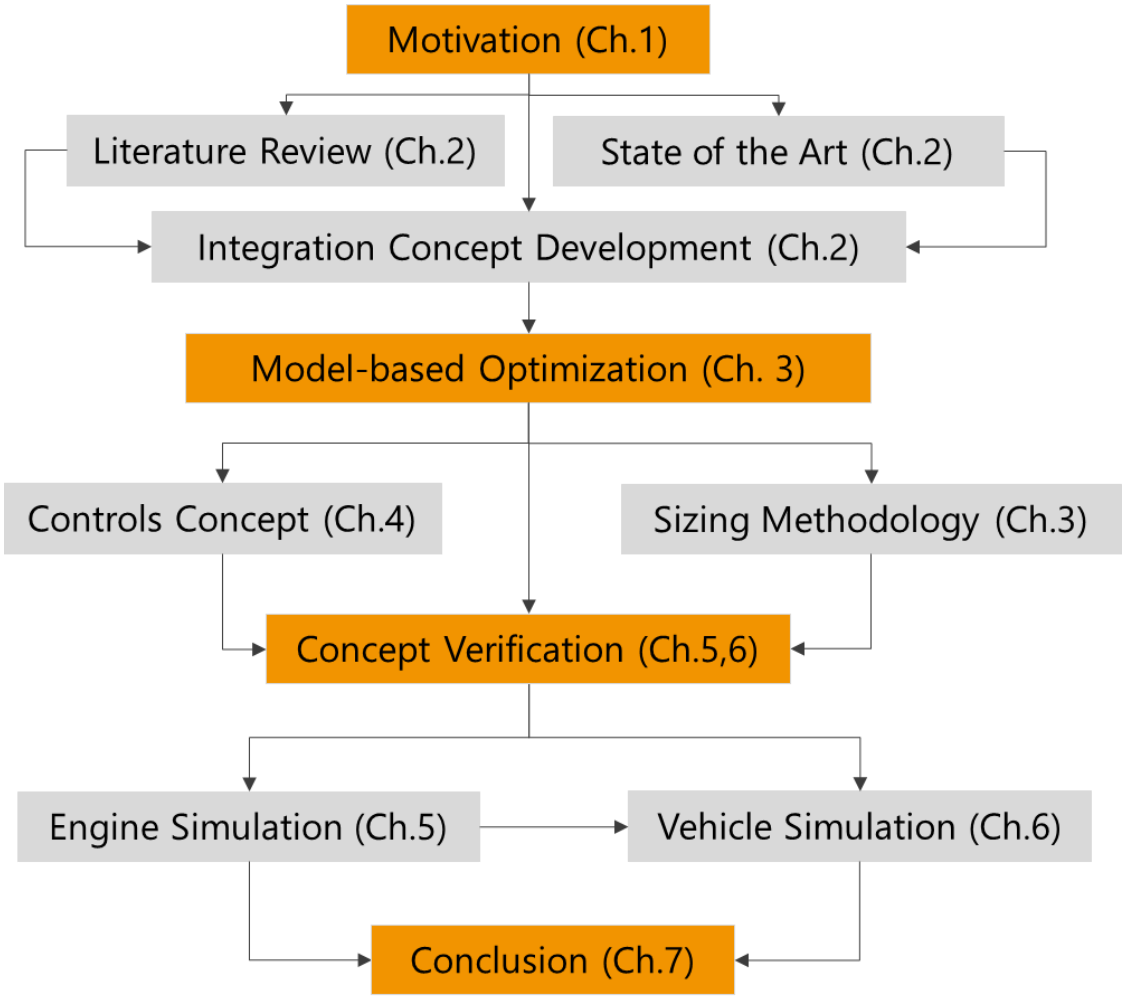

Figure 2 Dissertation outline showing the different tasks conducted during the research.

2 Integration Concept Development

This chapter reviews the past research conducted in the area of mild hybridization, supercharging and exhaust energy recovery to reduce fuel consumption. The key findings from the various research studies have been summarized to understand the potential and limitations of each technology area. The chapter then investigates the prior art developed to integrate these technologies on the engine and also discusses their limitations. Based on the identified methods and the opportunities for improvement, a novel integration concept has been proposed that enables highly efficient mild hybridization, supercharging and exhaust energy recovery functionality on the engine, while minimizing cost and package.

2.1 Literature Review

Low voltage (48V) electrification is a practical, low-cost technology that enables fuel consumption reduction through the electrification of engine accessories, regenerative braking, engine start-stop, and torque assist [3]. Generally, a belt-driven integrated starter generator (B-ISG) unit system is applied to achieve the mild hybrid capability while minimizing base engine design changes. However, such systems are limited to light-duty engines due to belt power transfer and pulley speed-ratio limits as identified by Yoon et al. [4]. Medium and heavy-duty diesel engines typically need much higher starting torque than what can be provided by the B-ISG systems and therefore they either require a separate engine starter along with B-ISG or they switch to an integrated starter-generator (ISG) system that is directly geared into the engine crankshaft [3]. With maximum motor power capabilities of up to 25kW [5], these systems offer significant fuel savings for not just light duty applications, but also for medium and heavy-duty urban vocation applications, which are subjected to low-speed and frequent start-stop driving. De Cesare et al. [6], in their analytical study for passenger SUV application, show that a highly integrated 48V mild hybrid system can achieve 23.7% increase in fuel economy over baseline vehicle on NEDC cycle. On real world drive cycles, Liu et al. [7] show up to 4% fuel savings in 80% of the drive cycle data collected from mild hybrid passenger cars without including fuel savings from start-stop. The paper does provide an idling percentage vs fuel saving dataset which can be used to estimate an approximately 11% overall fuel savings for a typical start-stop percentage of 19%. In medium heavy-duty application, Dahodwala et al. [8] predict up to 12% reduction in CO_2 emissions for a class 6-7 urban vocation truck on ARB transient cycle with a 48V ISG system. Lastly, EPA's regulatory impact analysis on implementation of greenhouse gas phase 2 emission standards estimated 5% increase in fuel efficiency of heavy-duty pickups and vans with a 7kW mild hybrid system [3]. The analysis also estimated a 22% increase in fuel efficiency of the applications with the implementation of 50kW strong hybrid system [3]. Based on the results of the analysis, it can be argued that a reasonable estimate of fuel consumption reduction on heavy-duty pickups and vans with a 25kW MHEV system would be at least 10%.

Engine downsizing and/or downspeeding, enabled by an advanced boosting system, can significantly decrease fuel consumption while maintaining engine performance [9, 10]. Both technologies increase engine relative torque (e.g., Brake Mean Effective Pressure BMEP) at a similar or lower friction level thereby improving mechanical efficiency of the

engine. Additionally, a reduction in the total in-cylinder surface area with the downsized engine can reduce in-cylinder heat loss. The advanced boosting system may include two-stage turbocharging, which is generally more efficient than an alternative system consisting of an E-booster [9]. However, when combined with regenerative braking, the fuel consumption reduction potential of E-booster exceeds that of a two-stage turbocharging system as the power for E-booster comes from vehicle energy recuperation [9]. With regards to the extent of fuel consumption reduction, the studies show a wide range depending on the application and degree of engine downsizing/downspeeding. King et al. [11] successfully performed downsizing by 60% on a 5L V8 gasoline engine by using a novel BSG integrated supercharger which achieved 22% reduction in fuel consumption on the FTP-75 cycle with no additional technologies implemented. For an on-highway medium heavy-duty diesel engine, Joshi et al. [10] predict that 4.6% reduction in fuel consumption can be realized on HDFTP engine test cycle with 200rpm engine downspeeding and an E-booster. In another study, Keidel et al. [12] simulated a supercharged heavy-duty diesel engine in a vocational application with 400 rpm downspeeding to achieve a 4-6% improvement in fuel economy on the HHDDT transient cycle. Lastly, for long haul Class 8 truck applications, Smith [13] predicted that an E-compressor can enable 43% engine downsizing when combined with other 48V components such as EGR pump, ISG and a sufficiently large battery pack. This advanced engine package was predicted to achieve a 14% increase in vehicle fuel economy over HHDDT Cruise cycle.

Waste heat recovery systems such as organic Rankine cycle (ORC) bottoming cycles or further expansion of exhaust gas through a turbocompound turbine can be used for partial recovery of fuel energy which is otherwise wasted (lost) in the exhaust. For heavy duty diesel engines, the wasted heat energy in the exhaust can be as high as 30% of the total fuel energy. While the ORC systems typically have a higher fuel consumption reduction potential in comparison to turbocompounding [3, 14], the technology is still in the prototype stage of development [15]. On the other hand, mechanical turbocompounding has already been applied to production on multiple heavy-duty engine platforms for both on-highway and off-highway applications [16, 17]. For both these technologies, the primary challenge lies in routing the power generated by the turbogeneration device back into the powertrain or vehicle. At high engine loads where the power output from the ORC expander or the turbocompound turbine is high, mechanical integration would be the most efficient approach; however, at low engine loads a mechanically integrated system would introduce parasitic losses [18]. Conversely, an electrical integration approach can allow for efficient ORC expander and turbocompound turbine operation, without inducing drag on the engine at low engine loads. However, at high engine speed and loads, the recovered energy must go through the mechanical to electrical to mechanical energy conversion cycle before the power can be supplied to the engine cranktrain. Multiple energy conversion cycles adversely impact the efficiency of power delivery from the waste heat recovery system to the engine. Other challenges of waste heat technologies include reduction of exhaust enthalpy into the aftertreatment system which can impact its performance [10, 19]. With respect to the potential of these waste heat recovery technologies, Callahan et al. [18] reported an overall benefit of 2.5% with the turbocompound technology implemented on a MY2010 Daimler DD15 heavy duty diesel engine. Similarly, Joshi et al. [10] predicted 1-

2% reduction in engine fuel consumption at higher engine speed and load with the turbocompounding system on a medium heavy-duty diesel application. Volvo claimed that the addition of the turbocompound system on their MY2017 D13 engine provided up to 6.5% reduction in fuel consumption [20]. In case of waste heat recovery using bottoming cycles, Xu et al. [21] document a 10% reduction in fuel consumption by Cummins using ORC system on a heavy-duty engine. This comprehensive review paper on waste heat recovery reports a range of 2-10% for reduction in fuel consumption in multiple simulation and experimental investigations [21].

While the three technology areas described above (electrification, advanced boosting, and waste heat recovery) show significant potential in reducing engine fuel consumption, independent implementation of all three technologies on the engine can lead to a significant increase in engine cost, package and complexity. Several technologies have been developed recently to combine these technology areas and increase the fuel consumption benefit to technology cost ratio. SuperGen [11, 22] provides one solution for combining supercharging and mild hybridization by integrating the B-ISG and E-booster into one device with the use of eCVT. The potential fuel consumption reduction with this combined supercharging and mild hybridization technology for a passenger car application was reported at 16% by King et al. In another integrated approach called SuperTurbo [23, 24, 25], the main engine turbocharger was coupled to a CVT and connected to the engine crankshaft, thereby enabling supercharging as well as turbocompounding capability. The technology achieved 28% engine downsizing on a heavy-duty off-road application with a 13.1% reduction in engine fuel consumption [25]. The technology also provided benefits in achieving ultra-low NOx emissions on heavy duty engines by reducing transient NOx and by improving aftertreatment thermal management [24]. An alternate concept eTurbo, is an integrated air system technology that integrates an electric motor on the turbocharger shaft to provide electric supercharging and electric turbocompounding capability [26, 27, 28]. With the eTurbo technology, Song et al. [28] predicted a 5.1% reduction in engine fuel consumption on FTP-75 drive cycle for a medium heavy-duty vehicle without engine downsizing/downspeeding. In passenger car application, Cooper et al. [26] showed that along with a 70% reduction in engine transient response time, eTurbo achieved a 2.9% reduction in vehicle fuel consumption from exhaust energy recovery on NEDC cycle.

Overall, the three integrated technologies (SuperGen, SuperTurbo and eTurbo) have been successful in combining two out of the three key technology areas of electrification, waste energy recovery and supercharging. However, a technology concept that combines all three technology areas (electrification, advanced boosting, and waste heat recovery) is yet to be widely researched. The next section describes the construction and functionality of the three integrated concepts discussed so far in more detail.

2.2 State of the Art

Over the past two decades, multiple integrated concepts have been patented and developed to enable supercharging, exhaust energy recovery, and mild hybridization. In 2006, Moeller et al. patented a power-split supercharging system that also provided belt starter-generator (BSG) capability known as SuperGen [11]. The novel concept couples secondary

compressor, engine crank pulley and two electric machines through a planetary drive to provide a power-split secondary compressor drive as well as belt starter-generator (BSG) functionality. A schematic of the SuperGen concept is shown in **Figure 3**. The engine crank pulley (10) is connected to the carrier of the first planetary set (12) while the compressor (2) is connected to the sun gears (22,32) of both planetary sets (12,14). The rotor of the first electric machine (26) is connected to the ring gear of first planetary set while the rotor of the second electric machine (42) is connected to the ring gear of the second planetary set. Lastly, the ring gear of first planetary set (24) is connected to the carrier of second planetary set (34). The arrangement allows for variable speed control of the secondary compressor (2) while also providing high-efficiency power-split energy transfer to the secondary compressor (mechanical from engine and electrical from electric machine 42). The system also provides the necessary gear reduction of up to 10:1 between the engine crank pulley and secondary compressor. The technology was further developed and successfully applied for engine downsizing to enable 16% reduction in fuel consumption [11]. Overall, while the technology efficiently integrates supercharging and mild hybridization, it does not consider integration of turbogeneration from excess exhaust energy.

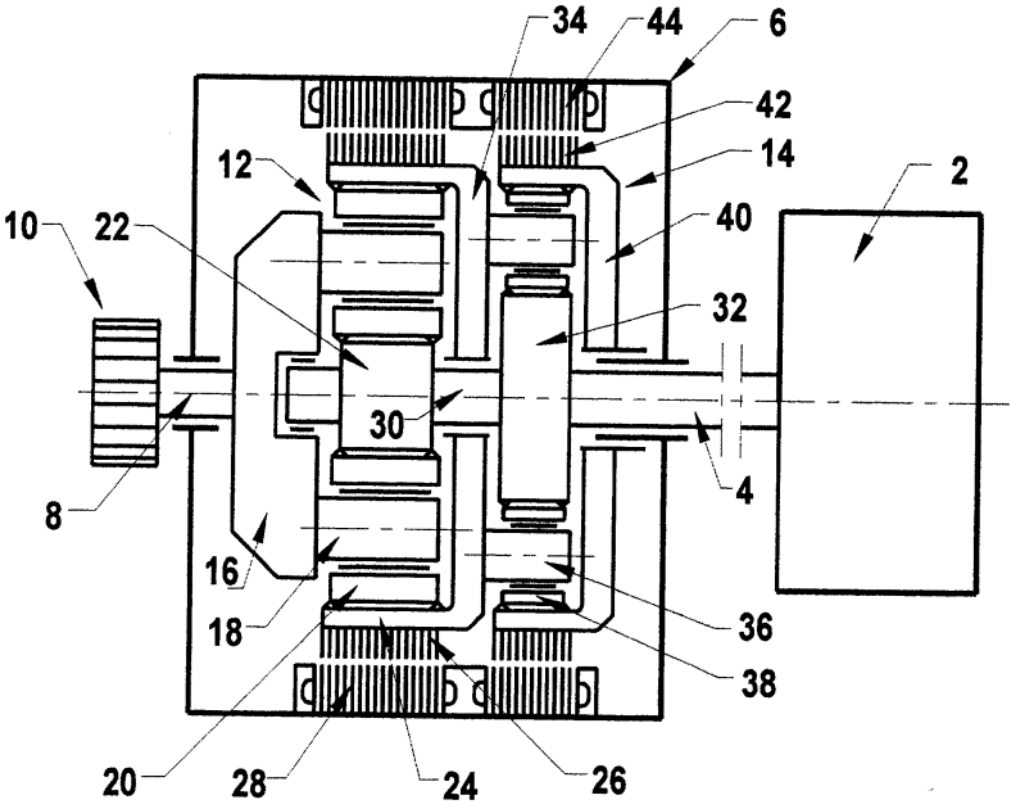

Figure 3. SuperGen supercharging system by Moeller et al [11, 29] (2 Secondary Compressor, 10 FEAD pulley, 28 First Electric Motor-Generator, 44 Electric Motor-Generator, 12 First Planetary Set, 14 Second Planetary Set).

Another integrated technology called the SuperTurbocharger applies a similar approach of coupling crankshaft and turbomachinery components using a variable ratio transmission drive. Patented in 2017 by Brinks et al., the concept enables mechanical supercharging and turbogeneration by coupling the main engine turbocharger to engine crankshaft through a traction drive and a toroidal CVT coupling. As shown in **Figure 4**, the main engine turbocharger shaft (320) is connected to the high-speed traction drive (308) which is then connected to the engine crankshaft through a CVT unit (310). During transients, the CVT unit is controlled to drive the turbocharger at higher speeds using the engine crankshaft, to achieve a faster response. At higher engine speed and loads, the turbocharger speed is again adjusted by the CVT actuator to enable turbogeneration from excess exhaust energy. While the system provides highly efficient mechanical power transfer between engine crankshaft and turbocharger at high loads, it can also lead to increased parasitic losses on the engine at lower speed and loads. Furthermore, since the system is implemented on the main engine turbocharger, the potential of supercharging and turbogeneration is limited to single stage air system. For a two-stage air system with a secondary compressor and a turbogeneration turbine, the concept wouldn't allow for independent speed control of secondary compressor and turbogeneration turbine, which would significantly limit the combined turbocharger efficiency. Overall, the SuperTurbocharger offers an efficient method for integration of mechanical supercharging and turbogeneration on engines with single stage air systems. The technology has already been developed and has demonstrated up to 13.1% reduction in fuel consumption on a heavy-duty diesel engine [24, 25].

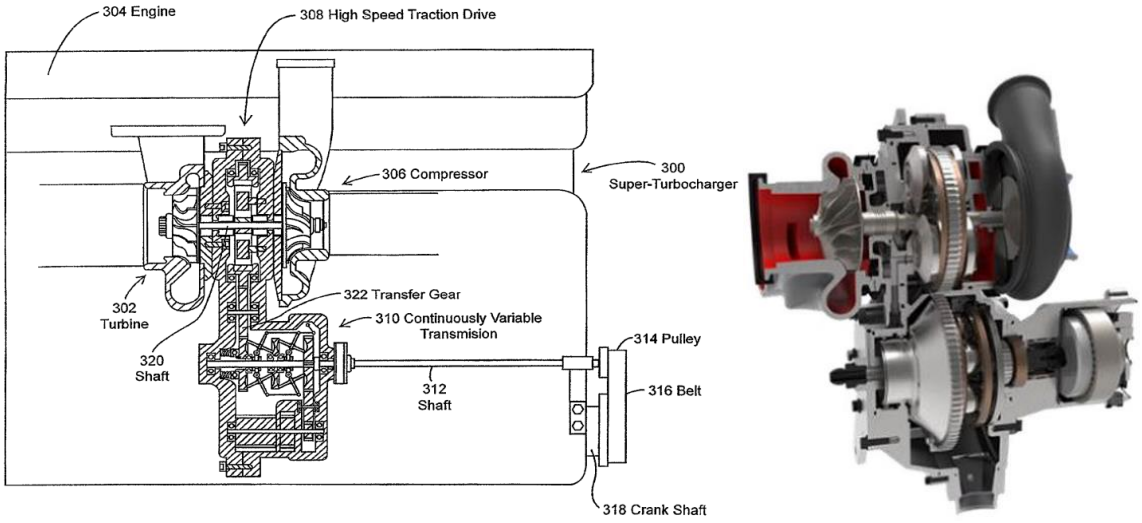

Figure 4 SuperTurbocharger internals show the planetary traction drive and CVT [30, 25]

Similar to the Superturbocharger, BorgWarner's eTurbo [26, 31] is another concept that integrates electrical supercharging and turbogeneration technologies by simple implementation of an electric machine on turbocharger shaft. As shown in **Figure 5**, the electric motor-generator (22) is integrated in the housing (20) between the compressor and turbine, with the rotor (24) attached to the turbocharger shaft. At lower engine speed and high loads, the electric motor assists the turbocharger to increase boost and achieve higher low-end torque. The assist from electric motor also helps spool up the turbocharger faster

and reduces engine transient response time. At higher engine speed and loads, the electric machine holds the turbocharger at a lower speed to allow energy recovery from exhaust gas flow, that would have otherwise been bypassed through the turbine wastegate. While this concept avoids an engine friction increase due to absence of coupling with engine crankshaft, the power transfer efficiency between eTurbo components and engine is low due to multiple energy conversions (for example mechanical to electrical to mechanical during turbogeneration). Furthermore, since the concept was developed for main engine turbocharger, the combined turbocharger efficiency and engine performance is limited to single stage turbocharger system. For two stage turbocharger systems, even if the eTurbo was utilized to integrate a secondary compressor and a turbogeneration turbine, the concept would not allow for independent control of the secondary compressor and turbogeneration turbine, leading to lower overall turbocharger efficiency.

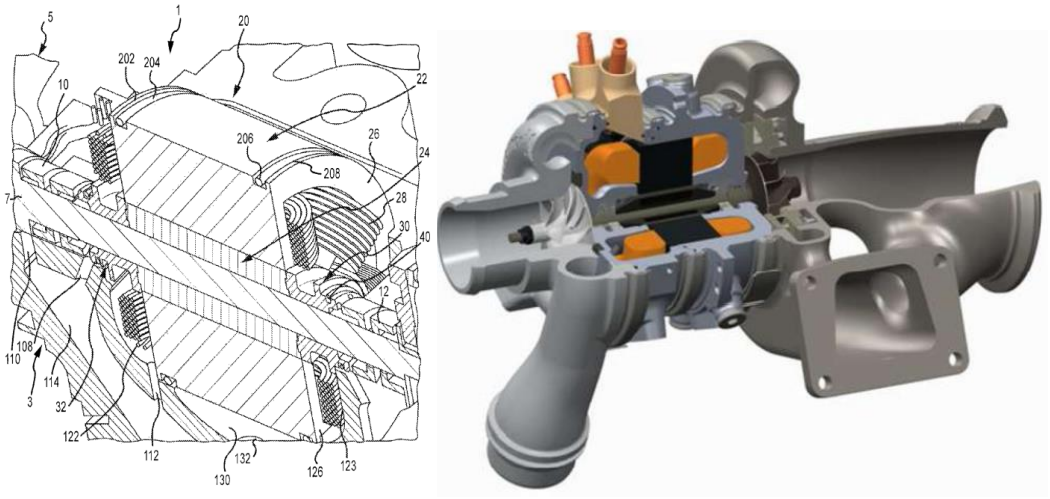

Figure 5 Section of BorgWarner's Electrically Assisted Turbocharger (eTurbo) [26, 31]

Lastly, Johnson [32] recently proposed an integration system that applies variable ratio transmission systems to couple turbomachinery components, electric motor and crankshaft. However, the concept has not been developed so far and its viability is unknown.

2.3 Proposed Concept

Based on section 2.1 and 2.2, the following concepts can be proposed for an integrated solution that provides supercharging, turbogeneration, and mild hybridization functionality on an engine.

- **Independent Integration**: The concept integrates a turbocompound or an ORC turbine, a secondary compressor and an integrated starter generator unit on the engine as shown in **Figure 6A**. The turbine is integrated with a dog-clutch and an electric motor to allow mechanical as well as electrical power transfer between the turbine and the engine. As described in section 2.1 and 2.2, mechanical power transfer is most efficient at high speed and loads while electrical turbogeneration, enabled by dog-clutch, is most efficient at lower engine speed and loads. The

secondary compressor functions independent of the turbocompound/ORC turbine and is powered by an electric motor. The integrated starter-generator (ISG) system provides the mild hybridization functionality of start-stop, regeneration and torque assist. As described in section 1.2, the primary challenge with such a system is the integration cost and increase in engine package size.

- **e-Turbo and ISG**: The concept is based on an electrically assisted turbocharger (eTurbo) that enables electrical supercharging and electrical turbogeneration. An ISG has also been added to enable mild-hybrid functionality as shown in **Figure 6B**. The eTurbo would be applied in addition to the base engine turbocharger to maximize combined turbocharger efficiency and hence engine fuel savings. While the concept seems cost effective, primary challenges include high exhaust energy conversion losses due to electrical power transfer and speed constraint between secondary compressor and turbogeneration turbine.
- **SuperTurbocharger and ISG**: As shown in **Figure 6C**, the concept utilizes a Superturbocharger in addition to the base engine turbocharger. The ISG system is added separately to the engine. The operation of SuperTurbocharger is similar to that of an eTurbo except that the shaft connecting secondary compressor and turbogeneration turbine is mechanically coupled to the engine crankshaft with a variable speed drive. While this concept enables higher efficiency of turbogeneration at higher power output, at lower engine speed and loads, the SuperTurbocharger can add frictional drag force to the crankshaft leading to increased fuel consumption. Furthermore, the SuperTurbocharger does not allow for independent secondary compressor and turbogeneration turbine speed control, which is essential to operate both components at high efficiency.
- **SuperGen + Powersplit Turbogeneration**: Lastly, the concept shown in **Figure 6D** combines SuperGen with a powersplit turbogeneration system. The concept allows for independent speed control of secondary compressor and the turbogeneration turbine. It also allows for both mechanical and electrical power transfer between the turbogeneration turbine and the engine. Another advantage of the concept is that the secondary compressor is connected to the engine through a speed coupling. The coupling helps in operating the secondary compressor at optimal speed while minimizing energy conversion losses between engine and secondary compressor. Furthermore, the electric motor-generator unit on the ring gear of SuperGen's planetary drive also provides the functionality of an ISG system. Overall, while this concept seems to be most fuel efficient in comparison to others, it has a relatively higher cost and a larger package size.

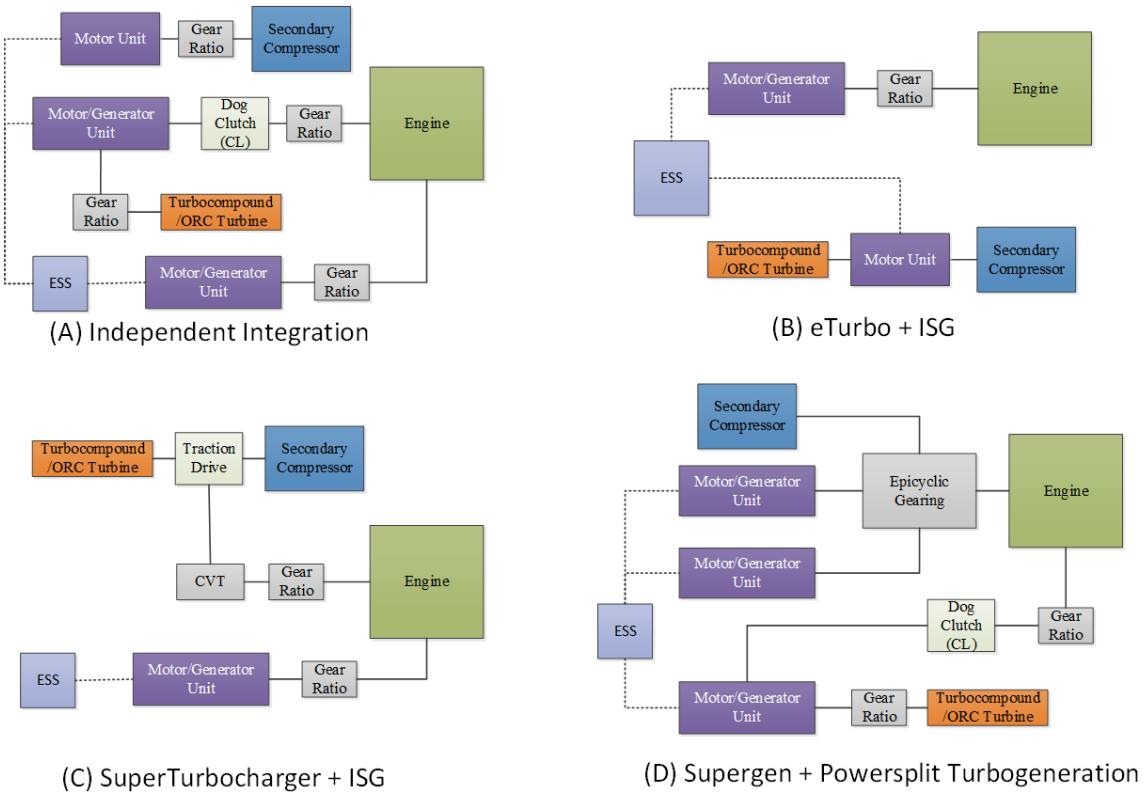

Figure 6 Integration concepts based on state-of-the-art technologies

Upon completion of an assessment of state-of-the-art technologies and a thorough literature review, significant gaps were identified in the efficiency, functionality, cost and packaging of the integration concepts described above. The key learnings from the assessment that can potentially address these identified gaps are:

- Since turbomachinery components spin at much higher speeds than engine, a speed coupling is needed to integrate them with the engine crankshaft and/or a motor-generator unit
- Direct integration of motor-generator unit in the engine cranktrain is needed to achieve mild hybrid capability
- Since most integrated concepts utilize multiple motor-generator units of similar power level in different regions of the engine operating map (supercharging at low speed high load / turbogeneration at high speed high load / regen and start-stop during no load), attempt should be made to utilize same motor-generator for multiple operation to reduce cost, packaging and weight increase
- Both mechanical and electrical method of engine integration is required for turbogeneration turbine to maximize power transfer efficiency
- Variable speed control is required on secondary compressor and turbogeneration turbine to maximize turbocharger efficiency
- High ratio geartrain with high mechanical efficiency is required between turbogeneration turbine and engine crankshaft to maximize power transfer efficiency

- Secondary compressor bypass is needed at higher engine speed and loads to minimize pumping losses
- In case of turbocompounding, a turbine bypass is needed for aftertreatment warmup

Based on these learnings, a novel integration concept was explored to integrate the secondary compressor, turbogeneration turbine, engine crankshaft and electric motor-generator. Since turbomachinery typically spins at much higher speed than engine crankshaft (at approximately 30x), a direct coupling of compressor or a turbine to the engine would require high gear reduction leading to low mechanical efficiency. Furthermore, a direct coupling to engine crankshaft would make the speed of turbomachinery component a function of engine speed leading to lower isentropic efficiency. Therefore, a speed coupling such as a planetary gear set would be required to integrate turbomachinery to the engine. The next step was to decide the placement of the four components on planetary gear set. The component operating at highest speed is typically the turbine while the component with lowest speed is the engine. The highest gear ratio in a planetary gear set is between sun gear and planetary gear carrier when the ring gear is fixed. Therefore, the turbine should be placed on the sun gear while the engine on the carrier gear with the ring gear fixed using a brake. The secondary compressor could then be coupled to the ring gear with a gear reduction as it is only required at low engine speeds and high loads. The approach would also allow for reduced number of gear interface between turbine and engine crankshaft thereby increasing mechanical efficiency during turbogeneration. The electric motor-generator unit could then be placed between the carrier gear and the engine with a clutch in between to allow for optimal turbogeneration at low engine loads and better control over secondary compressor at low engine speed and high loads. This concept was termed as the integrated turbogeneration electrification and supercharging (ITES) system. As shown in **Figure 7**, the system eliminates the use of separate electric motor/generator for secondary compressor and turbocompound turbine/turbine expander and eliminates the fluid coupling. The concept was granted a patent in the year 2019 and assigned to Joshi et al. [33].

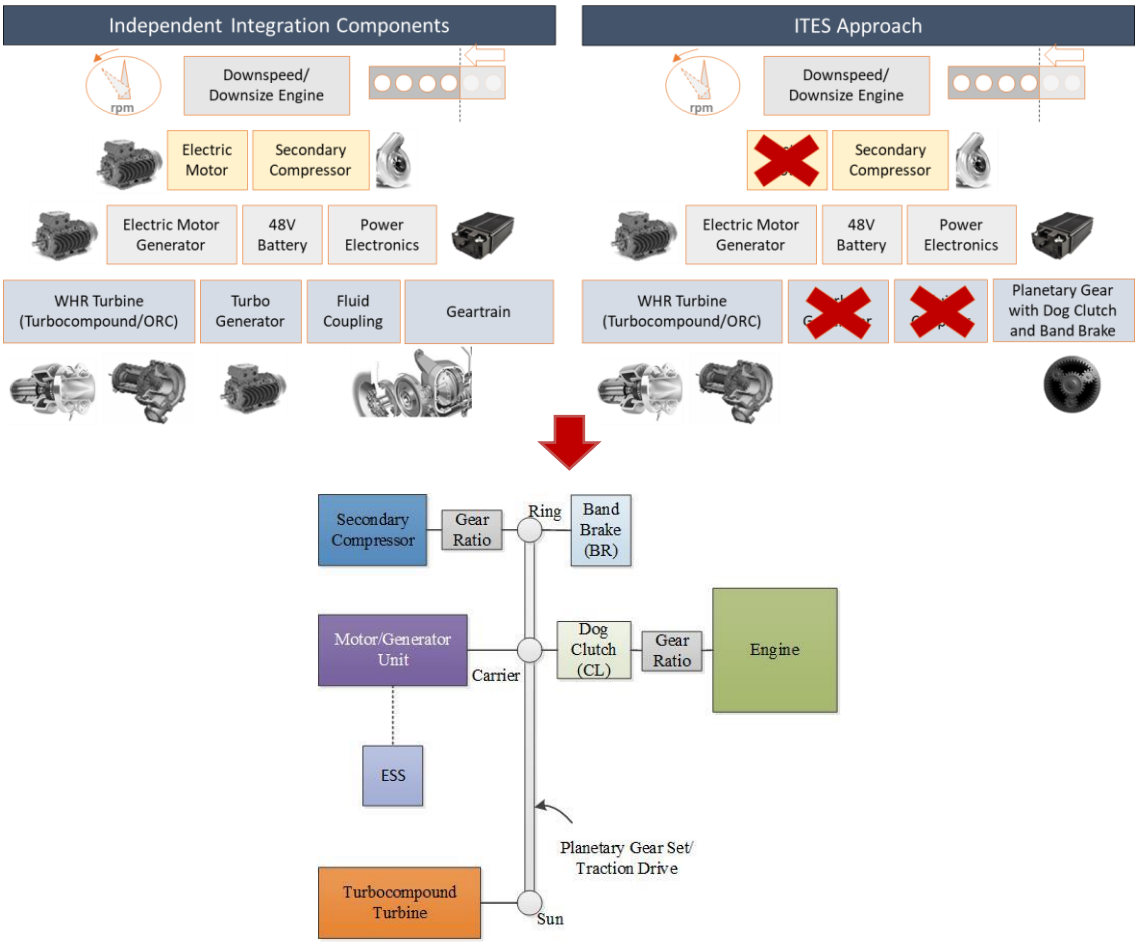

Figure 7 ITES integration approach in comparison to the independent integration ideal technology package.

The ITES unit is applied in addition to the base engine turbocharger and consists of a planetary gear set that has a secondary compressor connected to the ring gear, turbocompound turbine or ORC expander connected to the sun gear and an electric or hydraulic motor/generator connected to the carrier gear. The unit also consists of two actuators in the form of a dog clutch and a band brake. The dog clutch is implemented between the carrier and the gear connected to cranktrain, while the band brake is installed on the ring gear to stop secondary compressor from rotating when it is bypassed. **Figure 8a** shows a planetary gear lever diagram of ITES unit wherein all components and the basic linkages between them are shown. A more detailed layout of ITES unit including engine air system layout and geartrain is shown in **Figures 8b and 8c**.

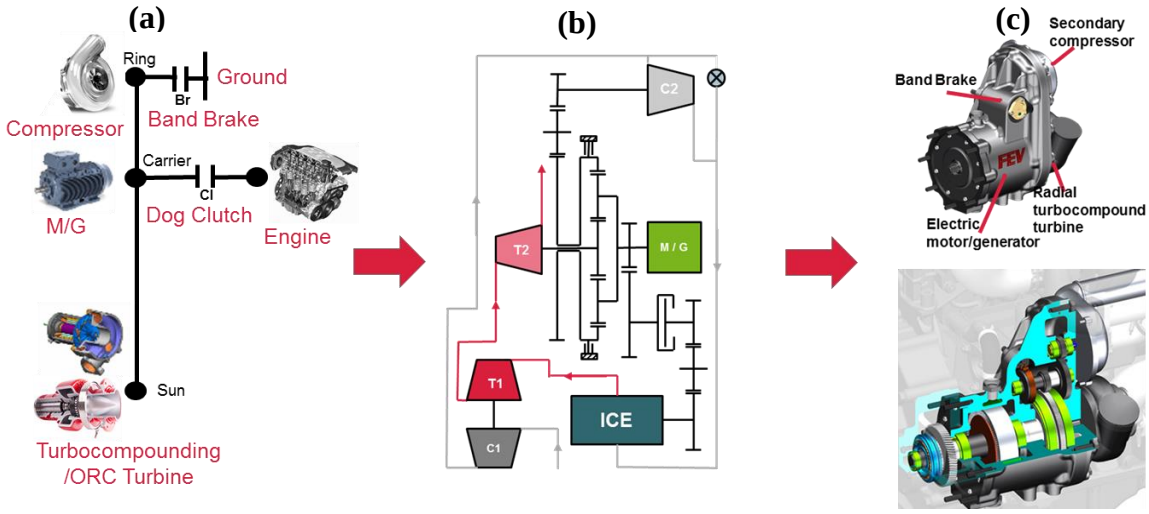

Figure 8 ITES system layout on planetary gear level diagram (a), with engine airpath (b) and in a cutaway section on engine (c)

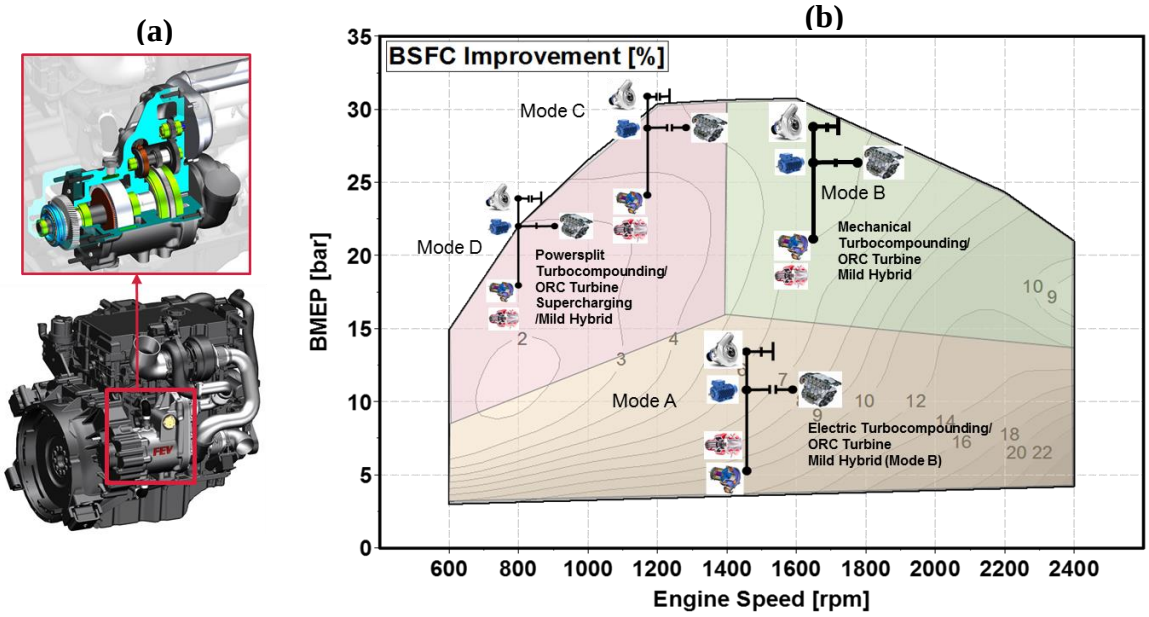

Figure 9 ITES system integration on engine (a) and different modes of operation on the engine map (b)

As shown in **Figure 9** and **Table 1** there are four different operating modes (A-D) that are possible with ITES based on the clutch and brake position.

- In mode A, the clutch between the engine cranktrain and the carrier gear (CL) is open while the band brake (BR) on the ring gear is engaged. This mode enables electric turbocompounding as the power from the turbocompound turbine is converted into electrical energy by the electric motor/generator. This mode is typically applied at low engine loads (region 1), where the turbocompound turbine power output is low and thus no drag or parasitic loss is applied to the engine cranktrain. Aftertreatment thermal

management is also possible in this mode through control of turbocompound turbine speed to generate back pressure.

- In mode B, the clutch between the engine cranktrain and the carrier gear (CL) is engaged while the band brake (BR) is still engaged. In this mode, mechanical as well as power-split turbocompounding is achieved as the power from the turbocompound turbine can either be transmitted to the engine cranktrain or to the electric motor/generator. Since the dog clutch is engaged, the motor generator unit can also be utilized for engine torque assist, regenerative braking and starting the engine.
- In mode C, the band brake (BR) is released, the secondary compressor bypass valve is closed and the clutch (CL) is disengaged. The secondary compressor is now provided power by the turbocompound turbine and/or by the electric motor/generator depending on the boost pressure demand at a given engine speed and load. This mode emulates the operation of an electrically assisted turbocharger. Aftertreatment warm up is also possible in this mode through reduction of air-fuel ratio by reducing the boost level, and by controlling turbocompound turbine speed.
- Finally, in mode D, the clutch (CL) is engaged and the band brake (BR) is released in cases where torque assist is required from the electric motor/generator while the secondary compressor is active.

The choice between the four modes described above depends on the engine speed and load, battery state of charge (SOC), vehicle speed, driver pedal position and brake pedal position.

Table 1 ITES operation in different modes and their advantages over conventional independent integration approach

Mode	Dog Clutch	Brake/ Bypass	Typical Operating Area	Technology Enabled	Advantages over Conventional Independent Integration
A	Off	On	Low Load	• Electrical Turbocompounding • Thermal management	• Maximize TC efficiency through speed control • No parasitic drag on engine
B	On	On	High Speed and Low to High Load	• Mechnical Turbocompounding • Torque assist and regen	• Maximize TC power transfer efficiency at high power output with no losses through fluid coupling
C	Off	Off	Low Speed and High Load	• Powersplit supercharging • Thermal management	• Distribute secondary compressor power demand between TC and MG to maximize efficiency
D	On	Off	Low Speed and Low to High Load	• Powersplit supercharging • Start-stop, torque assist and regeneration	• Distribute secondary compressor power demand between TC, engine and MG to maximize efficiency

With regards to durability and reliability requirements of many heavy-duty applications, ITES system overcomes these challenges by housing all the rotating components within the engine geartrain assembly with lubrication and cooling connections from the engine block. Furthermore, the system eliminates the need for a wastegate or VGT actuator, and

promotes the use of a more durable, fixed-geometry high-pressure-stage turbine. The system can also eliminate/reduce the need of exhaust flap by assisting aftertreatment thermal management at low loads through speed control of turbocompound turbine. Overall, the durability and reliability risk of ITES system is low, since the system integrates existing engine technologies that have been applied in production while reducing the need of high-durability-risk components such as VGT and exhaust flap. In addition to benefit of aftertreatment thermal management, ITES system can also reduce transient PM emissions by providing on-demand boost from the driven secondary compressor [34]. This is especially beneficial for heavy-duty engines wherein trade-offs are typically made between transient PM emissions and engine transient response. For engines with high levels of EGR, the driven secondary compressor can help improve transient NOx control while the turbocompound turbine can improve the trade-off between EGR drivability at low NTE speeds and engine fuel consumption at peak power [18]. To evaluate these potential benefits and verify the viability of the concept, model-based assessments were conducted, as described in the next chapters. The assessments led to the development of methods for component sizing, control strategy and optimization of the novel concept.

3 Model-based Optimization

This chapter focuses on the functional verification, component sizing and geartrain optimization of the ITES concept through 1D multi-physics simulation. A generic model-based method for turbomachinery components, geartrain and battery capacity sizing has been proposed, that can be extended to other integration concepts. The target application for implementation of ITES concept was chosen as a Class 6-7 urban vocation truck with a medium heavy-duty diesel engine. This specific application was chosen due to its high fuel savings potential from mild hybridization (low-speed start stop driving), aggressive low-end torque requirements, high technology cost sensitivity and strong packaging constraints [8]. As shown in **Figure 10**, the baseline 6 cylinder 7.7L medium heavy-duty diesel engine was downsized to a 4 cylinder 5.1L and integrated with the ITES unit. A high-level cost and weight specification shows similar cost and weight between the baseline engine and the downsized engine. Furthermore, the ITES system is contained within the baseline engine envelope while reducing engine length by 18% for this application.

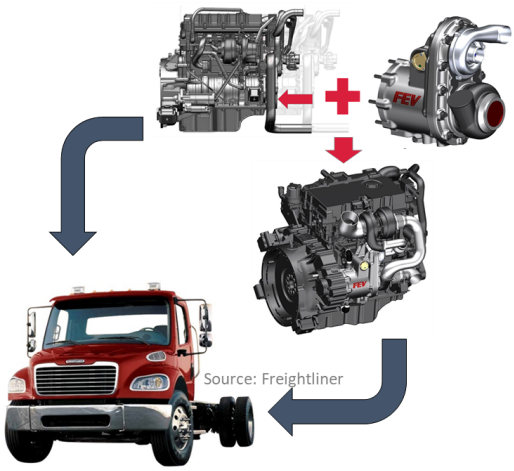

Parameter	Baseline Engine	Downsized Engine with ITES
Displacement [L]	7.7	5.1
No of Cylinder [-]	6	4
Bore [mm]	110	110
Stroke [mm]	135	135
Compression Ratio [-]	17.6	17.6
Peak Power [kW]	228@2200rpm	228@2200rpm
Power Density [kW/L]	29.6	44.7
Peak Torque [Nm]	1200	1200
Peak Cylinder Pressure [bar]	220	220
Air System [-]	Turbocharged with HP EGR	Turbocharged with HP EGR and ITES unit
Start-stop, Regen, Torque Assist [-]	No	Yes
Dimensions [mm]	1272x862x987	1045x864x984
Engine Weight [kg]	650	575
System Cost (DMC) [$]	13,000	12,500-13,000

Figure 10 Specifications of Class 6-7 urban vocation application with baseline and ITES system based powertrain

First, a 1D engine simulation model was developed for the baseline engine and validated against test data (Appendix A). Thereafter, the ITES system 1D model was developed and integrated with a downsized four-cylinder version of the baseline engine. Lastly, the ITES components were optimized through model-based optimization and a method for the same has been proposed.

3.1 Modeling Environment

In this dissertation, a commercially available multi-physics modeling software called GT-SUITE [35] has been applied for all model-based analysis. The class-leading 1D engine and vehicle system simulation tool has been applied successfully by both academia and industry for the past 20 years in multiple research and development programs. Furthermore,

many publications reviewed in section 2.1 have predominantly used GT-SUITE for system level analysis of novel engine air system concepts [10, 23, 27, 28]. The software provides validated physics-based sub-models of engine and vehicle components that can be readily combined and applied for system simulation. At the same time, validation of the system models is essential for such model-based evaluations.

Table 2 Engine sub-models used with GT-SUITE simulation tool [35]

Component/Process	Model
Compressor and Turbine	Manufacturer Provided Performance Maps
EGR Cooler/Charge Air Cooler	Semi-predictive Effectiveness Model
In-cylinder Heat Transfer	Woschni GT
Air path Heat Transfer	Colburn
Friction	Chen Flynn
Cylinder Filling/Air path	Navier-Stokes
Combustion/Fuel Injection	DI Pulse (GT Manual)
NOx Emission	Extended Zeldovich
Aftertreatment	Quasi-Steady Solver (GT Manual)
EGR, Lambda, Fueling Control	Model Based / PID

Table 2 shows the different physical models applied for modeling of engine components within GT-SUITE. In general, the complete air-path plumbing is modeled in 1D and solved using the Navier-Stokes equation. For convection heat transfer modeling of air path, Colburn correlation is applied [35]. To capture the impact of advanced air system technologies on combustion, 'DI-pulse' predictive combustion model is used. The combustion model divides the combustion chamber into three thermodynamic zones, specifically, the main unburned zone, the spray unburned zone and the spray burned zone. The modeling of physical processes in these zones, such as fuel injection, entrainment, evaporation, mixing, ignition, in-cylinder heat transfer, premixed combustion and diffusion combustion, is then achieved using standard modeling techniques described in Heywood Chapter 14 [36]. The predicted combustion temperature and in-cylinder composition of the combustion reactants is also used to predict in-cylinder NOx production through the Extended Zeldovich Mechanism. For engine friction modeling, Chen-Flynn expression with dependency on mean piston speed and cylinder pressure is applied upon validation against engine motoring friction data. For turbomachinery modeling, performance maps are obtained from the manufacturers and implemented in the model. Based on the inlet conditions and turbocharger speed, the maps calculate downstream pressure, temperature and shaft power. The aftertreatment system comprising of DOC, DPF, SCR and ASC is modeled as a pressure drop component to simulate exhaust restriction. However, to predict the impact of engine technologies on aftertreatment conversion efficiency, an empirical SCR catalyst mid-bed temperature model is applied [37]. The model predicts the SCR mid-bed temperature based on aftertreatment inlet conditions such as turbine outlet temperature, exhaust mass flowrate and ambient temperature. Lastly, in order to run drive cycles, the detailed engine model is converted to a fast-running model (FRM) by simplifying air path components, applying cylinder slaving and increasing discretization. **Figure 11** shows the

validated FRM model of the baseline engine that was able to achieve ~15X real-time speed with +/-5% accuracy on key performance parameters (Validation shown in Appendix A).

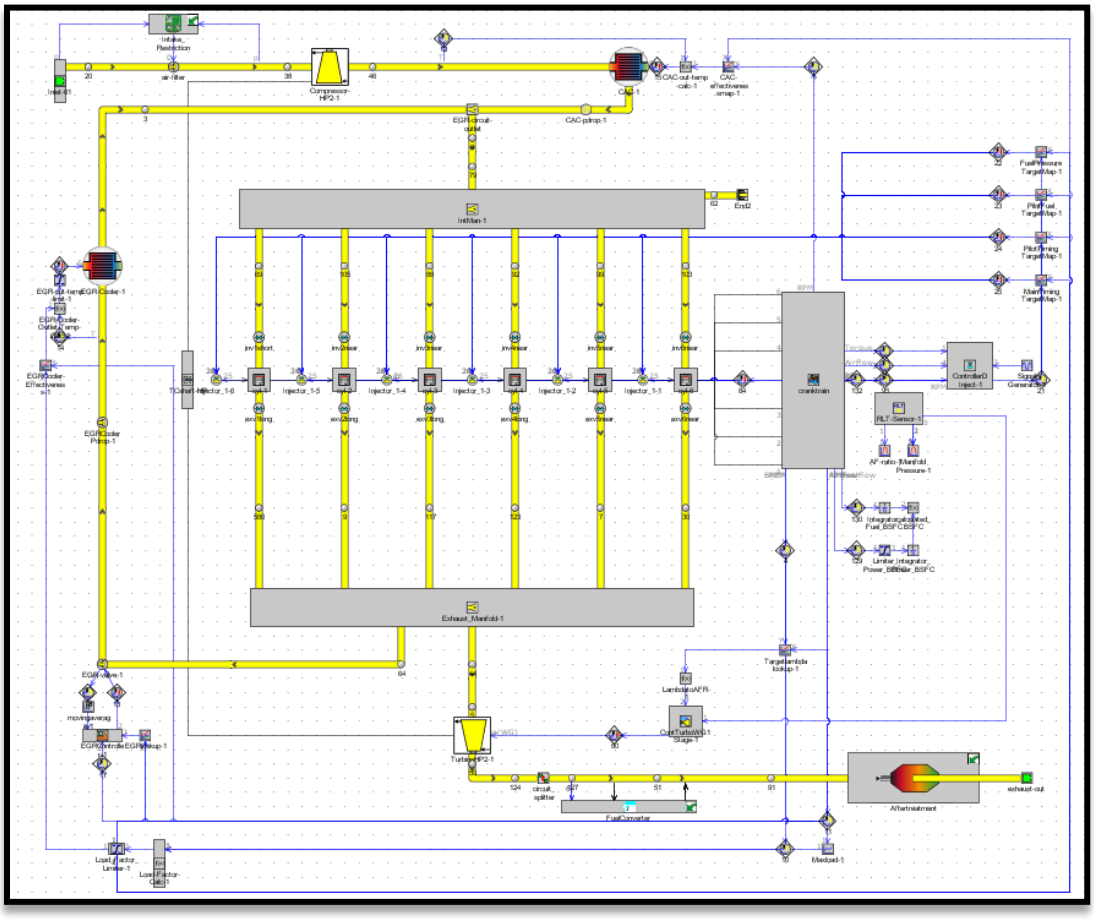

Figure 11 Baseline engine GT-SUITE 1D model that shows air path, cranktrain, power-cylinder, turbocharger, CAC, EGR cooler, controls and aftertreatment components.

Similarly, vehicle modeling was also conducted using GT-SUITE modeling software. The engine FRM model was integrated in a validated vehicle model (Appendix B) capturing vehicle body 1D longitudinal dynamics as shown in **Figure 12**. The various sub-systems within the vehicle model are typically modeled as follows:

- **Engine FRM Model**: The crankshaft of the engine FRM model is integrated with the vehicle driveline model as a lumped inertia component with excitation from cylinder pressure forces. The engine rotating assembly and all engine accessory drives are lumped into a single inertia component and connected to the automatic transmission through a torque converter. The vehicle controller converts the driver pedal input to engine torque request which is then sent to the engine fuel control unit to achieve the commanded engine torque. The vehicle controller also manages engine start-stop and idle functions. Engine auxiliary loads such as water pump, cooling fan, AC compressor, air compressor and power steering pump are modeled

by specifying power consumption vs engine speed curves. Typically, the auxiliary electrical loads are constant and applied as a fixed load to the alternator.

- **Transmission Model**: Each gear in transmission is modeled as a lumped inertia component in the drive line, with specified inertia, gear ratio, power transfer efficiency and shift time. The torque converter is modeled by specifying capacity factor and torque ratio tables as a function of speed ratio. The lockup clutch is modeled with specified actuation time and max static torque. Transmission shift strategy for upshifts and downshifts is specified as a function of vehicle speed and accelerator pedal position.
- **Driveline Component Models**: Shafts, axles, planetary gears and differentials are modeled with specified inertia, gear ratio and efficiency. The specifications are generally obtained from product specification datasheet.
- **Tractor and Trailer Model**: Tractor and trailer are modeled separately with the option to switch between vehicle configurations with and without trailer. Vehicle longitudinal dynamics are modeled with specified tractor mass, trailer mass, cargo mass, axle configuration, wheelbase, center of gravity, axle load distribution, tractor frontal area, tractor aerodynamic drag coefficient, delta frontal area from trailer addition, delta Cd from trailer addition. Tires are modeled as rigid (no slipping) with specified rolling radius and rolling resistance values. The values for aerodynamic drag coefficient and tire rolling resistance are typically calibrated to match the vehicle coast-down test data. Tire road interface, grades and environment conditions are also included in the model.
- **Battery Model:** Battery cells are modeled as an xRC equivalent circuit with specified resistance, capacitance and open circuit voltage curves. The cell characteristic curves are defined as a function of SOC, current and temperature. The cells are then combined in specified series and parallel arrangements to form a battery pack. It is assumed that all cells are balanced and do not have any spatial temperature variation temperature distribution at all times. The model allows for voltage and capacity variation by changing number of series and parallel cells. Conventional SOC model is applied which calculates battery SOC based on charge throughput for a given time. For 48V battery models, empirical correlation for prediction of battery life as a function of charge throughput and depth of discharge are also included.
- **Motor / Inverter Model**: Electric machines such as starter motor and ISG units are modeled as lumped inertia components with specified efficiency and torque generation characteristics. The torque and efficiency characteristics are specified as a function of DC voltage and component temperature. In cases where thermal sub-models are not developed, peak power output is applied for 30-60s before switching to continuous power rating.

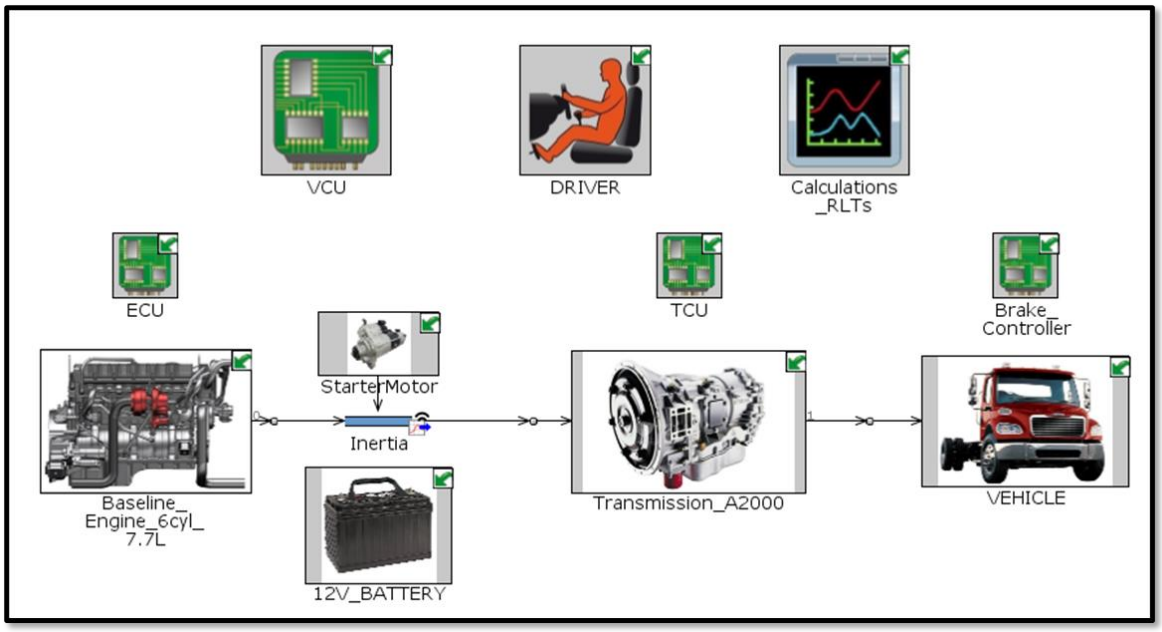

Figure 12 Vehicle propulsion system model in GT-SUITE capturing longitudinal dynamics

3.2 Downsized Engine with ITES Model

Once the baseline model was developed and validated against experimental data (Appendix A), the next step was to develop the model of downsized engine with the ITES unit. **Figure 13** shows the air system layout of the downsized engine in comparison to the baseline engine. While significant model changes were needed to develop the downsized engine model, validated sub-models of the baseline engine model were applied/preserved for consistency.

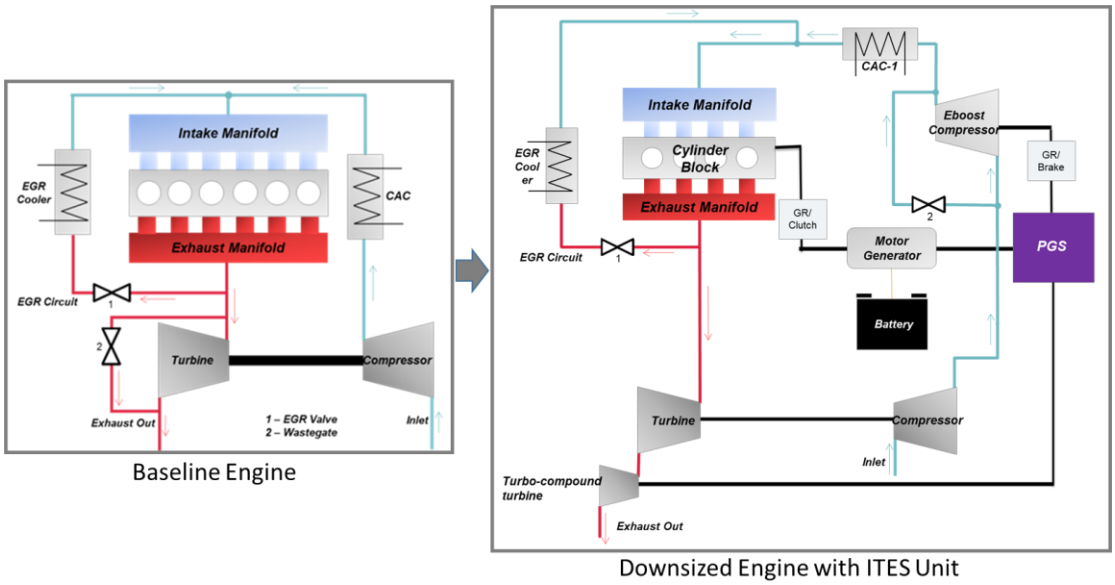

Figure 13 Comparison of baseline engine and downsized engine with ITES unit air system layout.

The following changes were made on the baseline engine model to develop the downsized engine model with ITES unit:

- **Combustion System:** Since the downsized 4-cylinder engine has the same piston bowl design, bore, stroke, compression ratio and connecting rod length, the DI-pulse combustion system model could be carried over from the baseline engine to the downsized engine power cylinder.
- **Cranktrain:** Two cylinder and their valvetrain components were removed from the model. The firing order was adjusted to 1-3-4-2 and firing separation adjusted to 180 degrees crank angle. Since four-cylinder engines typically need balance shafts and larger flywheel inertia to handle tortional vibrations, engine inertia was not changed. Friction model coefficient were also not adjusted and the FMEP was kept consistent between the baseline and downsized engine. The reduction in friction power (constant FMEP with reduced displacement) could be justified by reduction in number of piston-ring interfaces, water pump power reduction, oil pump power reduction and reduction in crankshaft/camshaft bearings.
- **Intake Side:** Since the downsized engine had the same rated power as the baseline engine no reduction in pipe diameters were applied. The intake manifold volume was proportionally adjusted for a 4-cylinder engine and the corresponding intake ports/valves were removed along with the two cylinders from baseline engine model. No changes were made to the intake restriction however a secondary compressor and its bypass route were added to the intake plumbing after the main engine compressor. The charge air cooler size was not increased as the secondary compressor would be bypassed during rated power operation. While an intercooler could have helped reduce the secondary compressor power consumption for same amount of air flow, no intercooler was applied in this assessment to keep the system cost/complexity low. For higher efficiency, it would have been beneficial to introduce EGR upstream of the secondary compressor to take advantage of engine delta pressure. However, the EGR mixing point was kept the same as baseline engine (just before intake manifold) to maintain the durability of the secondary compressor and charge air cooler. At lower temperatures, EGR can condense into droplets and damage the secondary compressor wheel as well as cause soot/condensate build up in the charge air cooler.
- **Exhaust Side:** Exhaust restriction orifice diameter was maintained to represent the same aftertreatment system as the baseline engine. The turbocompound turbine was added between the main engine turbine and the aftertreatment system. The main engine turbine was replaced with a high efficiency fixed geometry turbine without wastegate to maximize combined turbocharger efficiency. Section 3.3 describes how the turbocompound turbine and main engine turbine were sized for the downsized engine. The exhaust manifold volume was reduced corresponding to the cylinder reduction and no changes were made to the EGR route.
- **ITES System**: The planetary gear set internals, secondary compressor gear reducer and engine gear reducer were all modeled as inertia components with a specified ratio and efficiency. As shown in **Figure 14**, the efficiency (including

bearing losses) and inertia numbers for each component was obtained through a geartrain analysis, conducted using KiSSsoft software by the design engineers at FEV North America, Inc. During the optimization process, the analysis was conducted multiple times to close the loop between 1D GT-SUITE simulations and geartrain analysis.

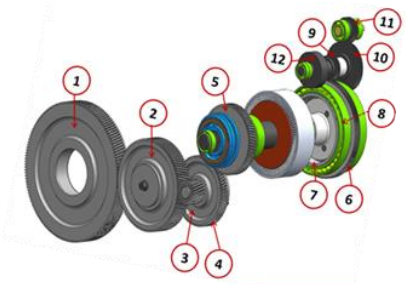

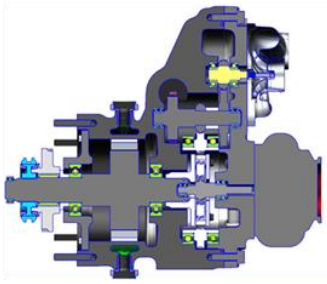

Gear #	Description	Quantity	Mass [kg]	Inertia [kg.mm2]
1	Crank Gear	1	6.30	45971
2	First Idler	1	2.40	7966
3	Compound Idler - Small	1	0.08	21.8
4	Compound Idler - Big	1	0.80	1288
5	eMotor Gear	1	1.30	2034
6	Ring Gear	1	1.75	7171
7	Planet Gear	3	0.10	18.8
8	Sun Gear	1	0.15	6.9
9	Compressor Idler - Small	1	0.09	20.8
10	Compressor Idler - Big	1	0.40	315
11	Compressor Gear	1	0.07	18.2
12	Band Brake Shaft	1	0.60	1618

FEV Limits	1.4	1.2
Component	Safety Root [-]	Safety Flank [-]
CS gear	3.5437	3.4356
Idler1	2.5853	2.1452
Idler2.1	4.4005	2.1452
Idler2.2	3.5608	2.3566
eMotor gear	3.7121	2.3579
Sun/Turbine	4.085	1.7124
Planets	3.9823	1.7199
Ring inside	4.7646	3.3993
Ring outside	3.1431	2.1661
Idler3.1	3.3483	2.1661
Idler3.2	5.0463	2.2745
Comp gear	5.1056	2.2745

Figure 14 ITES geartrain analysis conducted by design team at FEV North America, Inc. (taken with permission)

The key equations from the static analysis of the ITES planetary gear set are shown below:

$$\omega_{em} = \omega_{turb}\frac{S}{R+S} + \frac{\omega_{comp}}{G_{comp}}\frac{R}{R+S}$$

$$\omega_{eng} = \frac{\omega_{em}}{G_{eng}}$$

$$T_{em} + \frac{T_{eng}\eta_{eng}}{G_{eng}} = -\frac{R+S}{S}T_{turb}\eta_{sc} = -\frac{R+S}{R} * \frac{T_{comp}G_{comp}}{\eta_{cr}\eta_{comp}}$$

Where:

ω_{em}/T_{em} is the electric motor-generator angular velocity/torque
ω_{turb}/T_{turb} is the turbocompound turbine angular velocity/torque
ω_{comp}/T_{comp} is the secondary compressor angular velocity/torque
ω_{eng}/T_{eng} is the engine angular velocity/torque

S is number of sun gear teeth
R is number of ring gear teeth
G_{comp} is the secondary compressor gear reduction
η_{comp} is the efficiency of compressor gear reduction
G_{eng} is the engine gear reduction
η_{eng} is the efficiency of engine gear reduction
η_{sc} is the efficiency of power transfer from sun gear to carrier gear
η_{cr} is the efficiency of power transfer from carrier gear to ring gear

Other ITES components such as the dog clutch and band brake were modeled as simple on/off angular velocity constraints with a specified engagement/disengagement time. As described in section 3.1, the secondary compressor and turbocompound turbine were modeled using performance maps from suppliers. Similarly, the 48V electric motor-generator unit was also modeled as map-based object with specified efficiency and lumped inertia from supplier data. Lastly, a 2RC equivalent circuit model for the 48V A123 Li-Ion LFP battery was taken from Lee et al. [38] and implemented in the GT-SUITE model. An empirical battery aging model was also implemented in the GT-SUITE model for battery life predictions. The aging model has been discussed in more detail in chapter 6 wherein the battery size was further optimized on vehicle drive cycle [39]. For initial investigations, a rule-based ITES mode control strategy was implemented based on expected optimum ITES mode for a given engine operating region (**Figure 9**). The sizing and optimization of all the ITES components including gear ratios, secondary compressor size, turbocompound turbine size, electric motor-generator were conducted using this simple rule-based control strategy, as discussed in section 3.3.

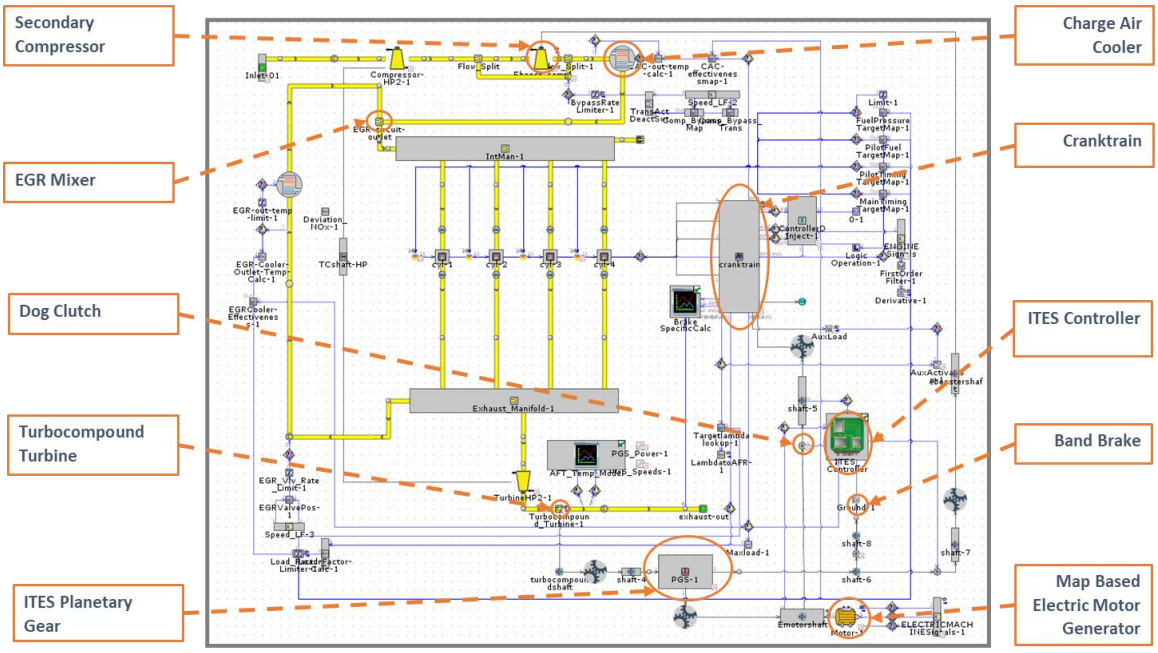

Figure 15 GT-SUITE model for the downsized engine with the ITES unit.

In the first step, proper functioning of the standalone ITES system model was verified by imposing speed and torque boundary conditions to different components. This process also helped in determining the preliminary gear ratios for the planetary gear set, engine gear reduction and compressor gear reduction. Once the standalone ITES model verification was completed, the standalone model was integrated with the modified version of the baseline engine model as shown in **Figure 15**. With the completion of all the modifications in the baseline model and the addition of the ITES system component models, the downsized engine with ITES system model was developed**.** The model was verified for flow and ODE convergence in steady state operation before moving on to the sizing and optimization of ITES components and engine turbomachinery.

3.3 Sizing and Optimization

The key components that needed to be optimally sized on the downsized engine with ITES system were the main engine turbine, main engine compressor, turbocompound turbine, secondary compressor, engine gear reduction, compressor gear reduction, planetary gear ratio, electric motor-generator and 48V battery pack. The objective of component sizing methodology was to maximize system efficiency, maintain system durability, minimize package size and minimize cost. First the turbomachinery components were sized assuming independent integration of secondary compressor and turbocompound turbine. Once the turbomachinery components and their optimum operating speeds were determined, the planetary gear ratio, compressor gear reduction and engine gear reduction were selected to maximize the efficiency of the turbomachinery at selected key engine operating points. Thereafter, the electric motor-generator was sized to provide/absorb the power from the turbomachinery components as well as provide the mild hybrid capability. Lastly, the 48V battery pack was sized to match the power demand of the electric motor-generator. Further optimization of the battery pack, based on battery life and energy management on drive cycles, was done through vehicle simulation in Chapter 6.

3.3.1 Turbomachinery Sizing

In the first step, the size of main engine compressor, main engine turbine and the turbocompound turbine was optimized at peak power and peak torque operating points, where the secondary compressor is typically bypassed. The main engine compressor was sized such that the peak power operating point aligned with the maximum efficiency line of the compressor map. This approach was adopted to maximize compressor efficiency at rated engine speed operating points, where the HDFTP cycle runs. Regarding the main engine turbine and turbocompound turbine, a preliminary assumption was made on the size based on expected pressure ratio and flowrate). The turbocompound turbine was connected to the engine crankshaft with a specified gear reduction to ensure that turbocompound turbine operated along best efficiency line. Steady-state engine simulations were run at peak power and peak torque operating points to evaluate the different turbocharger sizes against airflow target, EGR target, efficiency and altitude margin.

Figure 16 compares the location of operating points on the baseline engine versus the downsized engine. Since the downsized engine needed high pressure ratio to meet airflow

requirements, a new compressor type was selected with more pressure ratio capability at the expense of slightly lower efficiency. The efficiency loss on the compressor side was balanced by a higher efficiency main turbine that was implemented alongside the turbocompound turbine. Typically, the efficiency of main engine turbine is limited to maintain higher exhaust manifold pressure than intake manifold pressure to achieve EGR drivability. However, when a turbocompound turbine is implemented, it automatically creates the necessary back pressure on the exhaust manifold to drive high pressure EGR. Therefore, the main engine turbine efficiency can be maximized to the component design limitations. The main engine turbine on the downsized engine with the ITES system was up to 7% more efficient than the baseline engine turbine.

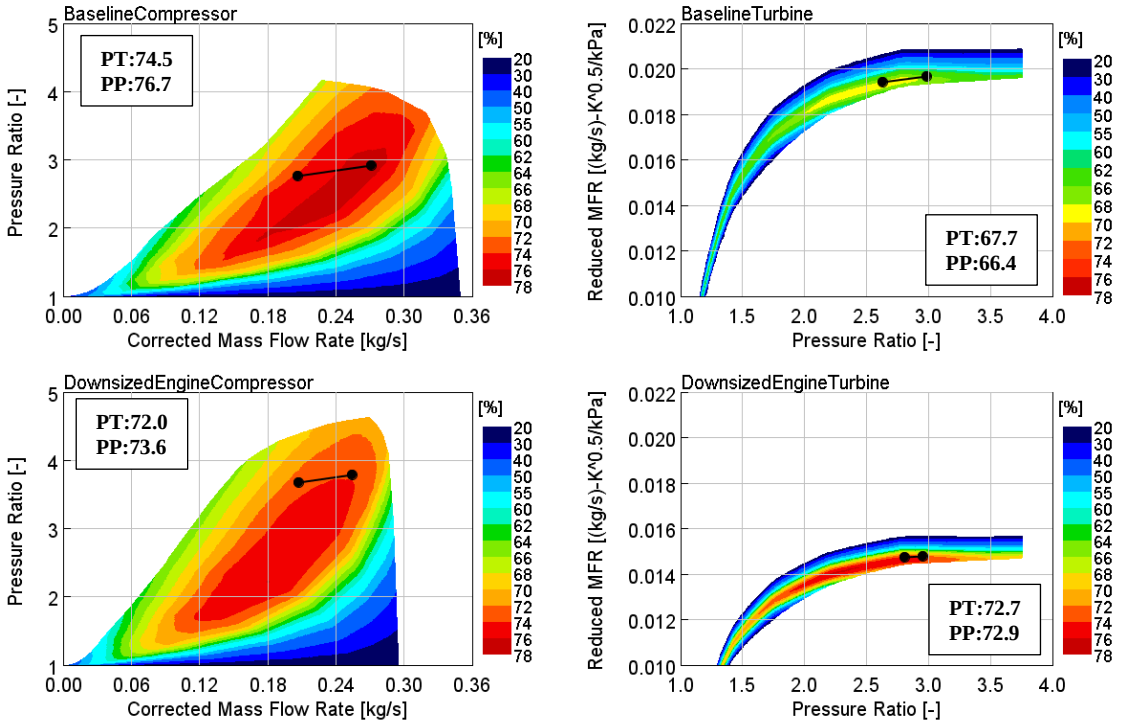

Figure 16 Main engine turbocharger sizing for the downsized engine with ITES system. The two operating points are the peak power on right (2200rpm 228kW) and peak torque on left (1600rpm 1200Nm) on the line plot.

To optimize the turbocompound turbine and main turbine size, a sweep on turbocompound turbine size was run while modulating the main engine turbine size to maintain air fuel ratio at peak power and peak torque operating points on the downsized engine. Since the turbocompound turbine eliminates the need of wastegate, it was necessary to ensure that air fuel ratio targets from the baseline engine can be met at peak power and peak torque operating points of the downsized engine. The objective of the sweep was to identify the optimum turbocompound turbine size that would maximize the extraction of energy from the exhaust gas while minimizing the added back pressure on the engine and the resulting increase in pumping work.

Figure 17 shows the impact of turbocompound turbine size on engine fuel consumption for a constant air fuel ratio target. As the turbocompound turbine nozzle size was reduced to increase the pressure ratio (lower turbine massflow multiplier), the turbocompound turbine was able to extract more work from the exhaust gas which led to higher power output. However, with the increase in pressure ratio, the turbine efficiency reduced due to higher flow losses within the turbine. Furthermore, the back pressure on the engine and the pumping work also increased, leading to a higher BSFC. On the other hand, at very low pressure ratios (higher turbine massflow multiplier), the turbocompound turbine work extraction reduces significantly, leading to slight increase in BSFC. Therefore, it was concluded that an optimal pressure ratio/turbocompound turbine power range exists that can achieve low fuel consumption at full load operating points. Based on the results, a turbocompound turbine mass multiplier of 0.96 was selected to minimize BSFC at full load operating points and maximize turbocompound turbine power at lower engine speed and loads.

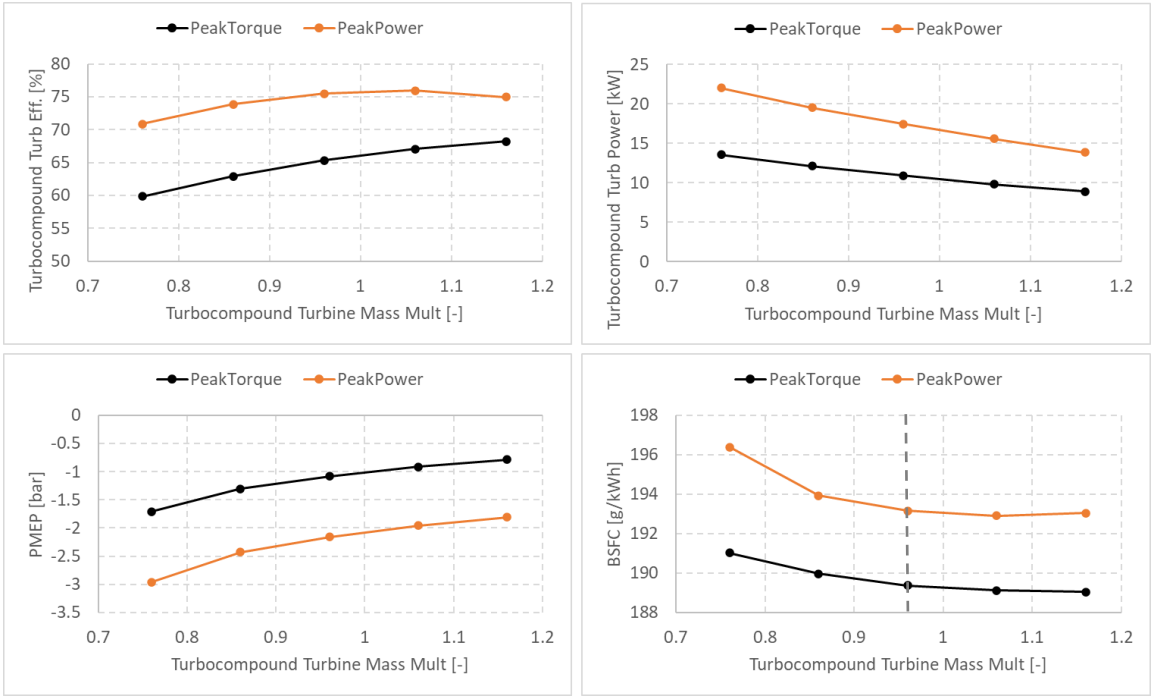

Figure 17 Turbocompound turbine sizing analysis for peak power (2200rpm 228kW 20.4AFR) and peak torque (1600rpm 1200Nm 19.4AFR) operating points at constant AFR (maintained by varying main engine turbine size)

The next step was to determine the size of the secondary compressor to achieve the low end torque targets on the downsized engine. An initial selection was made based on the required airflow, pressure ratio and package size, which was then simulated in GT-SUITE. The secondary compressor speed was directly controlled using a simple PID controller to achieve the air fuel ratio target. Thereafter, the secondary compressor size was varied in simulation to ensure that the operating points lie in high efficiency region of the secondary compressor map while maintaining greater than 10% surge margin on the main engine compressor. **Figure 18** shows the final match that was achieved on the downsized engine

in comparison to the baseline engine. Apart from 600rpm full load operating point, all other operating points lie in high efficiency island of the secondary compressor map. While the secondary compressor size could have been reduced further to tradeoff efficiency between 600rpm full load and rest of the low-end torque points, the efficiency of 800-1200rpm full load points was prioritized. This was because the 600rpm full load point is typically only visited during engine ramp up and is more of a transition point in engine test cycles. The region from 800-1200rpm full load is a more critical region for achieving high cycle-averaged engine efficiency.

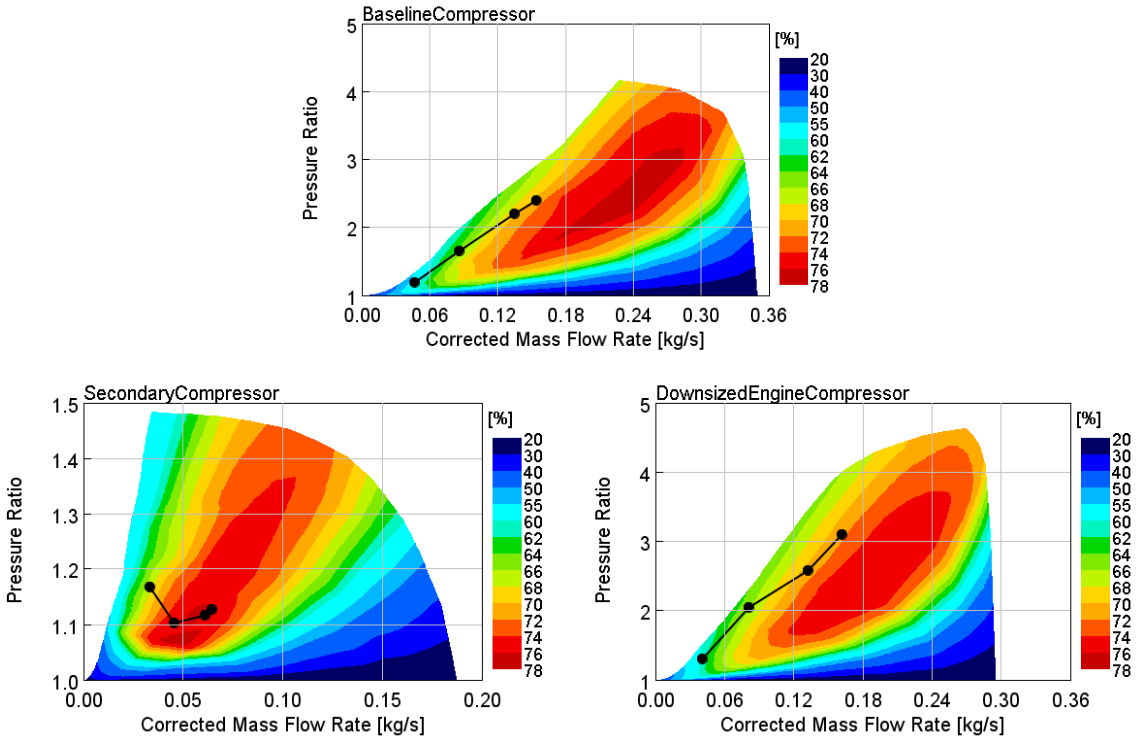

Figure 18 Low end torque operating points (600-1200rpm full load) match for the baseline and the downsized engine.

Now that all the turbomachinery components were selected and optimum operating speeds determined, the next step was to determine the planetary gear ratio, compressor gear reduction and engine gear reduction that could achieve the optimum speed targets on each of the turbomachinery components. Finally, a verification of the selected turbomachinery size was done through steady state engine mapping simulation with the selected ITES geartrain ratios.

3.3.2 ITES Geartrain Sizing

Based on the turbocompound turbine size and optimum operating speed an overall ratio of 25:1 was identified between the turbcompound turbine and engine crankshaft at peak power operating point. Therefore, the product of planetary gear ratio ((R+S)/S) and engine gear reduction was determined to be 25:1. While a single planetary gear ratio can vary from 3:1 to 10:1, a planetary gear ratio of 4:1 to 6:1 was recommended from the greatrain

analysis (discussed in section 3.2) to achieve high durability and efficiency. Based on this recommended range and an estimated range for compressor gear reduction, a DoE was conducted in mode C (band brake open/dog clutch open) at 1200rpm full load operating point. The specific operating point was selected as it was the highest engine speed and load at which the secondary compressor was active. **Figure 19** shows the key results from the DoE wherein the planetary gear ratio and secondary compressor gear reduction parameters were swept. The carrier gear speed was controlled using a PID controller to target the desired air fuel ratio at the operating point. As shown in the figure, while the AFR could be maintained within the steady state tolerance of the controller for most DoE cases, the AFR target could not be achieved above compressor gear reduction of 10. For the key performance metric BSFC, the secondary compressor gear reduction showed higher sensitivity with optimum in the range of 5:1 to 9:1 ratio, depending on the planetary gear ratio selection. The BSFC contour plot also showed multiple combination of compressor gear reduction and planetary gear ratio that could be applied to minimize fuel consumption. To narrow down the selection, the secondary compressor power consumption plot further showed that the secondary compressor power consumption was minimized at higher compressor gear reduction of 7:1 to 9:1., which was desirable for sizing of motor-generator.

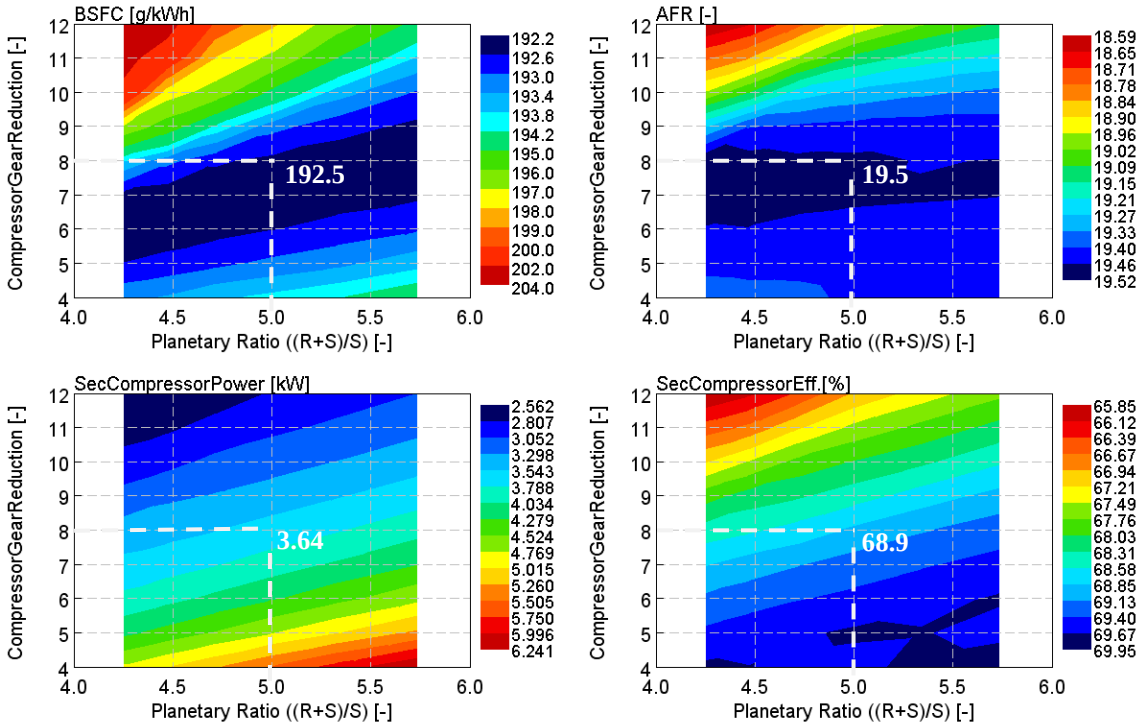

Figure 19 Planetary gear and compressor gear reduction optimization DoE run at 1200rpm full load operating point.

Overall, the analysis showed that a range of 7:1 to 9:1 for secondary gear reduction and a corresponding range of 4.25:1 to 5.73:1 for planetary gear ratio was optimum. Furthermore, since an overall ratio of 25:1 was desired between turbocompound turbine and engine crankshaft, an optimum engine gear reduction range of 5.88:1 to 4.36:1 was determined. The last factor that led to the final decision on the exact gear ratios was the engine starting

torque requirement and maximum engine speed constraint. Based on available benchmark data, a minimum engine starting torque of 300Nm and a maximum engine overspeed constraint of 3000rpm was required for the 5.1L downsized 4-cylinder engine. With the maximum possible motor-generator torque of 60Nm and maximum motor speed of 15000rpm (discussed in section 3.3.3), an engine gear reduction of 5:1 was selected to meet the engine starting torque requirement (60x5=300Nm) as well as prevent motor-generator overspeed at engine red line conditions(3000x5=15000rpm). Correspondingly, a planetary gear ratio of 5:1 and a secondary compressor gear reduction of 8:1 was finally selected.

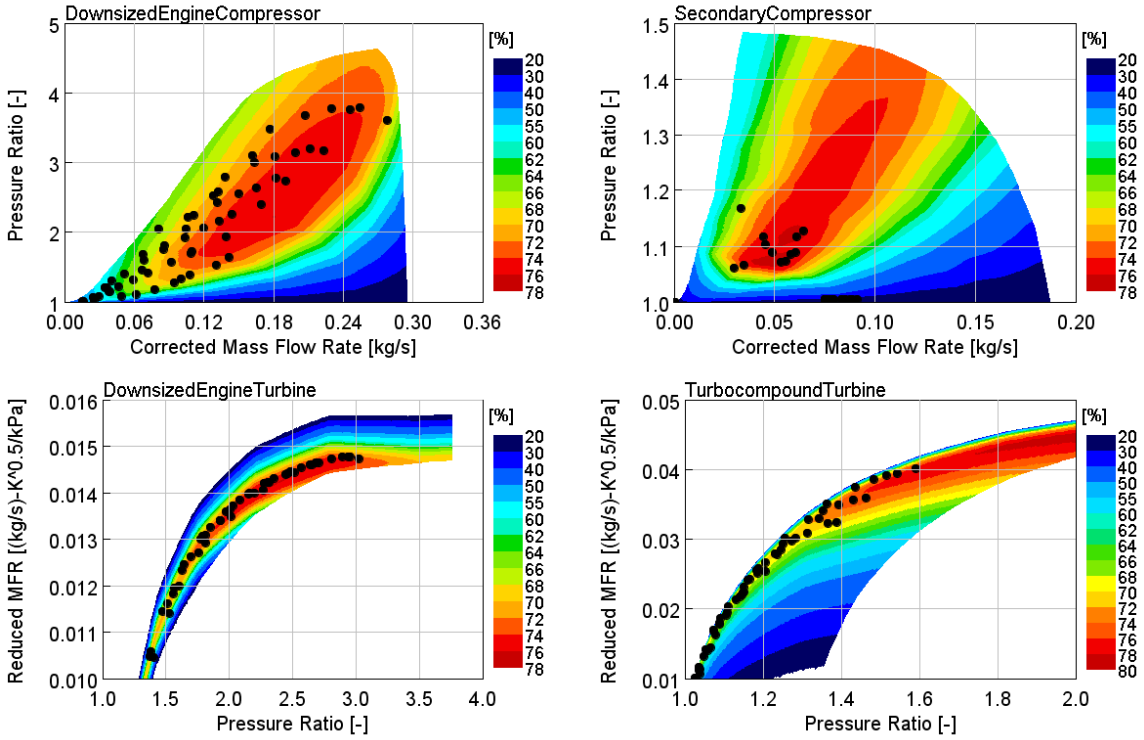

Figure 20 Final turbomachinery match on engine mapping with the selected ITES geartrain ratios.

Once, the ITES geartrain ratios were finalized, an engine mapping simulation was run on the downsized engine model to verify the turbomatch. As shown in **Figure 20**, all the turbomachinery components were well matched to the engine mapping operating points above 20% engine load.

3.3.3 Electric Motor-Generator and Battery Pack Sizing

Since the motor-generator unit was placed between the planetary gear set carrier and engine crankshaft, a higher speed and smaller diameter low voltage electric machine was most desirable. Based on the packaging constraints, cost and 48V system power limitations, a 155mm casing diameter 20kW/12kW peak/continuous rating electric motor-generator was selected. The electric motor-generator was a coolant cooled permanent magnet synchronous machine with a starting torque capability of 60Nm, a maximum speed range

of 15,000 rpm and a maximum motor-inverter combined efficiency of 92%. **Figure 21** shows the continuous torque and power curves for the electric machine measured at a coolant temperature of 85°C.

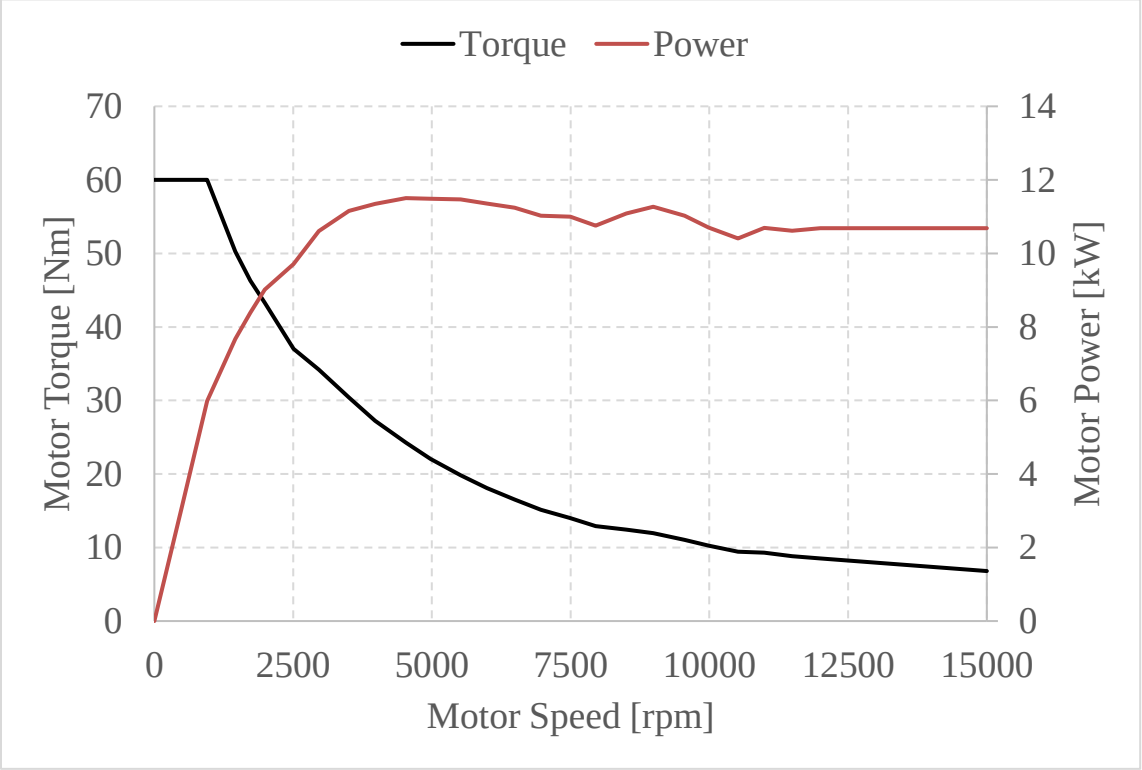

Figure 21 Continuous torque and power characteristics of a 12kW 48V coolant cooled permanent magnet electric motor-generator tested at 85°C coolant temperature.

Lastly, to meet the electrical requirements of the 48V electric motor-generator, a Lithium Iron Phosphate (LFP) chemistry based high power battery module from A123 systems was selected [38]. While LFP Li-Ion cells have less energy/power density in comparison to Nickel Manganese Cobalt (NMC) based Li-Ion cells, the LFP chemistry offers higher durability, lower cost and longer life, which is critical for medium and heavy duty vehicles [40]. As shown in **Table 3**, the module comprises of 14 cells in series and 1 in parallel arrangement to achieve nominal voltage of 48V and nominal capacity of 8Ah. For engine simulation assessment discussed in chapter 5, an initial battery capacity of 32Ah/1.536kWh (four 8Ah modules arranged in parallel) was assumed and modeled to meet the 12kW continuous discharge/charge power requirement of the electric motor-generator. At 48V, 12kW of power output corresponds to 250A of DC current requirement. Hence, with a 10C discharge power capability of the battery cell, a 32Ah pack capacity was needed to achieve maximum power capability of the motor-generator. The battery pack capacity was further optimized in chapter 6, based on vehicle drive cycle simulation wherein the drive cycle energy storage and battery life requirements were also considered.

Table 3 A123 48V battery module specification [38].

Specification	Value
Cell Chemistry	LFP
Cell Arrangement	14S1P
Nominal Voltage	48V
Nominal Capacity	8Ah
Max Power Discharge (60s)	7.5kW
Continuous Charge/Discharge Rate	10 C
Weight	8kg
SOC Range	30-80%

4 Control Strategy Development

As expected for a highly integrated system, a robust control strategy was extremely critical for realization of powertrain performance and emissions benefits. At any given instant during vehicle operation, the ITES mode and corresponding electric motor-generator torque had to be optimized for maximizing system efficiency, while meeting transmission input torque request. For all the preliminary sizing investigations in chapter 3, a simple rule-based ITES mode strategy was applied for steady state engine operation as shown in **Figure 21** (left). The strategy was developed based on expected optimal ITES mode in the different operating regions of the engine map without active use of mild hybridization strategies such as engine load shift and torque assist. The three engine operating regions and the corresponding motor-generator control is summarized as follows:

- At lower engine loads (green region), wherein the turbocompound turbine power was low, mode A was applied, and the motor-generator torque was adjusted to target maximum efficiency on the turbocompound turbine.
- At higher engine speed and high loads (red region), wherein the turbocompound turbine was high, mode B was applied, and the motor-generator torque was set to 0 to allow all the power from the turbocompound turbine to be directly transmitted to the engine crankshaft.
- At lower engine speed and high loads (purple), wherein the secondary compressor is active, mode C was applied, and the motor-generator speed was controlled to target desired air-fuel ratio.

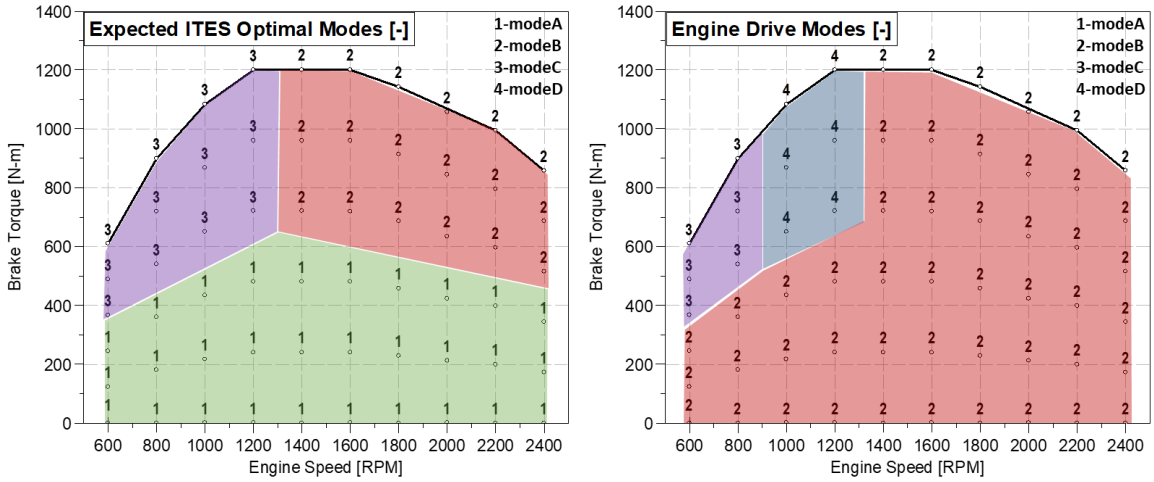

Figure 22 Expected optimum ITES modes for minimizing engine fuel consumption (left) and ITES mode to ensure connection between electric motor-generator and engine crankshaft (right).

While this engine-focused rule-based strategy was expected to be optimal for steady state engine operation, it was sub-optimal when considered with mild hybridization strategies that included SOC dependency. For example, at high SOCs, it would have been more beneficial to run in engine drive modes (**Figure 21** right) and meet the transmission input torque demand with assist from ITES electric motor-generator. On the other hand, at low

SOCs, it would have been more beneficial to run the ITES electric motor-generator in generation mode and increase load on the engine to reduce cycle-averaged BSFC. Similarly, at low SOCs, it would have been more beneficial to run in mode D at low engine speed and high loads to charge the battery with power from engine crankshaft. As shown in **Figure 21** (right), mode D could not be applied to engine speeds of 600-800rpm. This was due to the high compressor pressure ratio requirements at such low engine speeds, which required independent control of ITES electric motor-generator to spool up the secondary compressor.

Furthermore, for transient operation with high acceleration demand, it would be necessary to switch to mode C at low engine speed and loads to help spool up the secondary compressor. Similarly, at higher engine speed and low loads, mode B would need to be always applied with maximum assist from motor-generator torque to achieve a fast load response. Lastly, a robust control strategy for mode switching would be necessary to ensure speed match between the carrier gear and the engine crankshaft before engagement of the dog clutch. Based on these assessments a three-layer control strategy has been proposed for the ITES system as described below:

- **Steady State Control:** Run an offline optimization using equivalent consumption minimization strategy (ECMS) to determine optimal ITES mode and ITES motor-generator torque command for a given SOC, engine torque demand and engine speed in steady state operation. Apply this strategy until a transient event is detected or a mode change request is detected that requires engagement of dog clutch.
- **Transient Control:** Detect transient event based on rate of change of accelerator pedal and activate transient maps for ITES mode and motor-generator torque control. Apply until a mode change request is detected that requires engagement of dog clutch.
- **Mode Switch Control:** Detect mode change request that requires engagement of dog clutch. Actively control motor-generator torque to achieve speed match and engage dog clutch to complete mode transition.

The next sections describe these three control strategy layers in more detail. Thereafter, a complete schematic of ITES system control strategy and its integration with vehicle ECU has been presented.

4.1 Steady State Control

The steady state control for ITES system was developed on the basis of equivalent consumption minimization strategy (ECMS). The strategy has been shown to be derived from optimal control theory concept of Pontryagin's Minimum Principle (PMP) and has been widely used for real-time supervisory control of hybrid vehicles [41]. As the name suggests, ECMS strategy is based on conversion of battery power consumption to equivalent fuel, which is then added to engine fuel consumption to create an equivalent fuel consumption variable. The minimization of this equivalent fuel consumption variable then results in the determination of the control variables that are close to optimal. The strategy can be applied through an offline optimization process, wherein optimal multi-

dimensional maps of control variables can be developed as a function of state variables. **Figure 23** shows an overview of this offline optimization process that was applied to develop these optimal multi-dimensional maps for steady-state control of the ITES system.

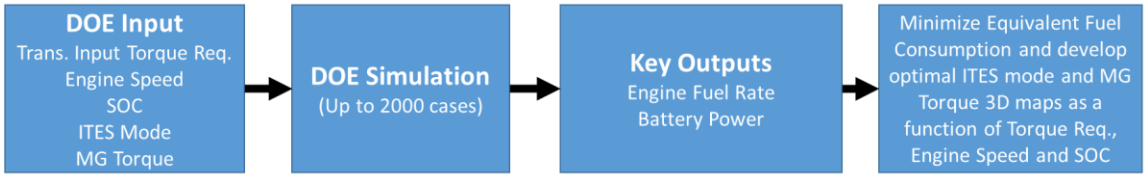

Figure 23 Steady state optimal ITES mode and motor-generator torque map development process.

Using the high-fidelity GT-SUITE model of the downsized engine with the ITES system, a large-scale design of experiments was run with state variables of engine speed, transmission input torque request and SOC, as well as control variables of ITES mode, motor-generator torque command and engine torque. Based on the results for a given SOC, engine speed and transmission input torque request, equivalent fuel consumption was calculated for every combination of ITES mode, ITES motor torque and engine torque that met the transmission input torque request. Thereafter, the ITES mode, ITES torque and engine torque that corresponded to minimum equivalent fuel consumption were selected as optimum. The process was repeated for the complete possible range of transmission input torque request, SOC and engine speed. As a final result of the offline optimization, 3D maps for ITES mode and corresponding ITES motor-generator torque were defined as a function of transmission input torque request, engine speed and SOC.

$$J(TorqReq,\ SOC,\ EngSpd,\ Mode,\ MG\_Torq) = m_f + f(SOC)\frac{BSFC}{n_{elec}}P_{batt}$$

Where:

m_f = *engine fuel flow rate in (g/hr)*

$f(SOC) = 1 - (2 * \frac{SOC - SOC_{target}}{SOC_{max} - SOC_{min}})^{\alpha}$

$BSFC$ = *engine brake specific fuel consumption (g/kWhr); Assumed 231g/kWh*

$n_{elec} = n_{elecd}$ *, combined electrical system efficiency in discharge, Assumed 0.9*

$n_{elec} = 1/n_{elecc}$ *, combined electrical system efficiency in charge, Assumed 0.9*

P_{batt} = *Battery power consumption/generation*

The equation above shows the equivalent fuel cost function that was minimized to determine the optimal values of control variables. The battery power was converted into net electrical system power by dividing/multiplying the electrical system efficiency, based on the sign of battery power. Thereafter, the electrical system power was converted into equivalent fuel by multiplying it with cycle averaged brake specific fuel consumption of the engine. To consider the impact of SOC on battery power and achieve charge sustain, a penalty factor term was added to battery equivalent fuel term. As shown in **Figure 24**, the function is designed to increase weightage on battery equivalent fuel term at lower SOCs

in order to reduce battery power consumption. On the other hand, at high SOCs, the penalty factor becomes large negative which promotes higher battery power consumption to minimize the equivalent fuel consumption.

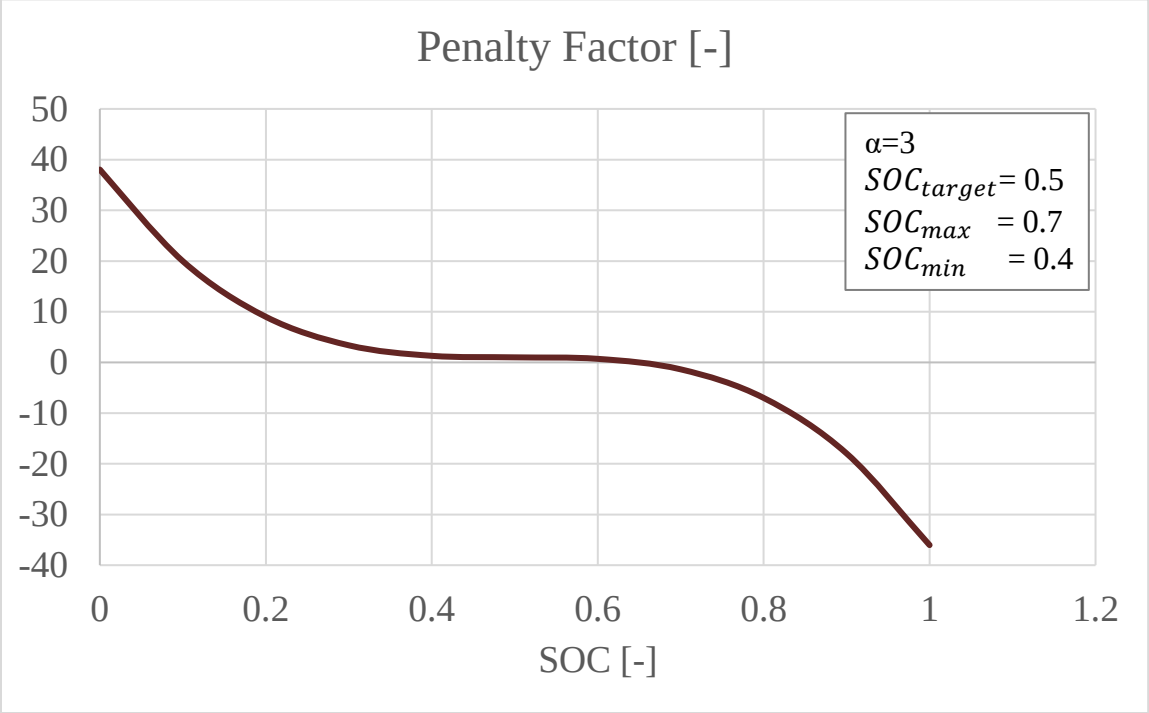

Figure 24 Penalty factor function used in the ECMS strategy equivalent fuel consumption calculations.

An example of the equivalent fuel consumption minimization process has been shown in **Figure 25**. For a given engine speed of 800rpm, load request of 20% and fixed ITES mode B, motor torque was swept from minimum to maximum while adjusting engine fueling to meet transmission input torque request. As the motor torque was increased, engine fuel consumption reduced while battery power consumption increased. While engine fuel consumption was similar for the three shown SOC cases, battery equivalent fuel showed a strong dependence on the SOC due to penalty factor term. At low SOCs and high penalty factor, battery equivalent fuel curve had a higher slope in comparison to engine fuel curve, which led to the selection of minimum possible motor torque to minimize total equivalent fuel consumption. Alternatively, at high SOCs and low penalty factor, the battery equivalent fuel curve had much lower slope in comparison to engine fuel curve, which led to the selection of high motor torque to minimize total equivalent fuel consumption. For mid SOC range, the battery equivalent and engine fuel consumption curves had similar slopes, which led to an optimal motor torque of -11Nm that minimized the equivalent fuel consumption. The solution also showed that for operation around target SOC and low engine loads, it was most beneficial to increase engine load and reduce engine BSFC while storing the excess engine power into the battery for future use.

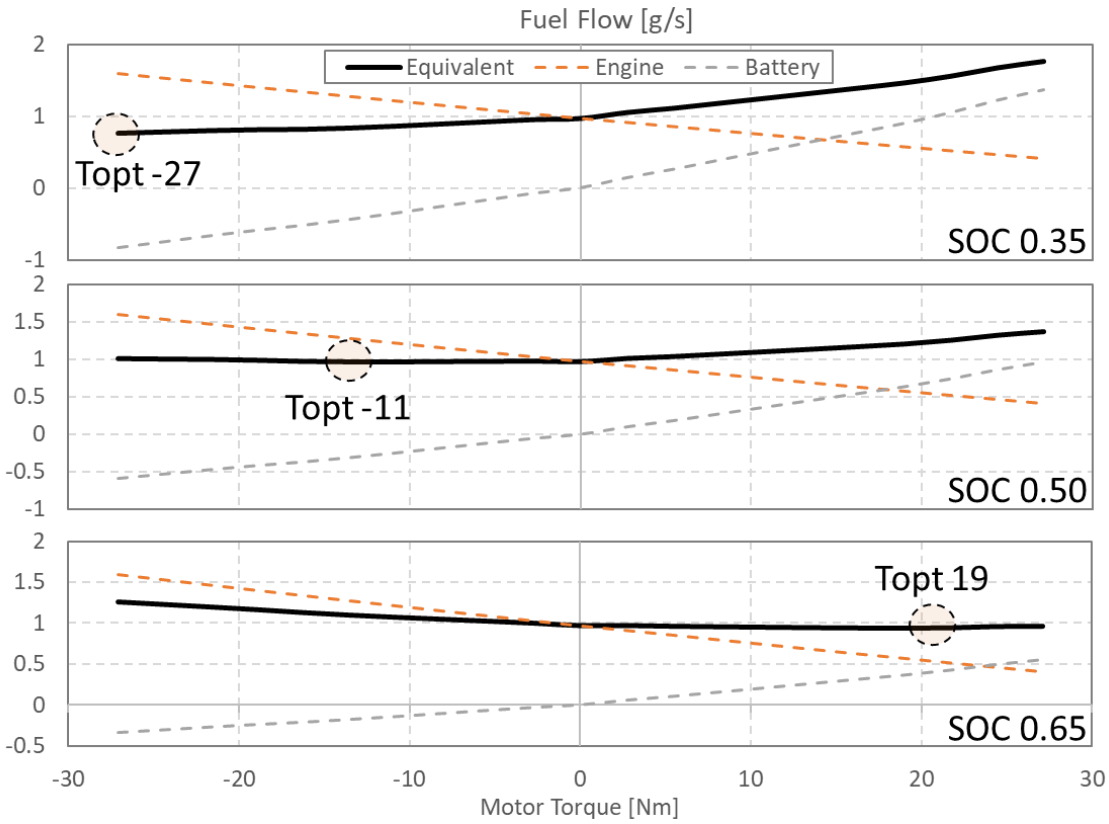

Figure 25 ECMS based minimization of equivalent fuel at 800rpm and 20% load request with three different SOC levels in mode B.

While only mode B calculations are shown in **Figure 25**, equivalent fuel consumption was also calculated with other possible ITES mode and motor torque combinations, that met the load torque request and engine AFR target. Thereafter, the ITES mode and the motor torque combination that corresponded to minimum equivalent fuel consumption was selected as optimal. The final optimal ITES mode and motor-torque combinations that were selected for the specific operating point of 800 rpm and 20% load request are shown in **Figure 26** as a function of SOC. As expected at low battery SOC, ITES mode B (mode 2) with a negative motor torque is most optimal as it helps charge the battery as well as increase the engine load to regions with lower brake specific fuel consumption. In the mid SOC range, it was more optimal to run in ITES mode A (mode 1), wherein the motor-generator was disengaged from the engine crankshaft and was used to control the speed of turbocompound turbine to maximize efficiency. Lastly, at high SOCs, it was again more optimal to run in mode B (mode 2) with a positive motor torque to discharge battery and assist the engine in meeting load request.

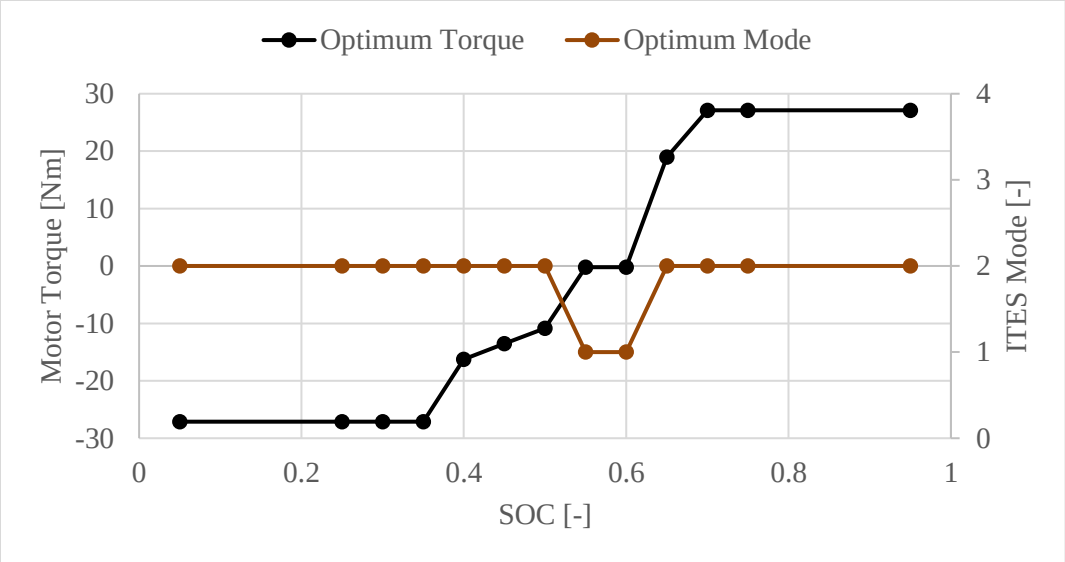

Figure 26 Optimal ITES mode and ITES motor-generator torque command as a function of SOC at 800rpm 20% load request. Motor torque amplified by a factor of 5 at crankshaft due to gear ratio.

After the optimization process was completed, the final steady-state 3D optimal control maps were implemented in the GT-SUITE model of the downsized engine with ITES system. As shown in **Figure 27**, the optimal control tables of ITES mode and corresponding motor torque were defined as a function of load request and engine speed for multiple SOCs, ranging from 0.1 to 0.9 in steps of 0.05.

ITES Steady State Map Modes (SOC=0.3)										
Load/RPM->	600	800	1000	1300	1400	1600	1800	2000	2200	2400
0	2.0	2.0	2.0	2.0	2.0	2.0	2.0	2.0	2.0	2.0
0.2	2.0	2.0	2.0	2.0	2.0	2.0	2.0	2.0	2.0	2.0
0.4	2.0	2.0	2.0	2.0	2.0	2.0	2.0	2.0	2.0	2.0
0.6	3.0	3.0	3.0	3.0	2.0	2.0	2.0	2.0	2.0	2.0
0.8	3.0	3.0	3.0	3.0	2.0	2.0	2.0	2.0	2.0	2.0
1	3.0	3.0	3.0	3.0	2.0	2.0	2.0	2.0	2.0	2.0

ITES Steady State Map MG Torque (SOC=0.3)										
Load/RPM->	600	800	1000	1300	1400	1600	1800	2000	2200	2400
0	-33.9	-27.1	-22.0	-18.1	-15.0	-12.9	-11.9	-10.2	-9.3	-8.5
0.2	-33.9	-27.1	-22.0	-18.1	-15.0	-12.9	-11.9	-10.2	-9.3	-8.5
0.4	-30.5	-27.1	-22.0	-18.1	-15.0	-12.9	-11.9	-10.2	-9.3	-8.5
0.6	-0.3	-3.6	-2.1	-3.2	-15.0	-12.9	-11.9	-10.2	-9.3	-8.5
0.8	-0.7	-6.2	-3.0	-4.4	-15.0	-12.9	-11.9	-10.2	-9.3	-8.5
1	-3.6	-2.3	-5.1	-6.9	-15.0	-12.9	-11.9	-10.2	-9.3	-8.5

ITES Steady State Map Modes (SOC=0.6)										
Load/RPM->	600	800	1000	1300	1400	1600	1800	2000	2200	2400
0	1.0	1.0	1.0	1.0	1.0	1.0	1.0	1.0	1.0	1.0
0.2	1.0	1.0	1.0	1.0	1.0	1.0	1.0	1.0	1.0	1.0
0.4	2.0	2.0	2.0	1.0	1.0	1.0	1.0	1.0	1.0	1.0
0.6	3.0	3.0	3.0	3.0	2.0	2.0	2.0	2.0	1.0	2.0
0.8	3.0	3.0	3.0	3.0	2.0	2.0	2.0	2.0	2.0	2.0
1	3.0	3.0	3.0	3.0	2.0	2.0	2.0	2.0	2.0	2.0

ITES Steady State Map MG Torque (SOC=0.6)										
Load/RPM->	600	800	1000	1300	1400	1600	1800	2000	2200	2400
0	0.0	-0.1	-0.4	-0.6	-0.9	-1.4	-1.5	-1.6	-2.2	-3.1
0.2	-0.1	-0.2	-0.4	-0.6	-0.8	-1.1	-1.7	-2.2	-2.2	-3.7
0.4	0.0	0.0	0.0	-1.5	-2.1	-2.7	-3.1	-3.8	-4.0	-5.1
0.6	-0.3	-3.6	-2.1	-3.2	0.0	0.0	0.0	0.0	-6.6	0.0
0.8	-0.7	-6.2	-3.0	-4.4	0.0	0.0	0.0	0.0	0.0	0.0
1	-3.6	-2.3	-5.1	-6.9	0.0	0.0	0.0	0.0	0.0	0.0

ITES Steady State Map Modes (SOC=0.9)										
Load/RPM->	600	800	1000	1300	1400	1600	1800	2000	2200	2400
0	2.0	2.0	2.0	2.0	2.0	2.0	2.0	2.0	2.0	2.0
0.2	2.0	2.0	2.0	2.0	2.0	2.0	2.0	2.0	2.0	2.0
0.4	2.0	2.0	2.0	2.0	2.0	2.0	2.0	2.0	2.0	2.0
0.6	3.0	3.0	3.0	3.0	2.0	2.0	2.0	2.0	2.0	2.0
0.8	3.0	3.0	3.0	3.0	2.0	2.0	2.0	2.0	2.0	2.0
1	3.0	3.0	3.0	3.0	2.0	2.0	2.0	2.0	2.0	2.0

ITES Steady State Map MG Torque (SOC=0.9)										
Load/RPM->	600	800	1000	1300	1400	1600	1800	2000	2200	2400
0	33.9	27.1	22.0	18.1	15.0	12.9	11.9	10.2	9.3	8.5
0.2	33.9	27.1	22.0	18.1	15.0	12.9	11.9	10.2	9.3	8.5
0.4	33.9	27.1	22.0	18.1	15.0	12.9	11.9	10.2	9.3	8.5
0.6	-0.3	-3.6	-2.1	-3.2	15.0	12.9	11.9	10.2	9.3	8.5
0.8	-0.7	-6.2	-3.0	-4.4	15.0	12.9	11.9	10.2	9.3	8.5
1	-3.6	-2.3	-5.1	-6.9	15.0	12.9	11.9	10.2	9.3	8.5

Figure 27 ECMS strategy based steady state optimal maps for ITES mode and corresponding ITES motor-generator torque in Nm defined as a function of requested normalized load and engine speed in RPM.

4.2 Transient Control

Once the steady state control algorithm was developed, the strategy was evaluated on HDFTP transient cycle through engine simulation. The evaluation was done to understand the key shortcomings of the steady state control strategy and how a transient control strategy could be developed to mitigate them. As shown in **Figure 28**, the challenge with steady state control (NoCtrl) was observed during torque response at low engine speeds. The highlighted circle shows the slow torque response of the downsized engine with ITES system in comparison to the baseline engine. In general, it is expected that a downsized will have a slower torque response in comparison to a larger displacement engine due to higher air-fuel ratio at low loads, which allows for faster increase in fueling. However, the objective of the ITES system was to mitigate such limitations on the downsized engine with the help of secondary compressor. The secondary compressor does ramp up eventually as the pedal request increases above the threshold for inducing an ITES mode switch. However, the delay caused by ITES mode switch event and secondary compressor ramp up leads to an overall slower torque response in comparison to the baseline engine.

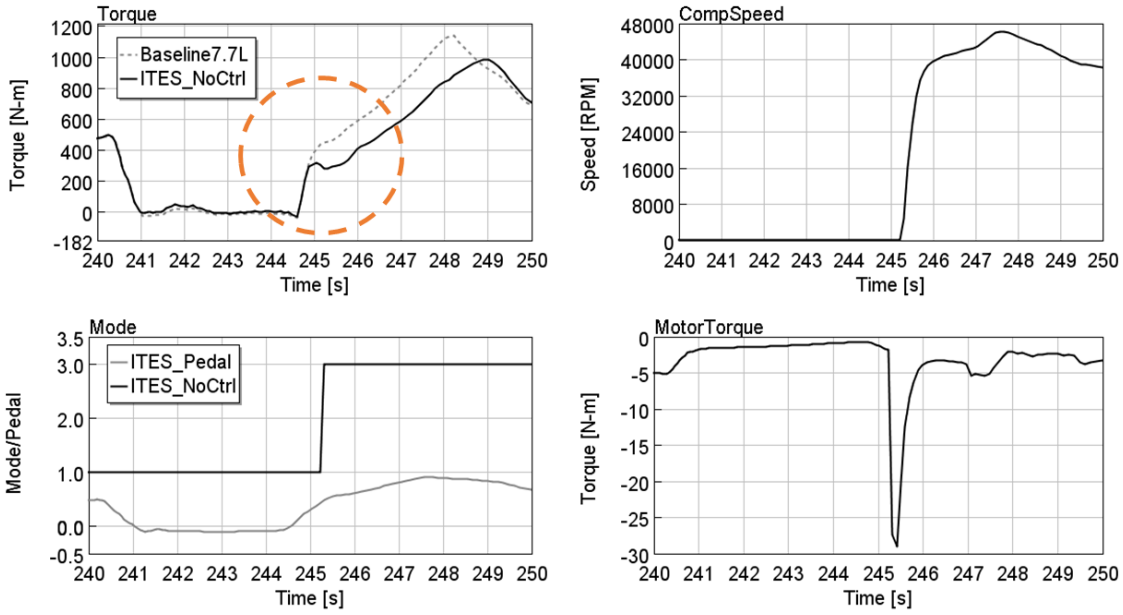

Figure 28 Comparison of torque response for the baseline and downsized engine with ITES system, during a portion of HDFTP engine certification cycle.

Based on the engine simulation results with the steady state control strategy, it was concluded that a transient control strategy would be needed to maximize engine torque response. The strategy would detect a rapid increase in pedal request and switch to a transient ITES mode/torque map to maximize engine performance. A schematic of the override of the steady state control strategy with the proposed transient strategy has been shown in **Figure 29**.

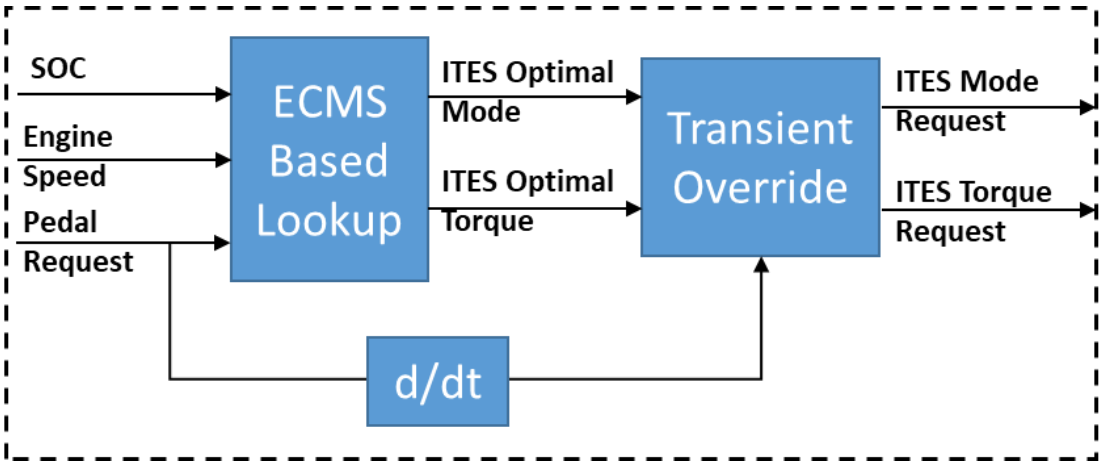

Figure 29 Transient control override method for the ITES supervisory controller

At engine speeds below 1400rpm, secondary compressor was enabled by implementing mode C at all requested loads in the transient ITES mode map. Consequently, the initial output of the air-fuel ratio based PID controller for motor torque was minimized (generation) to enable a fast ramp up of secondary compressor. At higher engine speeds, mode B was enabled at all requested loads to ensure that ITES motor can provide maximum torque assist to the engine crankshaft during transient override. **Figure 30** compares the ITES operating modes and corresponding motor-generator torque between the steady state operation and transient override.

ITES Steady State Map Modes (SOC=0.6)

Load/RPM->	600	800	1000	1300	1400	1600	1800	2000	2200	2400
0	1.0	1.0	1.0	1.0	1.0	1.0	1.0	1.0	1.0	1.0
0.2	1.0	1.0	1.0	1.0	1.0	1.0	1.0	1.0	1.0	1.0
0.4	2.0	2.0	2.0	1.0	1.0	1.0	1.0	1.0	1.0	1.0
0.6	3.0	3.0	3.0	3.0	2.0	2.0	2.0	2.0	1.0	2.0
0.8	3.0	3.0	3.0	3.0	2.0	2.0	2.0	2.0	2.0	2.0
1	3.0	3.0	3.0	3.0	2.0	2.0	2.0	2.0	2.0	2.0

ITES Steady State Map MG Torque (SOC=0.6)

Load/RPM->	600	800	1000	1300	1400	1600	1800	2000	2200	2400
0	0.0	-0.1	-0.4	-0.6	-0.9	-1.4	-1.5	-1.6	-2.2	-3.1
0.2	-0.1	-0.2	-0.4	-0.6	-0.8	-1.1	-1.7	-2.2	-2.2	-3.7
0.4	0.0	0.0	0.0	-1.5	-2.1	-2.7	-3.1	-3.8	-4.0	-5.1
0.6	-0.3	-3.6	-2.1	-3.2	0.0	0.0	0.0	0.0	-6.6	0.0
0.8	-0.7	-6.2	-3.0	-4.4	0.0	0.0	0.0	0.0	0.0	0.0
1	-3.6	-2.3	-5.1	-6.9	0.0	0.0	0.0	0.0	0.0	0.0

ITES Transient Map Modes

Load/RPM->	600	800	1000	1300	1400	1600	1800	2000	2200	2400
0	3.0	3.0	3.0	3.0	3.0	2.0	2.0	2.0	2.0	2.0
0.2	3.0	3.0	3.0	3.0	3.0	2.0	2.0	2.0	2.0	2.0
0.4	3.0	3.0	3.0	3.0	3.0	2.0	2.0	2.0	2.0	2.0
0.6	3.0	3.0	3.0	3.0	3.0	2.0	2.0	2.0	2.0	2.0
0.8	3.0	3.0	3.0	3.0	3.0	2.0	2.0	2.0	2.0	2.0
1	3.0	3.0	3.0	3.0	3.0	2.0	2.0	2.0	2.0	2.0

Apply mode C to enable sec. compressor at low loads

Apply mode B to ensure torque assist from EM

ITES Transient Map MG Torque

Load/RPM->	600	800	1000	1300	1400	1600	1800	2000	2200	2400
0	-33.0	-27.0	-22.0	-17.0	-15.0	12.9	11.9	10.2	9.3	8.5
0.2	-33.0	-27.0	-22.0	-17.0	-15.0	12.9	11.9	10.2	9.3	8.5
0.4	-33.0	-27.0	-22.0	-17.0	-15.0	12.9	11.9	10.2	9.3	8.5
0.6	-33.0	-27.0	-22.0	-17.0	-15.0	12.9	11.9	10.2	9.3	8.5
0.8	-33.0	-27.0	-22.0	-17.0	-15.0	12.9	11.9	10.2	9.3	8.5
1	-33.0	-27.0	-22.0	-17.0	-15.0	12.9	11.9	10.2	9.3	8.5

Head start for AFR control PID to ramp up sec. compressor

Direct torque assist at crankshaft

Figure 30 Comparison of ITES operating modes and corresponding motor-generator torque in steady state and transient operation.

Lastly, the transient override maps were implemented in the ITES control strategy and verified through engine simulation on HDFTP cycle. The threshold for detection of transient event was determined by evaluating the typical rate of pedal increase for multiple torque ramps in the cycle. As shown in **Figure 31**, the transient override strategy (TransCtrl) was able to detect a fast torque increase request and apply mode C earlier in comparison to steady state strategy (NoCtrl). Overall, with the transient override function

in the ITES control strategy, the downsized engine with the ITES system was able to match the performance of baseline engine.

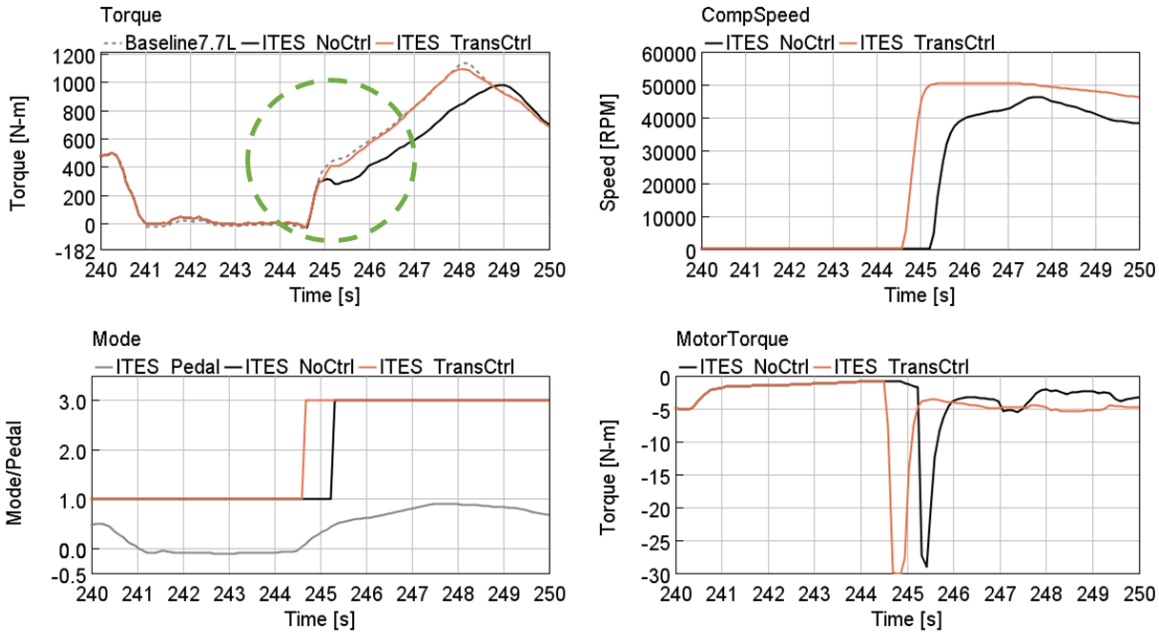

Figure 31 Comparison of torque response of downsized engine with (TransCtrl) and without (NoCrtl) transient control of ITES system in comparison to the baseline engine, during a portion of HDFTP engine certification cycle.

4.3 Mode Switch Control

The ITES system was conceptualized with the implementation of an electromechanically actuated dog-clutch between electric motor-generator and the geartrain connected to engine crankshaft. The objective was to maximize power transfer efficiency by avoiding oil drag, frictional and electrical losses associated with other types of clutches (wet/dry plate clutch). However, for a smooth engagement of dog-clutch, a speed match is required between the input and output shafts before engagement. It was envisioned that this could be achieved with the control of electric motor-generator torque to match the input shaft speed with the output shaft of the dog-clutch before clutch engagement. Therefore, anytime the ITES modes changed from A, C (dog clutch open) to B, D (dog clutch closed), a control function would be needed to achieve speed-match on dog-clutch before engagement. On the other hand, the electromechanically actuated band-brake inside the ITES system did not need any such speed-match function but rather a simple on/off actuation (normally in off position). To primarily address the speed match requirement at the dog-clutch and ensure a smooth transition, an expanded mode switch control function was developed and implemented in the ITES control strategy. As a first step, transient engine test cycle simulation was run with the control strategy described in section 4.2 to evaluate the performance without the expanded mode switch control. As expected, a large torque spike was observed in the clutch transmitted torque at the time of engagement of the dog-clutch without speed match, shown in **Figure 32**.

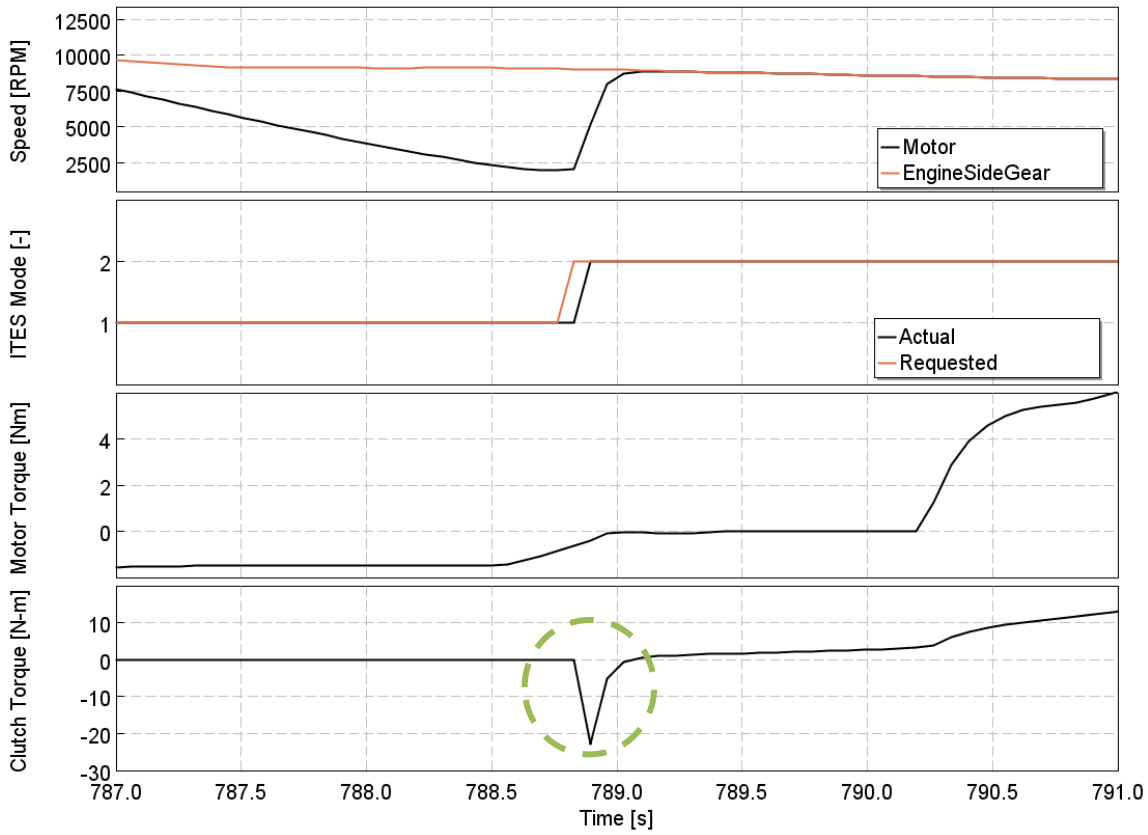

Figure 32 Mode A (1) to mode B (2) switching performance for a transient engine cycle simulation on the downsized engine model without the expanded mode switch control strategy for speed-match.

Based on the results, the simple mode switch control algorithm which converted the requested ITES mode to actuator positions was expanded to include speed-match control. Once a mode request was detected that would lead to the engagement of the dog clutch and, the absolute speed difference between input and output shafts (measured by motor and engine respectively) was determined to be more than a predefined threshold, speed-match PID was enabled. The PID controller then adjusted motor-generator torque to match the speed on the motor generator shaft with the output shaft of the dog-clutch (connected to engine crankshaft). As soon as the absolute speed difference between the input and output shafts of dog-clutch reduced below a predefined threshold, the actuator commands for band-brake, dog-clutch and ITES motor torque were sent to the components. The complete algorithm for mode switch control has been shown in **Figure 33**.

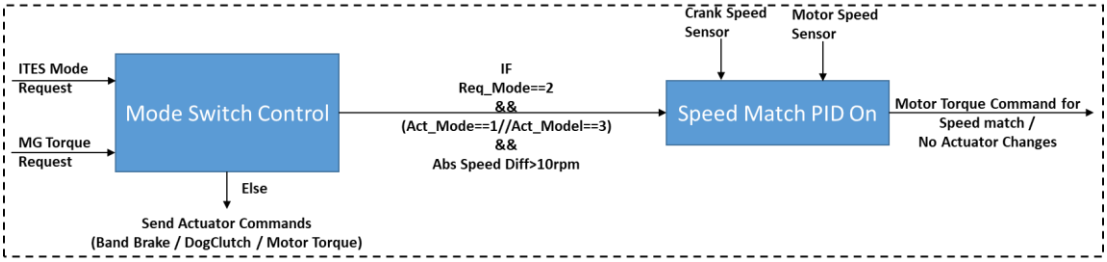

Figure 33 Base mode switch control function expanded to include speed match for dog-clutch engagement

Finally, the expanded mode switch control algorithm was implemented in the model for the downsized engine with the ITES system. As shown in **Figure 34**, the speed match function of the expanded mode switch control strategy (Ctrl) was activated when the requested mode was 2, the current mode was 1 and there existed a large speed difference between input and output shafts of the dog-clutch. The speed match PID then increased the speed of the motor to match the speed on the engine side gear. Once the absolute speed difference was within a predefined threshold, the dog-clutch was engaged and no torque spike was observed in the transmitted clutch torque, unlike the case without this expanded mode switch control as shown in **Figure 32**. The complete mode-switch process was completed within 500ms.

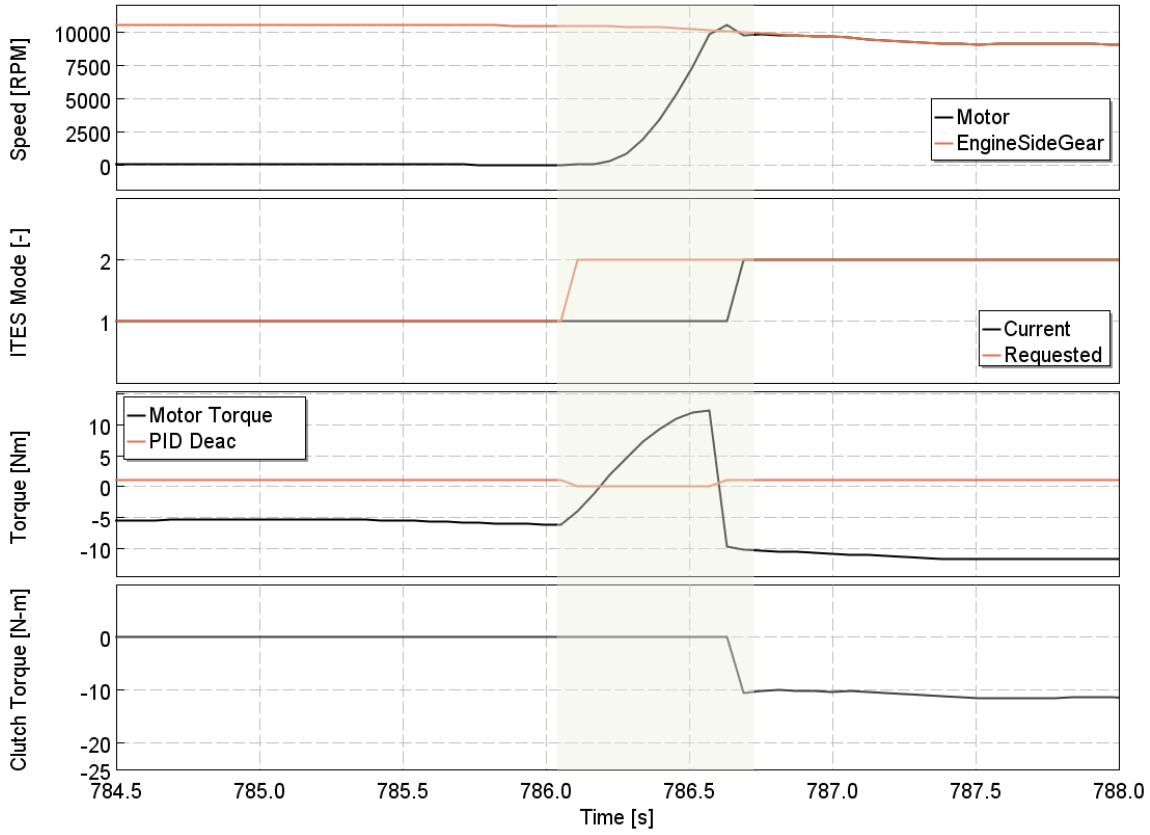

Figure 34 Performance with the speed-match activated mode switch control strategy.

4.4 Final Control Strategy and Vehicle Integration

The overall control scheme for the supervisory controller, ITES control module (ICM), engine control module (ECM) and battery management system (BMS) has been shown in **Figure 35**. The supervisory controller takes the input from accelerator pedal (position), brake pedal (position), antilock braking system (vehicle speed), BMS (SOC) and ECM (engine speed). The supervisory controller then determines the ITES mode request, the corresponding motor torque request and engine torque request based on steady state optimal control, transient override and hybrid function override. The engine torque request is sent to the ECM which then controls all engine actuators to meet the demanded engine torque. The ITES mode request and corresponding motor-generator torque command is sent to the ICM which controls the band-brake, dog-clutch and motor torque command to ensure smooth mode transitions. The ICM also receives the motor-generator electrical power limit from the BMS to ensure that the battery current limits are not exceeded. The next sections describe the supervisory controller and ITES control module in more detail.

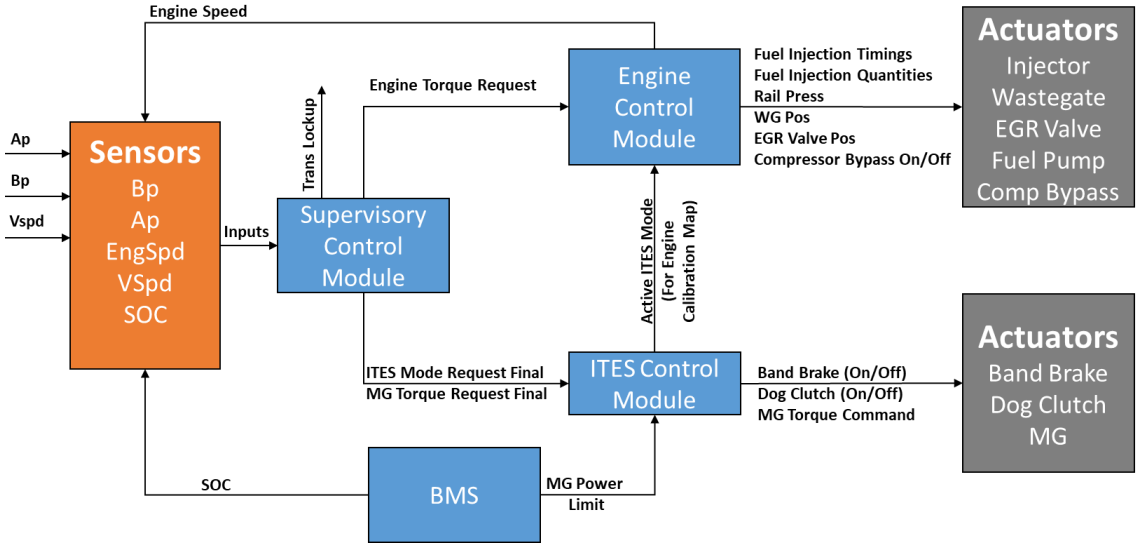

Figure 35 Schematic of the overall control interactions between supervisory control module, engine control module, ITES control module and BMS.

The objective of the supervisory controller is to determine the optimal ITES mode and corresponding motor torque that meets the driver request while maximizing system efficiency. **Figure 36** shows the details of the supervisory controller with respect to the overall control schematic shown in **Figure 35.** First the optimal ITES mode and torque is calculated based on requested engine torque, engine speed and SOC using the ECMS algorithm described in section 4.1. Thereafter, the transient override is applied, if the requested torque signal derivative is detected to be higher than a threshold. Lastly, hybrid function overrides are applied based on brake pedal, engine speed, vehicle speed and accelerator pedal input. The hybrid functions force mode B on the ITES system with a corresponding motor torque to achieve the start-stop, regeneration and e-creep functionality. Correspondingly, an engine torque request is also calculated by the supervisory controller to meet the overall driver torque request.

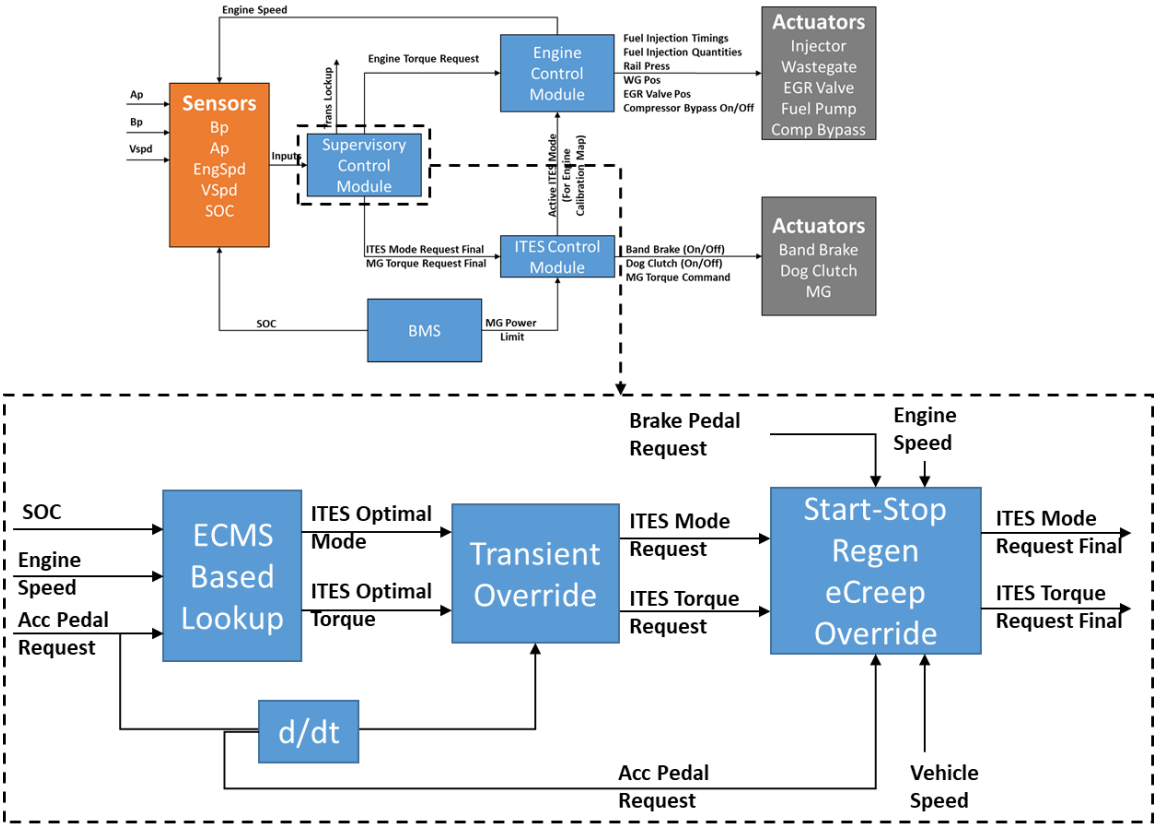

Figure 36 Details of supervisory controller showing steady state optimal control, transient override and hybrid function overrides.

Table 4 shows the different states within the supervisory controller, their transition conditions and the respective outputs to the actuators/controllers. The e-creep mode is activated at low vehicle speeds wherein the ITES system operates in mode B, lockup clutch is closed and ITES motor is commanded to meet driver torque demand. Once the vehicle reaches a speed threshold, the lockup clutch is opened and the engine fueling is enabled. The vehicle then runs in hybrid mode for all accelerator pedal demand greater than 0. The ITES mode and corresponding motor torque is selected based on ECMS based optimal control with transient override. During braking events, the ITES mode B is again activated, the lockup clutch is engaged and retarding torque from the motor is applied to enable regeneration. The motor regen torque is increased linearly as a function of brake pedal position with maximum regen torque at 10% brake pedal position. Further increase in vehicle retardation force is provided by the friction brakes. This is done to maximize regeneration before engagement of friction brakes, that leads to irrecoverable frictional losses. Once the vehicle speed drops below a threshold during braking, the lockup clutch is opened, and the friction brakes are actuated in the 0-10% brake pedal position as well.

Table 4 Supervisory control modes, transition conditions and actuator outputs.

Inputs To Supervisory Control	Acronym
Acc Pedal	Ap (0-1)
Brake Pedal	Bp (0-1)
Battery State of Charge	SOC (0-1)
Vehicle Speed	Vspd (0-120kmph)
Engine Speed	EngSpd (0-2400rpm)
Engine Max Torque at Current Engine Speed	Max_Eng_Torq (0-1200Nm)
Motor Min/Max Torque at Current Motor Speed	Max/Min_MG_Torq (-50 - 50 Nm)
Max Brake Torque at Current Axle Speed	Max_Brake_Torq (0-40,000Nm)
Engine Idle Governor Torque Command	Idle_Torq

Supervisory Control Modes	Condition	ITES Mode (Output)	Motor Torque Request (Output)	Engine Torque Request (Output)	Lockup Clutch (Output)	Friction Brake (Output)
eCreep	Vspd<=4 && Ap>0	2	Ap*Max_MG_Torq	0	Closed	0
Hybrid Mode	Vspd>5.25 && Ap>0	ECMS optimal mode with Transient Override	ECMS optimal mode with Transient Override	Ap*Max_Eng_Torq	Open	0
Regen Braking	EngSpd>710 && Bp>=0.01	2	Min(10*(Bp-0.1),1)*Min_MG_Torq	0	Closed	Max(0,(Bp-0.1)/0.9)*Max_Brake_Torq
Friction Braking Vehicle Stop	EngSpd<610 && Bp>=0.01	2	Min(10*(Bp-0.1),1)*Min_MG_Torq	Idle_Torq / 0 based on start-stop timer	Open	Bp*Max_Brake_Torq

The outputs from the supervisory control module are then sent to the ITES control module which ensures a smooth ITES mode transition and application of corresponding motor torque as described in **Figure 37.** The details of the mode switch control were previously discussed in section 4.3.

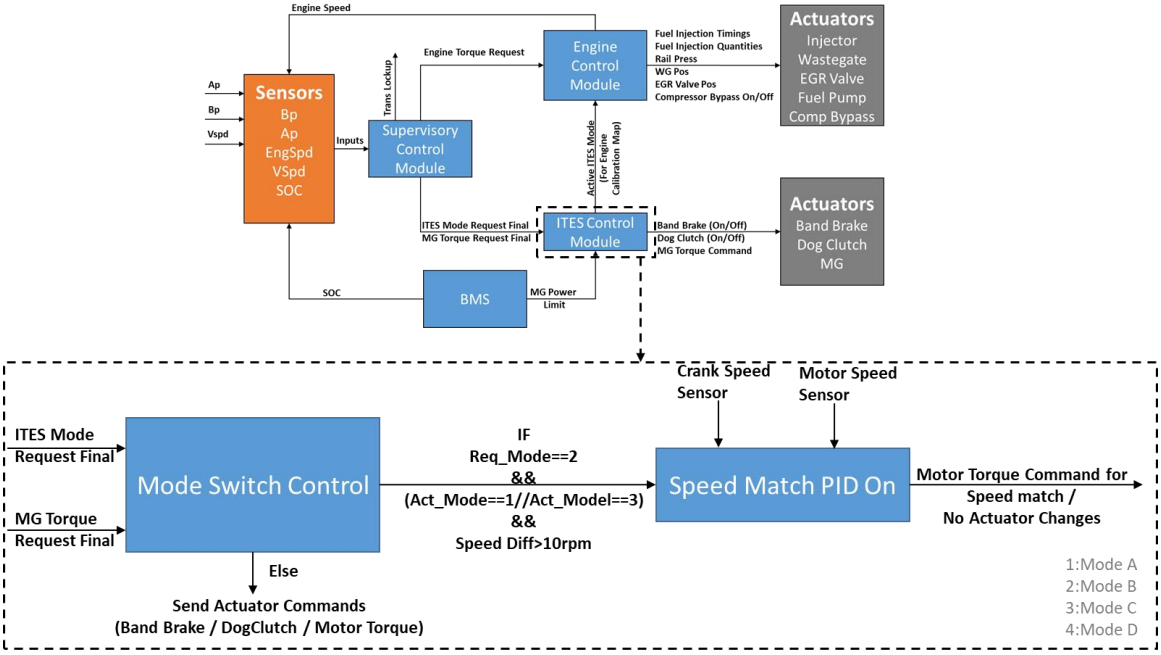

Figure 37 ITES control module details that show the implementation of expanded mode switch control strategy.

5 Engine Simulation Assessment

In this chapter, the performance and emission benefit of the downsized engine with the ITES system has been evaluated in comparison to the baseline engine through 1D engine simulation. Following the sizing of ITES system components (Section 3.3) and control strategy development (Chapter 4), a steady state engine map was simulated on the downsized engine model. The results were then compared against those from the baseline engine model for Brake Specific Fuel Consumption (BSFC), Brake Specific Nitrogen Oxides (BSNOx), Air-Fuel Ratio (AFR), Exhaust Gas Recirculation (EGR), turbine inlet temperature and peak cylinder pressure. Furthermore, to evaluate the impact of ITES system-based technology integration approach on system efficiency, the steady state performance of the downsized engine model with the ITES system was also compared against a downsized engine model with independent integration of mechanical turbocompounding, electric secondary compressor and integrated stater generator.

Thereafter, the aftertreatment temperature impact of engine downsizing with the ITES system was evaluated in comparison to the baseline engine. Furthermore, the capabilities of ITES system in aftertreatment system warmup were explored, and compared against other methods of aftertreatment thermal management such as exhaust throttle and exhaust variable valve timing.

Finally, the downsized engine model with ITES system was simulated on the Heavy Duty Federal Test Procedure (HDFTP) certification cycle and the results were compared against those from the baseline engine model. Apart from comparison of cycle-averaged performance and emissions metrics, the objective of the cycle assessment was to verify the intended function of the transient ITES control strategy and evaluate the load following capability of downsized engine.

5.1 Steady State Operation

For the boundary conditions shown in **Table A2**, steady state engine mapping was run on both baseline and downsized engine with the ITES system. The engine calibration parameters for main injection timing, AFR target and rail pressure were adjusted on the downsized engine to keep peak cylinder pressure, NOx emissions and turbine inlet temperature within limits as shown in **Figure 38**. Due to higher BMEP, the peak cylinder pressure and turbine inlet temperature increased on the downsized engine at all speed and loads. The most challenging engine operating region was higher speed and loads wherein the injection timing was retarded to maintain the peak cylinder pressure below the calibration limit of 220bar and turbine inlet temperature below the continuous limit of 680°C.

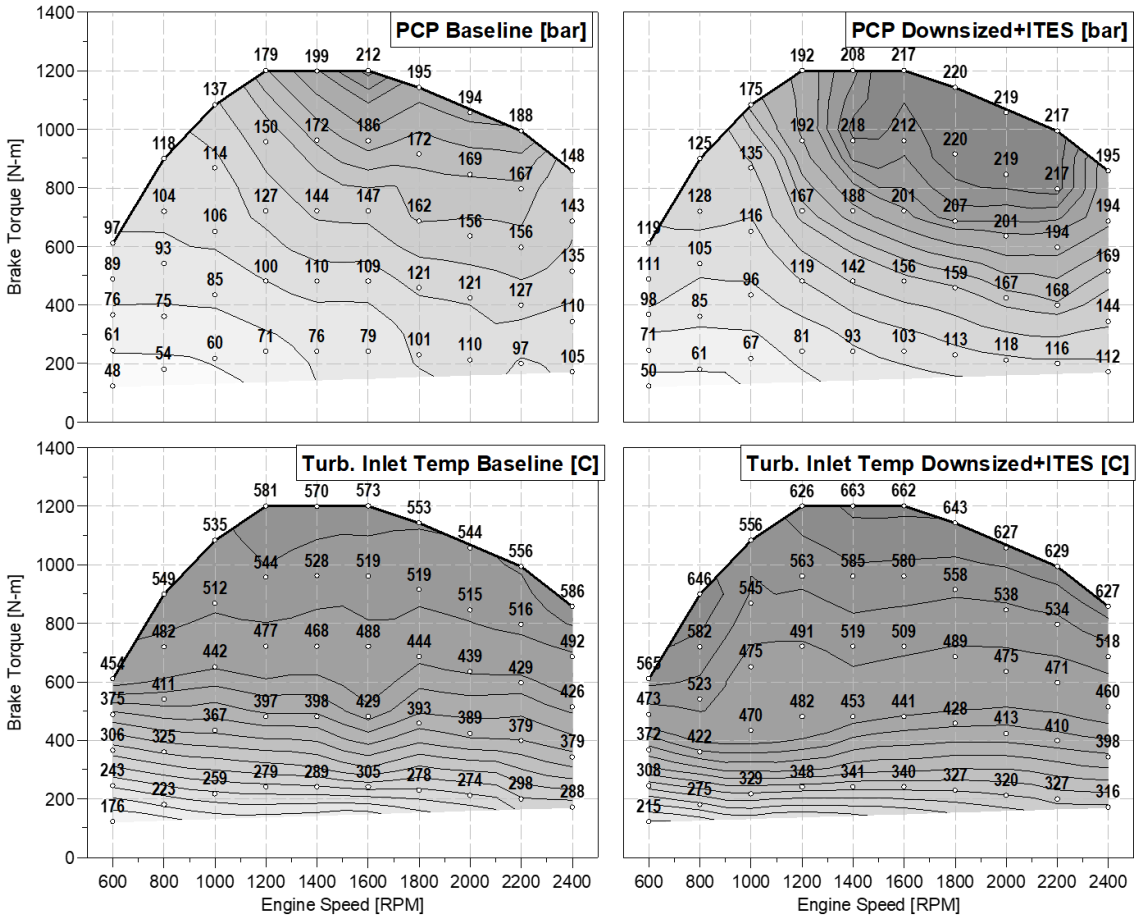

Figure 38 Peak in-cylinder pressure and turbine inlet temperature comparison between baseline and downsized engine with ITES system.

As shown in **Figure 39**, the EGR rates and lambda values on the downsized engine were targeted to be similar to baseline engine, except at lower engine speeds and high loads, where slightly lower lambda values were applied to control NOx and maximize combined turbocharger efficiency. At lower engine loads, where the gas exchange was dominated by piston motion, the lambda values on the downsized engine were inherently lower in comparison to the baseline engine. While the lower lambda values could potentially increase steady state engine out PM emissions at the expense of reduced engine out NOx and increased aftertreatment inlet temperature, the overall impact on cycle average PM emissions was expected to be minimal. This was because the engine does not typically run at lower engine speed and high loads for extended periods of time and also because the electrically driven secondary compressor within the ITES system could potentially reduce PM spikes during transient engine operation. Furthermore, with future developments on low PM combustion and NOx-based passive DPF regeneration systems, the regulatory risk of increasing engine out PM is much lower than that of increasing engine out NOx emissions.

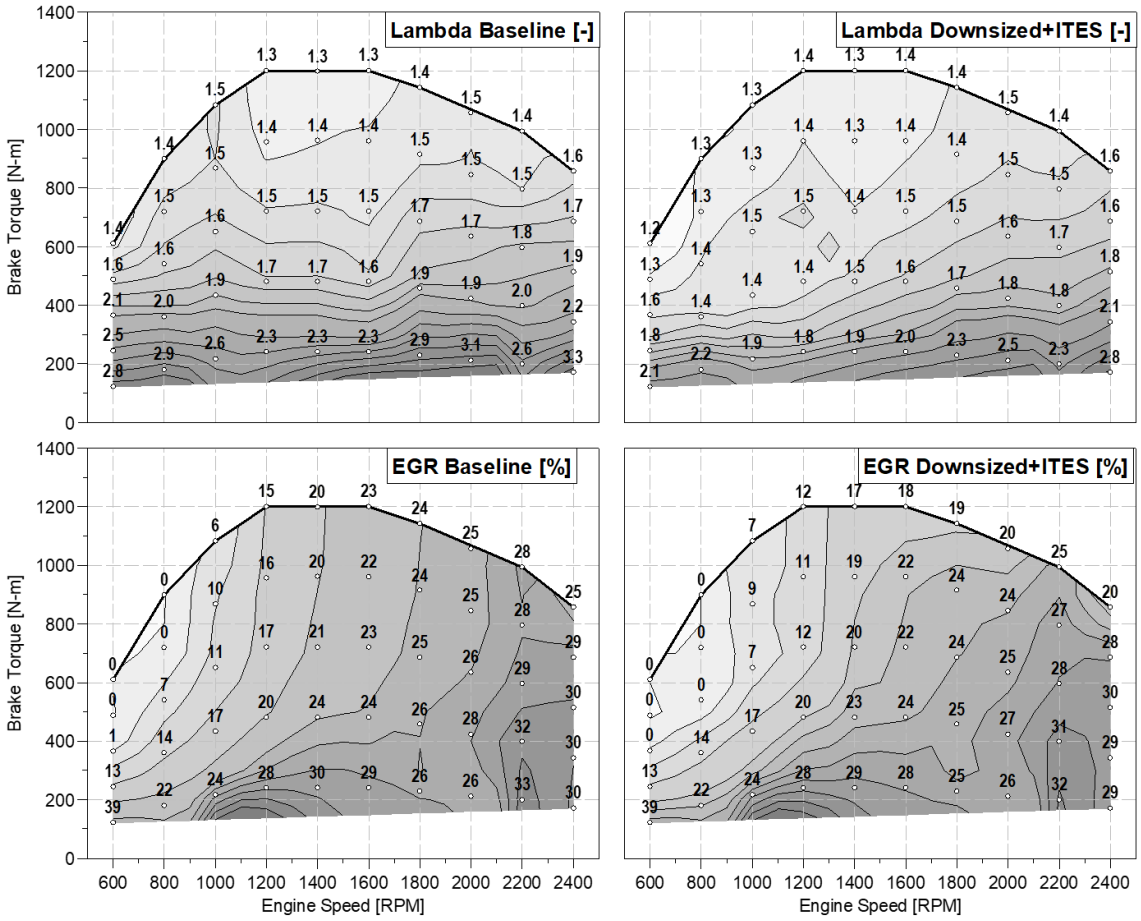

Figure 39 Comparison of EGR rates and lambda between baseline and downsized engine with ITES system.

The key performance metrics of BSFC and BSNOx have been shown for the baseline and downsized engine in **Figure 40**. The brake specific parameters were calculated by dividing the species flowrate in grams per hour with the sum of engine brake power (flywheel) and battery terminal charge power in kilowatts. As expected with engine downsizing, the highest benefit in engine BSFC was observed at higher engine speed and lower loads. The combined benefit of higher mechanical efficiency, improved turbomatch and turbocompounding moved the best BSFC island to higher engine speeds with a large region of the engine operating map below 190g/kWh. For most of the engine operating points in the Not-to-Exceed (NTE) zone [42], the BSFC benefit of engine downsizing with ITES system was in the range of 6-8%. At higher engine speed and loads, the benefit reduced due to retarded injection timing to keep peak cylinder pressure within limit. At lower engine speeds and high loads, the BSFC benefit was offset by secondary compressor power consumption. Overall, in the steady state operation, a power-weighted average BSFC reduction of 6.3% was predicted for the downsized engine with ITES, in comparison to baseline engine.

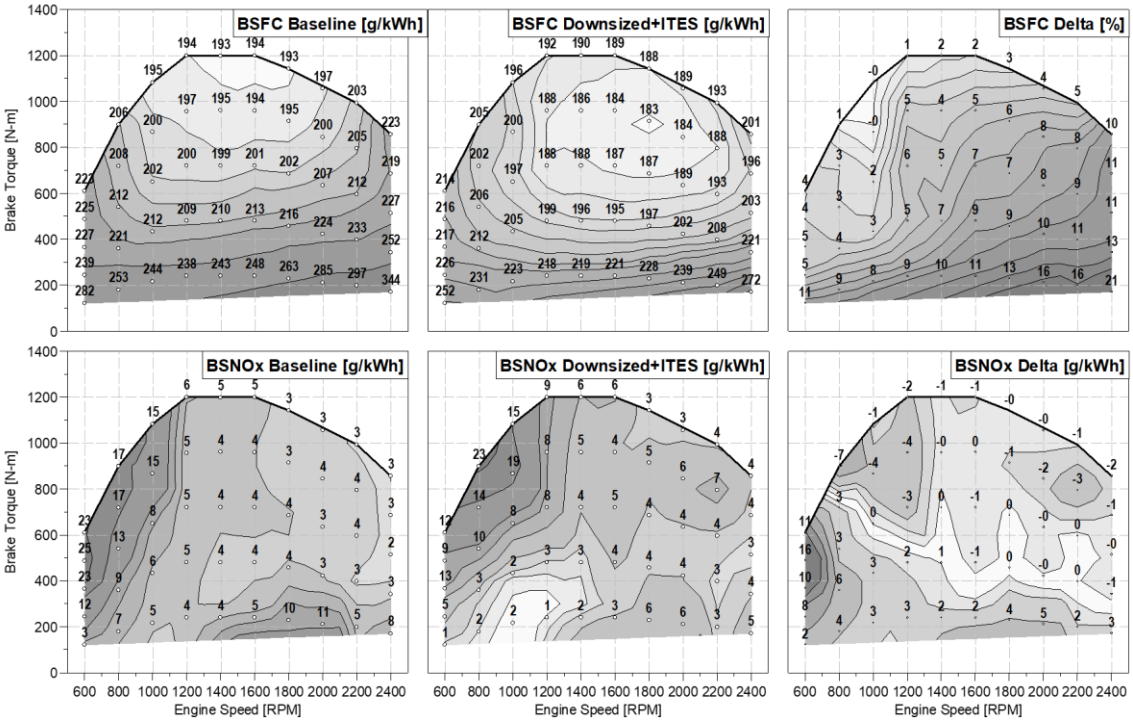

Figure 40 Comparison of brake specific fuel consumption (BSFC) and engine out brake specific NOx emissions (BSNOx) between the baseline engine and downsized engine with the ITES system.

With regards to BSNOx emissions, both the baseline and downsped engine showed very similar NOx emissions in the NTE zone due to similar EGR rates and lambda. While the BMEP increase with engine downsizing typically results in increased NOx emissions due to higher temperature and pressure during combustion, this effect was negated in this case due to application of retarded injection timing to limit peak cylinder pressure. At lower engine loads, a significant reduction in NOx emission was observed on the downsized engine due to reduced air-fuel ratios, resulting from reduced displaced volume. However, at lower engine speeds and high loads, a significant NOx increase was observed due to higher BMEP on the downsized engine. An injection timing retard in this region of the engine operating map was not very effective in reducing NOx without a significant penalty on engine torque and BSFC. Overall, in the steady state operation, a power-weighted average BSNOx reduction of 0.32 g/kWh was predicted for the downsized engine with ITES, in comparison to baseline engine.

While the above analysis showed the benefit of ITES system-enabled engine technologies over the baseline engine, it was also necessary to evaluate the technology integration approach of ITES system in comparison to that of independent integration. As shown in **Figure 41**, the ITES system model was converted to a model with independent integration of E-booster, mechanical turbocompounding and integrated starter-generator on the downsized engine. The turbomachinery size and gear ratios were maintained on the model with independent integration, for a direct comparison against the model with ITES system. The downsized engine model with independent integration was then run in steady state

operation on the engine map while maintaining the same calibration of EGR, lambda and fuel injection control parameters.

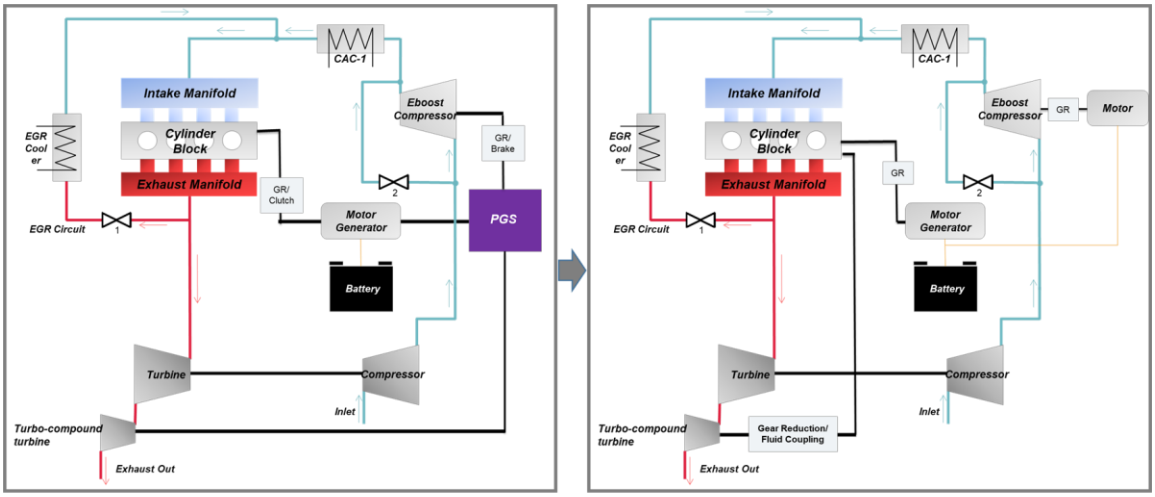

Figure 41 Downsized engine with ITES system model conversion to downsized engine model with independent integration of E-booster, Integrated Starter-Generator and Mechanical Turbocompounding.

In the first step, the performance of the turbomachinery was compared between the two architectures. As shown in **Figure 42,** the turbocompound (TC) turbine and secondary compressor operated at very similar power level at higher engine speed and loads, between the two cases. However, at higher engine speeds and low loads, where the ITES system switched to electrical turbogeneration, the TC turbine power was slightly higher for the ITES system due to higher TC turbine efficiency. Similarly at lower engine speeds and high loads the TC turbine efficiency/power was higher for the ITES system due to operation at optimum TC turbine speeds. Since the lambda values were consistent between the two architectures, the net increase in TC turbine power for ITES system led to higher pressure ratio across the TC turbine, which then resulted in higher exhaust manifold pressure. Consequently, for the ITES system, a higher secondary compressor power was applied by the lambda-based controller to increase the intake manifold pressure and thus maintain airflow. Furthermore, the figure also compares the motor-generator power consumption between the two architectures. The ITES motor-generator was able to recover a fraction of the exhaust energy through electrical turbogeneration at lower loads and through powersplit supercharging at lower engine speed and high loads. However, in the case of independent integration, all the energy recovered from exhaust gas was directly transmitted to engine crankshaft and therefore no electrical power generation was observed on the motor-generator.

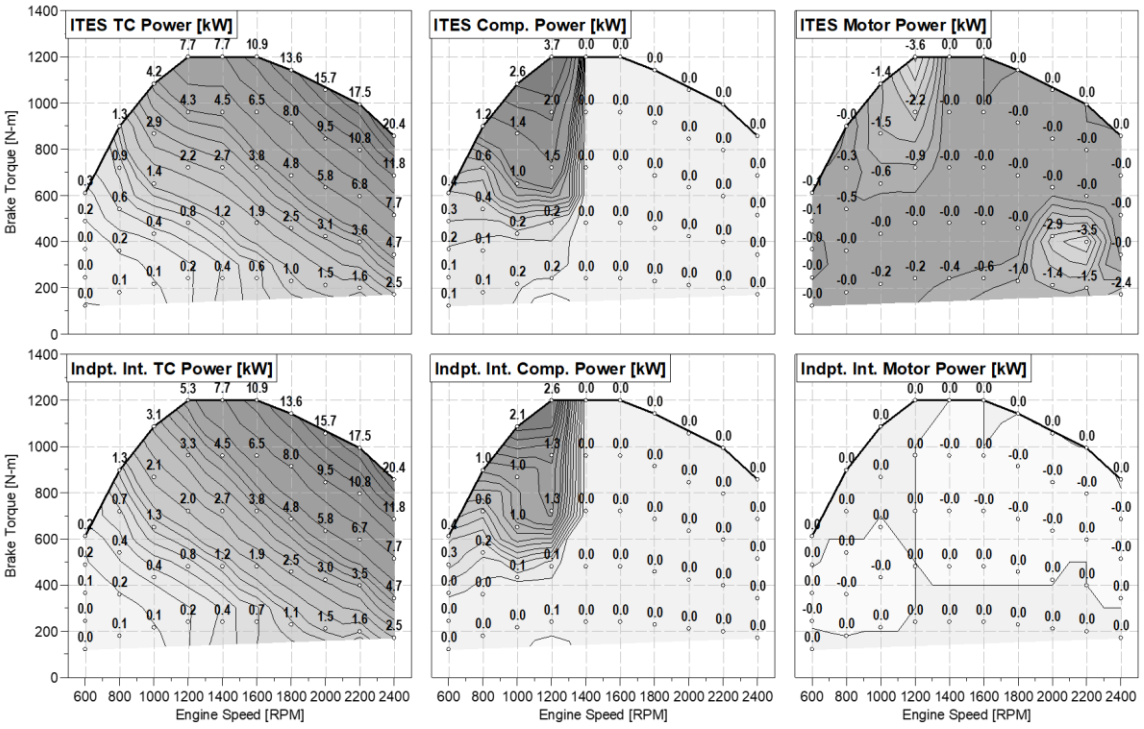

Figure 42 Comparison of turbocompound turbine fluid power, secondary compressor fluid power and motor-generator brake power between the downsized engine with ITES system and the downsized engine with independent integration.

Next, some more performance parameters such as the pumping mean effective pressure (PMEP), TC turbine efficiency and engine attachment power were compared between the downsized engine with ITES system and the downsized engine with independent integration. As shown in **Figure 43**, the PMEP was very similar between the two architectures however much higher TC turbine efficiency was observed on the ITES system due to operation at optimum turbine speeds. This benefit was primarily observed at higher engine speed and low load due to electrical turbogeneration, as well as at lower engine speeds and high loads, due to powersplit turbogeneration. At lower engine speed and high loads, some operating points showed lower TC turbine efficiency with the ITES system, due to calibration trade-offs between air-fuel ratio, BSNOx and BSFC.

At higher engine speed and low loads, a slight increase in PMEP (reduction in pumping work) was observed for the ITES system due to higher TC turbine efficiency at very similar turbine power. However, at lower engine speed and high loads, while the TC efficiency was higher for the ITES system, the TC turbine power, the secondary compressor power and the manifold pressures were also higher. This led to very similar pumping work between the two architectures. For the ITES system, the extra power generated from exhaust gas due to optimum TC turbine speed was partly stored in the battery and partly transferred to secondary compressor. Whereas for the independent integration architecture, the TC turbine efficiency was limited by speed constraint between TC turbine and engine crankshaft geartrain. Furthermore, the power generated by TC turbine could not be directly

transmitted to the secondary compressor, which would have led to multiple energy conversion losses.

Lastly, **Figure 43** also compares the engine attachment power (auxiliary power) between the two architectures. For the ITES system, the attachment power was only through ITES geartrain coupling however for independent integration approach, the attachment power was from mechanical turbocompounding and also from integrated starter-generator. At higher engine speed and loads, the attachment power was very similar between the two architectures as the ITES system operated in mechanical turbocompounding mode. However, at lower engine loads, the ITES system switched to electrical turbogeneration and hence the engine attachment power was near-zero. Similarly, at lower engine speed and high loads, the engine attachment power was near-zero for the ITES system, as it operated in powersplit supercharging mode with the dog-clutch disengaged between the crankshaft geartrain and carrier gear.

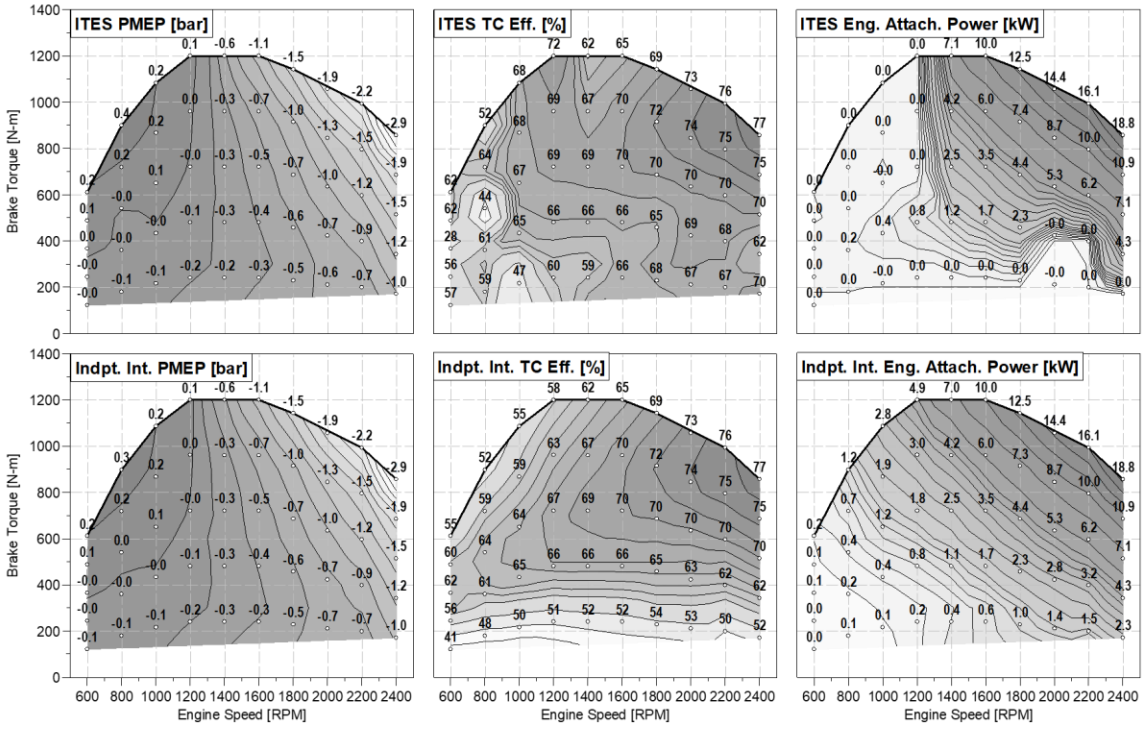

Figure 43 Comparison of pumping mean effective pressure (PMEP), turbocompound turbine efficiency and engine attachment power (motor/TC) between the downsized engine with ITES system and the downsized engine with independent integration.

Once the operation of turbomachinery and geartrain components was verified, BSFC and BSNOx were compared between the downsized engine with ITES system and the downsized engine with independent integration. As shown in **Figure 44**, at higher engine speed and loads, BSFC was nearly identical between the two architectures as the ITES system applied mechanical turbocompounding in that region. With the switch to electrical turbogeneration at lower engine loads, up to 2% benefit in BSFC was observed with the ITES system due higher TC turbine efficiency. At lower engine speeds and high loads,

BSFC benefit was again observed with the ITES system due to increased TC turbine efficiency and reduced energy conversion losses. With the ITES system, the energy from the TC turbine could be directly transmitted to secondary compressor, whereas in case of independent integration, the energy had to go through multiple conversion pathways (exhaust to engine to battery to secondary compressor), which led to efficiency loss. The BSNOx map was very similar between the two architectures with some differences at higher engine speed and low loads as well as at low engine speed and high loads. This was primarily due to the relatively small differences in air-fuel ratio and intake manifold temperature between the two models. For most operating points at low engine speed and high loads, a higher BSNOx was observed with the ITES system due to high secondary compressor power consumption and hence, higher intake manifold temperature. At higher engine speed and low loads, the gain in TC turbine efficiency led to slight increase in air-fuel ratio and hence, BSNOx emissions. Overall, it was concluded that in comparison to independent integration of technologies, the ITES system could achieve similar or higher benefit in BSFC on the downsized engine.

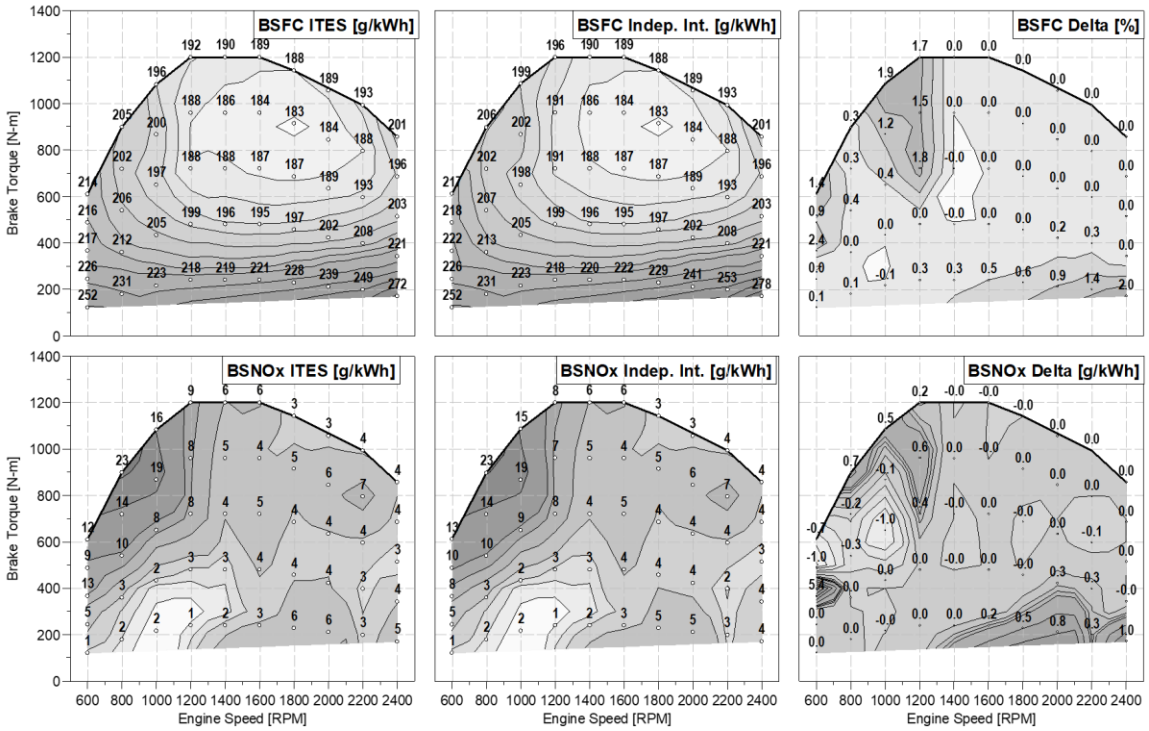

Figure 44 Comparison of brake specific fuel consumption and engine out brake specific NOx emissions between the downsized engine with the ITES system and the downsized engine with independent integration of mechanical turbocompounding, E-booster and ISG.

5.2 Aftertreatment Warmup

While the downsized engine with the ITES system showed significant benefit in fuel consumption without increase in engine out NOx emissions, it was also important to assess the impact of the technology on aftertreatment system performance. The key variable that impacts the aftertreatment system performance is the catalyst temperature. For diesel engines, the primary exhaust gas pollutant species are NOx and PM, which are treated by the Selective Catalytic Reduction (SCR) and Diesel Particulate Filter systems [36]. The activation temperature for SCR is typically 200°C while the minimum operating temperature for DPF to achieve passive PM reduction using NOx is 250°C [43, 44, 48]. In hot engine operation, it is desirable to maintain the SCR and DPF above these target temperatures to ensure emission compliance and minimize active DPF regeneration events. During cold starts, the engine is calibrated to maximize engine out exhaust temperature for a fast SCR warm-up while minimizing engine out NOx emissions [44]. This section evaluates the capability of ITES system in maintaining higher engine out exhaust temperature at low loads and in achieving faster aftertreatment warmup during cold starts.

First, the aftertreatment inlet temperature observed on the downsized engine with the ITES system was compared against the baseline engine in steady state hot engine operation. As shown in **Figure 45**, at lower engine loads, a higher aftertreatment inlet temperature was observed on the downsized engine with ITES system due to lower lambda values. This was primarily due to the reduction in displaced air volume on the downsized engine in comparison to baseline engine. Similarly, at lower engine speeds and high loads, the aftertreatment inlet temperature was higher for the downsized engine due to lower lambda values. In this region of the engine operating map, the lambda values were calibrated to improve turbomachinery efficiency and reduce NOx emissions while respecting the limits for maximum turbine inlet temperature and minimum air-fuel ratio. On the other hand, at higher engine speed and loads, the exhaust temperature of the downsized engine was lower in comparison to the baseline engine due to similar lambda values, higher engine efficiency and turbocompounding.

While the downsized engine with the ITES system showed a significant potential in maintaining >200°C aftertreatment inlet temperature at lower engine loads, further evaluation was done to explore the capability of ITES system in maximizing aftertreatment inlet temperature during warm-up mode. Typically, a warm-up mode engine calibration is applied to maximize engine out exhaust temperature while minimize engine out NOx emission during a cold start cycle [44]. Multiple engine calibration measures such as injection timing retard, post injection, closing of exhaust flap, early exhaust valve opening (for engines with exhaust cam phaser) and increased EGR rates are applied to reduce air-fuel ratio and increase exhaust temperature. Since the ITES system can operate in both mode A (electrical turbogeneration) and mode B (mechanical turbocompounding) at lower engine loads, the engine out exhaust temperature can be increased by either varying the speed of the TC turbine in mode A or by applying negative torque on the ITES motor to increase engine fueling in mode B.

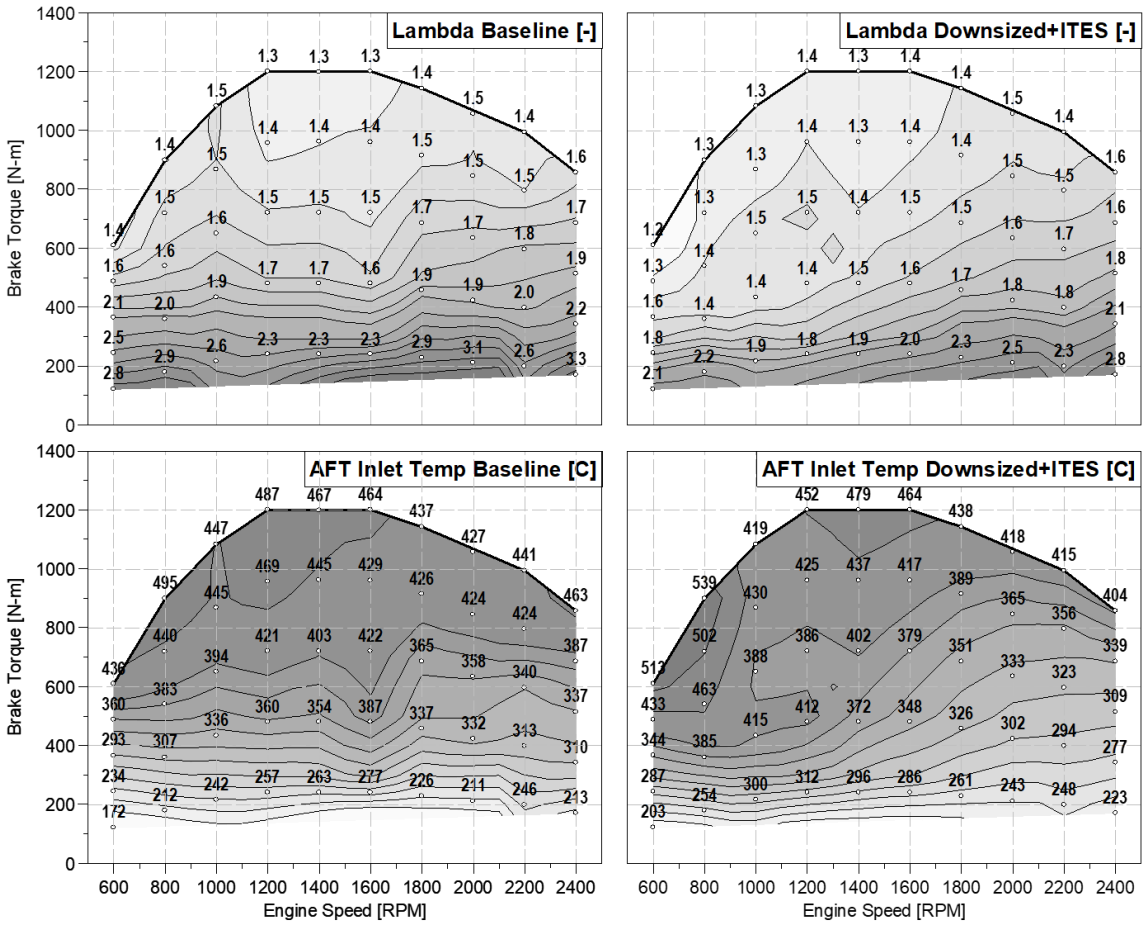

Figure 45 Comparison of lambda and aftertreatment inlet exhaust gas temperature between baseline and downsized engine with ITES system.

At higher engine speed and low load, the capability of ITES system in increasing aftertreatment inlet temperature through load shift in mode B was very limited. This was because of the reduction in motor torque with increase in engine speed. Therefore, the method of increasing aftertreatment inlet temperature by varying TC turbine speed in mode A to increase exhaust back pressure and reduce lambda was more effective. As shown in **Figure 46**, a sweep was run on the TC turbine speed by controlling motor torque in mode A at 1600rpm and 20% load. By reducing the ITES motor torque, the turbocompound turbine speed was increased, which led to lower TC turbine efficiency and hence higher back pressure on the engine. The higher back pressure then led to increase in engine pumping losses and hence increase in BSFC. Consequently, the air-fuel ratio also reduced which led to an increase in aftertreatment inlet temperature. As the figure shows, a 50°C increase in aftertreatment inlet temperature could be achieved with a 6% increase in fuel consumption.

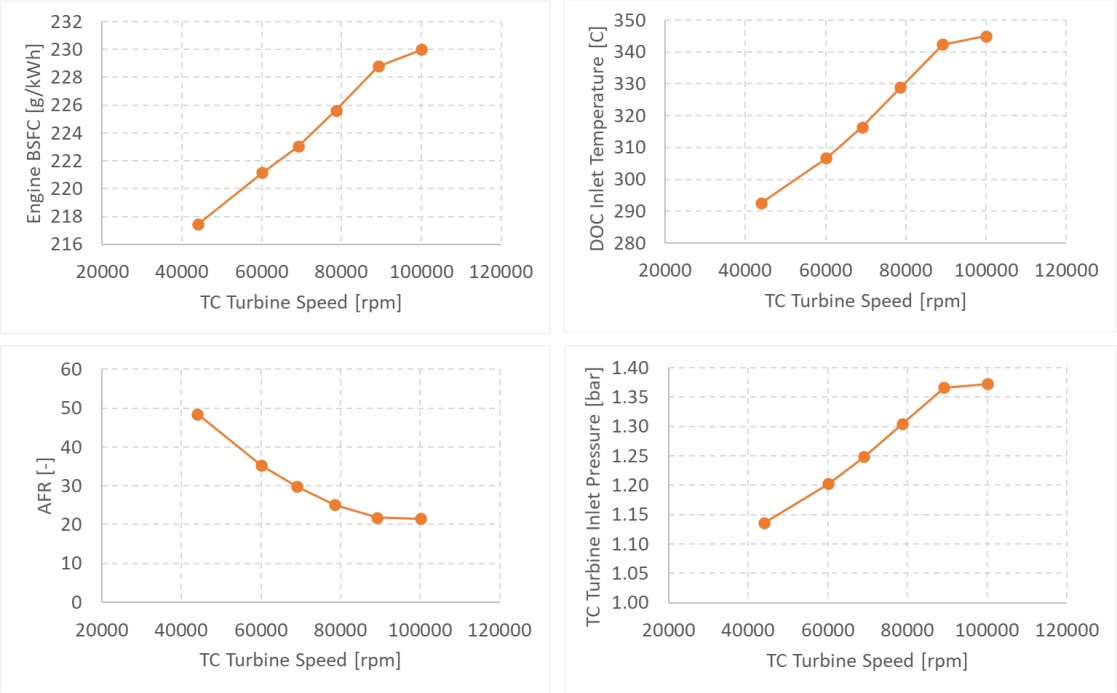

Figure 46 Aftertreatment warmup potential with ITES system in mode A at 1600rpm and 20% load.

At lower engine speed and low loads, since the TC turbine power output and exhaust flowrate was low, mode A was not very effective in reducing air-fuel ratio and increasing the aftertreatment inlet temperature. However, since the ITES motor torque was higher at lower engine speeds, significant load shift on the engine was possible in mode B. By applying a negative torque on the ITES motor-generator, which was mechanically connected to the engine crankshaft, the engine fuel flow and hence the aftertreatment inlet temperature could be increased, at the same flywheel output torque. The energy generated by the ITES motor could be stored in the battery and used later-on to provide torque assist to the engine. As shown in **Figure 47**, a sweep of ITES motor torque was run to increase engine attachment torque at idle. The engine load shift plot shows that up to 156Nm of engine load shift could be achieved with max generating torque applied on the ITES system. Due to this load shift, a DOC inlet temperature of 250°C was predicted at idle which was a significant benefit in comparison to standard ITES system calibration.

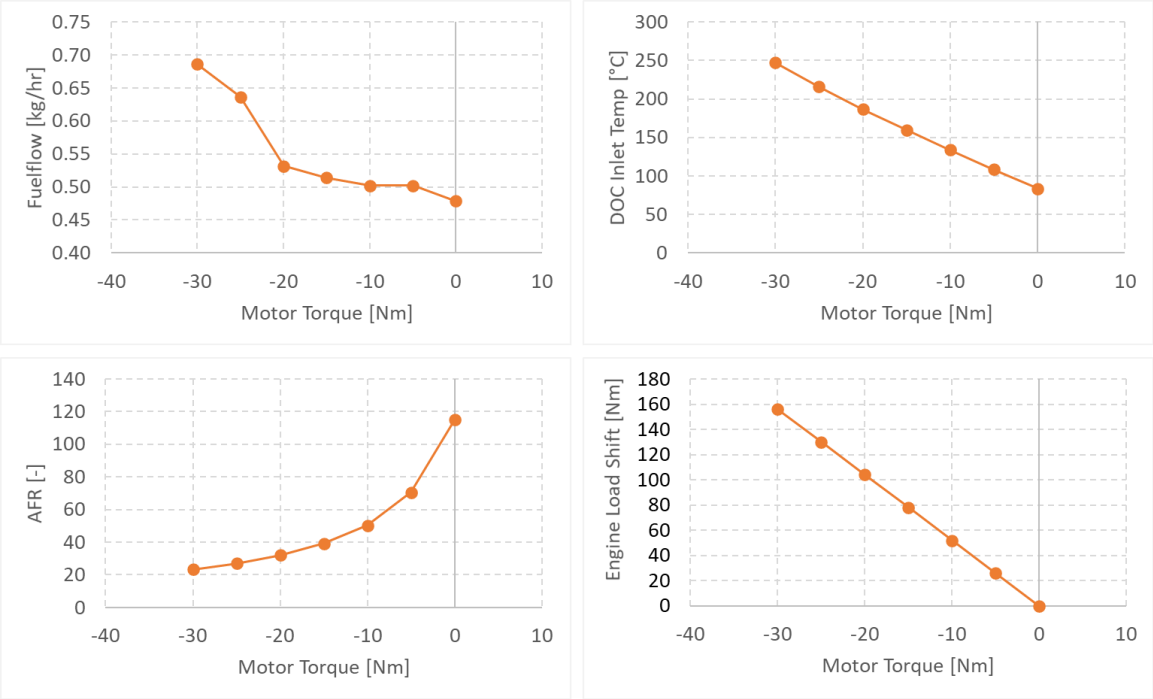

Figure 47 Aftertreatment warmup potential with ITES system in mode B at 600rpm and 0% load (idle).

To quantify the relative benefit of ITES system in comparison to competing technologies for aftertreatment warmup, a sweep of exhaust throttle and exhaust valve timing was run at both 1600rpm 20% load and 600rpm 0% load (idle) operating points. Since the aftertreatment warmup behavior is a function of both exhaust gas massflow and temperature, exhaust power was also included as a variable for comparison. **Figure 48** shows the comparison at 1600rpm 20% load wherein, for a given BSFC penalty, the ITES system was able to achieve higher exhaust power and temperature, in comparison to exhaust back pressure valve and exhaust variable valve timing. While the ITES system and the exhaust back pressure valve both achieved the same effect of increasing the exhaust back pressure on the engine, the exhaust back pressure valve also induced throttling losses in the exhaust path which led to higher fuel penalty. On the other hand, exhaust variable valve timing achieved the increase in exhaust power at the expense of reduced in-cylinder work due to earlier exhaust valve opening. In contrast, the ITES system was able to achieve increase in exhaust back pressure by extracting more work from the TC turbine and storing the energy in the battery for later use during engine torque assist.

The overall trend in air-fuel ratio and BSNOx showed the expected reduction with increase in exhaust temperature and power. The lowest air-fuel ratio was observed with the exhaust variable valve timing due to its highest sensitivity on gas exchange process. Since target EGR was maintained in the actuator sweeps, BSNOx reduction correlated well with AFR reduction.

Overall, while the ITES system showed a benefit over other technologies in efficiently increasing exhaust power and temperature, the maximum increase in exhaust temperature

was limited with ITES system due to TC turbine speed limitation. The highest potential for increase in exhaust power and temperature was observed with the exhaust back pressure valve.

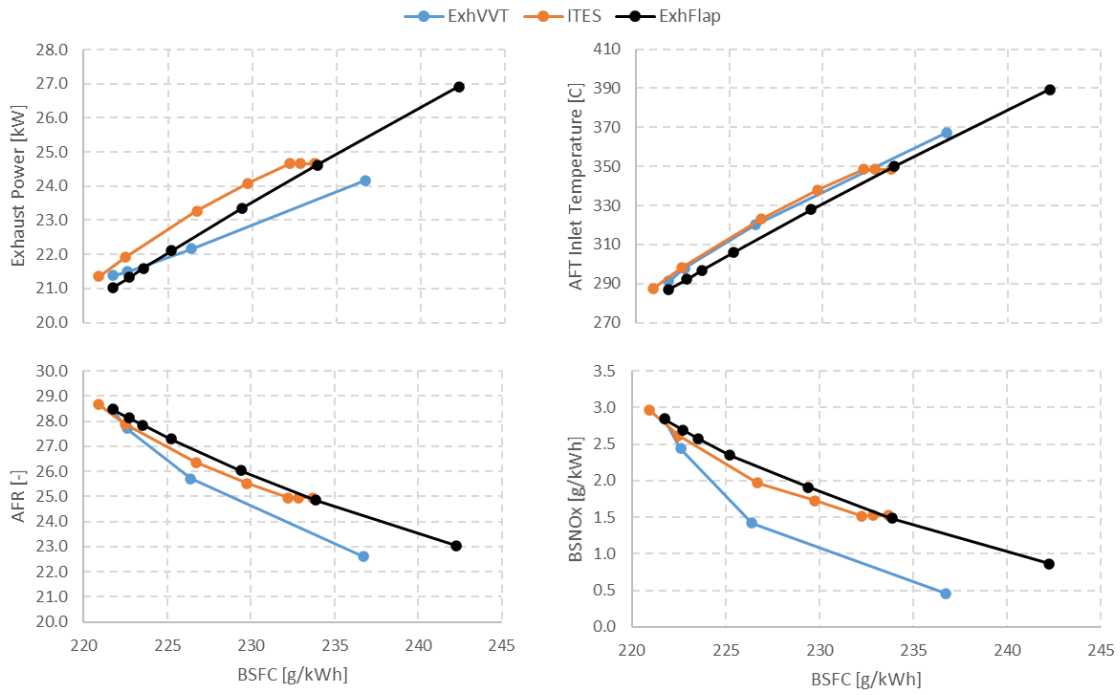

Figure 48 Comparison of aftertreatment warmup potential between Exhaust Variable Valve Timing (ExhVVT), ITES system and Exhaust Back Pressure Valve (ExhFlap) at 1600rpm and 20% load on the downsized engine.

A similar evaluation was conducted at 600rpm and 0% load (idle) operating point which is a critical operating point for regulatory cycles. At such low engine speeds where the exhaust mass flowrate is relatively low, the actuators in gas exchange path do not have much sensitivity in increasing exhaust power and temperature. As shown in **Figure 49**, the ITES system was able to efficiently achieve a remarkable increase in exhaust power and temperature in comparison to exhaust back pressure valve and exhaust variable valve timing. As described in **Figure 47,** this was due to increase in engine load torque from the ITES system which then increased engine fuel flow, exhaust massflow and exhaust temperature. An interesting behavior was observed on the BSNOx emissions, which increased initially with increase in engine fuel flow, however, as the air-fuel ratio reduced below 30, BSNOx emissions decreased due to lower local lambda during combustion. Overall, in comparison to exhaust pack pressure valve and exhaust variable valve timing, the ITES system predicted the most efficient and highest (>200°C) aftertreatment warmup potential at engine idle conditions.

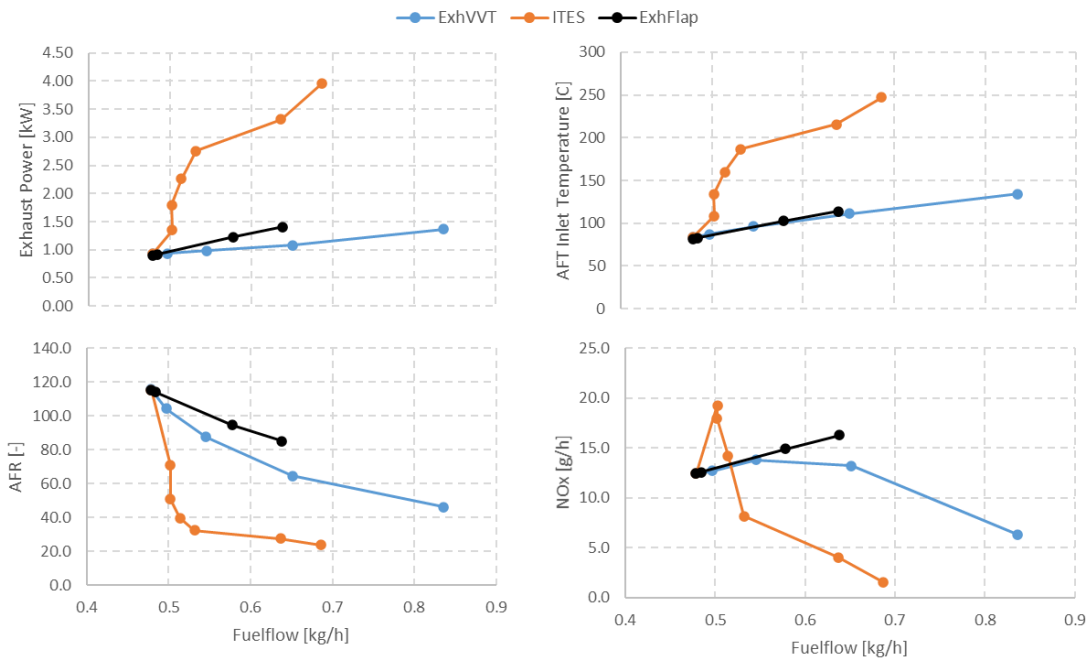

Figure 49 Comparison of aftertreatment warmup potential between Exhaust Variable Valve Timing (ExhVVT), ITES system and Exhaust Back Pressure Valve (ExhFlap) at 600rpm and 0% load (idle) on the downsized engine.

Once the ITES system's potential in aftertreatment warmup was quantified at few operating points, a complete engine mapping exercise was conducted to develop aftertreatment warmup mode calibration using the ITES system. At engine load below 20%, the ITES system mode and motor torque were swept to determine the optimum solution that could maximize exhaust temperature while minimizing fuel consumption penalty. **Figure 50** shows the comparison of the optimized ITES modes and motor torque during aftertreatment warmup and during standard operation at target SOC. At 0% engine load, the most efficient method for increasing aftertreatment inlet temperature was determined to be mode 2 (mechanical turbocompounding) with maximum generation torque on the ITES system motor. With the motor to crank speed ratio of 5:1, up to 150Nm of load shift could be achieved on the engine at idle speeds. However, at rated engine speed of 2200rpm, the load shift magnitude reduced to 46.5Nm due to motor power limit. At higher engine speeds and 20% load, it was observed that mode 1 (electrical turbogeneration) was a more efficient method of increasing aftertreatment inlet temperature. This was due to effective regulation of the TC turbine power to increase engine back pressure, engine pumping work and hence exhaust temperature. At engine loads above 20%, the calibration was identical between warmup mode and standard mode.

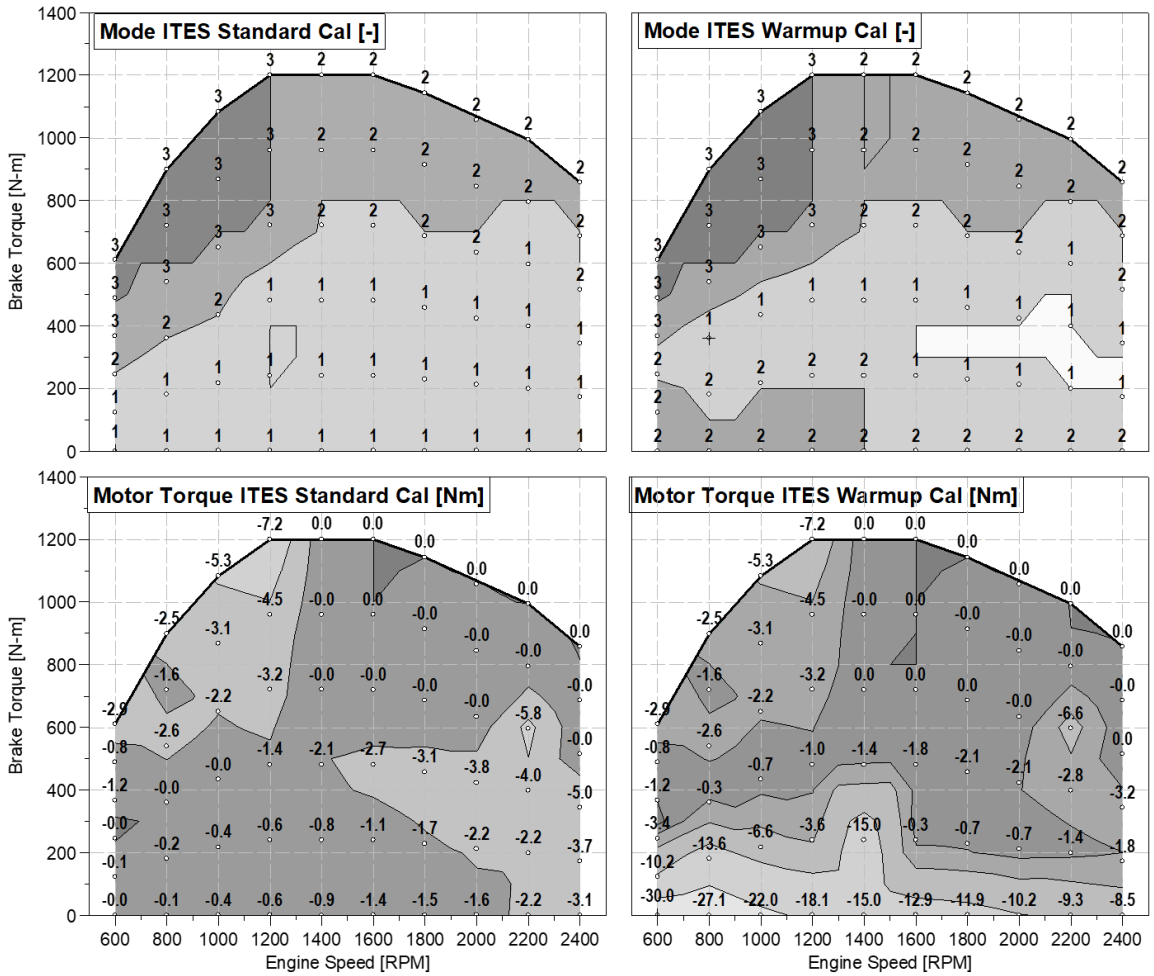

Figure 50 Comparison of ITES system steady-state calibration on the downsized engine in standard and warmup modes.

With the load shift and TC turbine speed adjustment in warmup mode, a significant reduction in lambda values was also observed at low loads. Consequently, the reduction in oxygen concentration also led to a reduction in engine out NOx emissions as shown in **Figure 51.** While the trend in NOx reduction is reasonably predicted, it should be noted that the magnitude of NOx reduction might have been over-predicted due to NOx model accuracy. The NOx model calibration did not include conditions with such low air-fuel ratios at low engine loads. Furthermore, the specific quantities were calculated by dividing the species flow rate in g/hr by the sum of engine brake power and battery terminal charge power in kW, as discussed in section 5.1. At higher engine loads, lambda values and engine out NOx were not impacted as the calibration was consistent between standard and warmup modes.

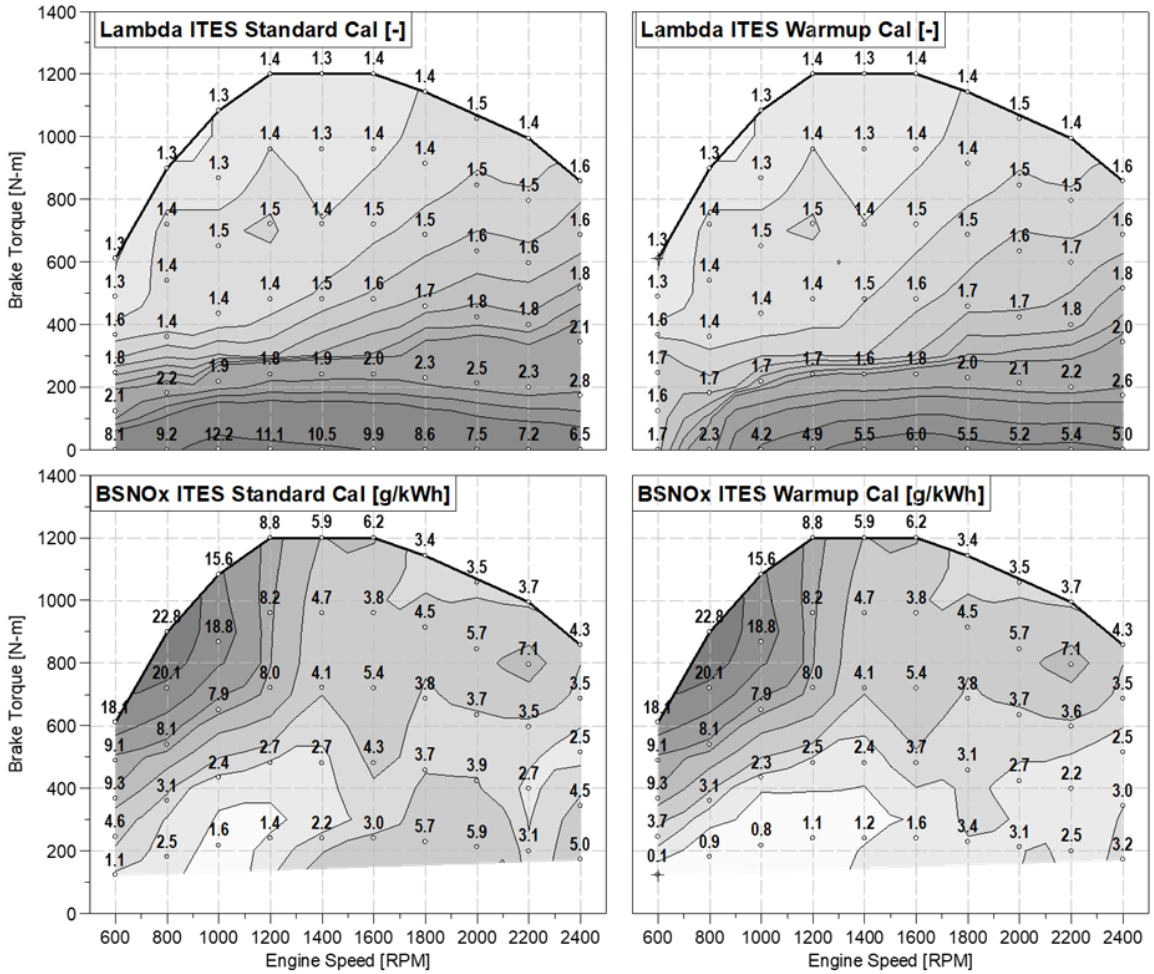

Figure 51 Comparison of lambda and BSNOx between standard and warm-up modes on the downsized engine with the ITES system.

Finally, the predicted rise in aftertreatment inlet temperature and the corresponding BSFC penalty in the warmup mode has been shown in **Figure 52**. At lower engine speed and loads where engine load shift was applied, >100°C increase in aftertreatment inlet temperature was predicted without any penalty in BSFC. This was primarily due to the increase in mechanical efficiency from increase in the ratio of indicated power to friction power. Since the flywheel output power was kept constant, the additional brake power produced by the engine was stored in the battery for later use. At higher engine speed and low load, >50°C increase in aftertreatment inlet temperature was predicted with up to 5% fuel penalty. Overall, the assessment concluded that apart from enabling fuel savings, the ITES system could also be utilized for efficient aftertreatment thermal management at low loads with a potential to increase aftertreatment inlet temperature by 50-100°C.

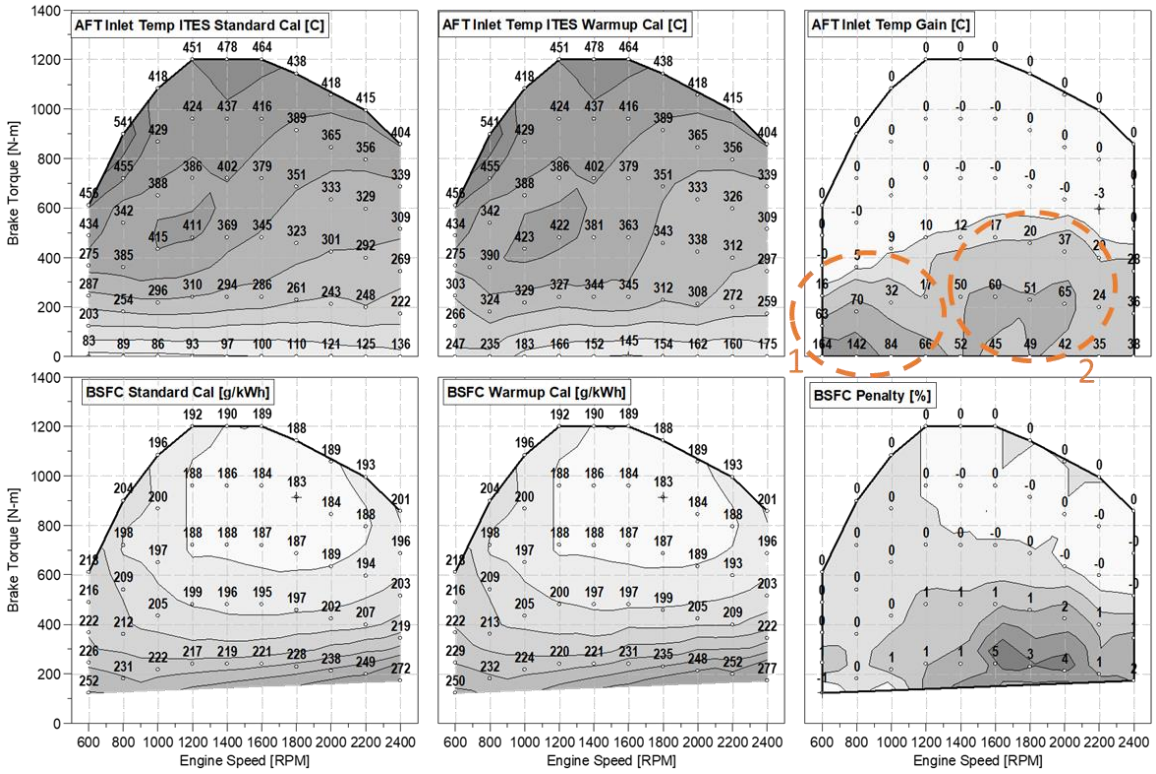

Figure 52 Comparison of DOC inlet temperature and BSFC between standard and warm-up modes on the downsized engine with the ITES system.

5.3 Transient Cycle

With the steady state performance quantified, the final step was to evaluate the transient performance of the downsized engine with the ITES system on Heavy Duty Federal Test Procedure (HDFTP) cycle. The HDFTP is an engine dynamometer test cycle for pollutant criteria and greenhouse gas emission certification [2]. As shown in **Figure 53**, the cycle predominantly operates at rated engine speed and medium load, where the fuel consumption benefit of the downsized engine with the ITES system is relatively high. The cycle also operates at around idle speeds for extended period, representing the typical driving conditions of urban vocational applications. Utilizing the transient control strategy developed for the ITES system in chapter 4 and the map-based open-loop engine calibration maps, hot-start FTP was run on the downsized engine with the ITES system and compared against baseline engine. The battery initial SOC was adjusted such that the difference between initial and final SOC was within 1%. Since the baseline engine model was validated against hot-start FTP cycle test data (Appendix A), the control strategy for EGR valve and injection parameters was kept consistent between the baseline engine and the downsized engine with the ITES system.

Thereafter, the benefit of the previously developed (section 5.2) ITES system calibration in warmup mode was evaluated on cold-start FTP cycle. The cold-start FTP cycles were simulated without any engine calibration changes in comparison to hot-start cycle to understand the direct impact of ITES system warmup calibration on cycle averaged BSFC,

cycle averaged BSNOx and SCR warmup time. To simulate cold-start HDFTP cycle, time-based engine coolant and oil temperature profiles were directly applied in the model from cold-start test data, and all initial wall/material temperatures in the model were initialized at 25°C.

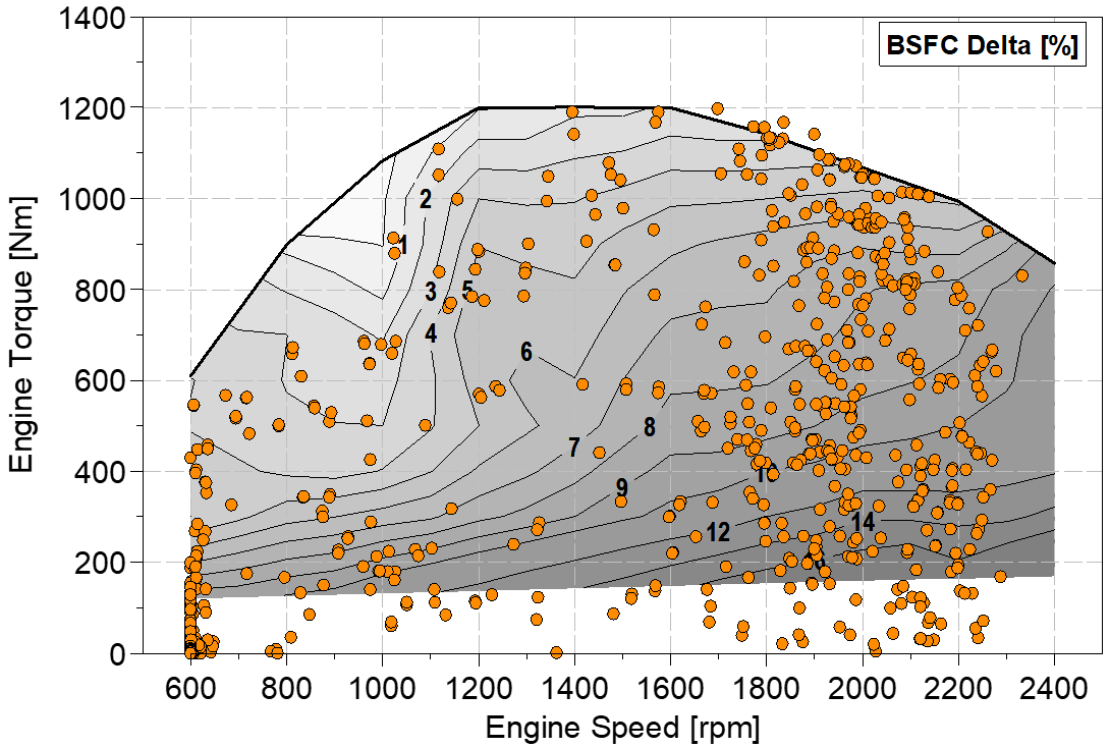

Figure 53 HDFTP cycle operating points on the BSFC delta map between the baseline engine and downsized engine with ITES system.

Figure 54 and **Figure 55** show the key performance and emission metrics on the hot-start HDFTP cycle for the baseline and downsized engine with the ITES system. Standard boundary conditions (Table **A2)** were applied for cycle simulation. As shown in **Figure 54**, the downsized engine was able to follow the demand torque with a regression coefficient >99%, which reaffirmed the confidence in the transient capability of the downsized engine with the ITES system. As expected, the air massflow rate on the downsized engine with the ITES system was reduced due to lower engine lambda values, higher engine efficiency and reduced engine displacement. By utilizing the engine mass flowrate and engine-out exhaust temperature prediction, a catalyst heat sink model [37] was implemented to predict SCR mid-bed temperature. Consistent with the observations made on **Figure 45**, the aftertreatment inlet temperature of the downsized engine with ITES system was lower in comparison to baseline engine due to higher engine efficiency and exhaust energy recovery from the TC turbine. However, the aftertreatment inlet temperature for the downsized engine with ITES system was still above the SCR light-off temperature in hot operation. Furthermore, in comparison to the baseline engine, the downsized engine with the ITES system showed a lower rate of SCR mid-bed temperature loss during idle portions of the FTP cycle (e.g., 200-400s). As shown in **Figure 45** earlier,

this was due to the higher engine-out exhaust temperatures at lower loads on the downsized engine with ITES system.

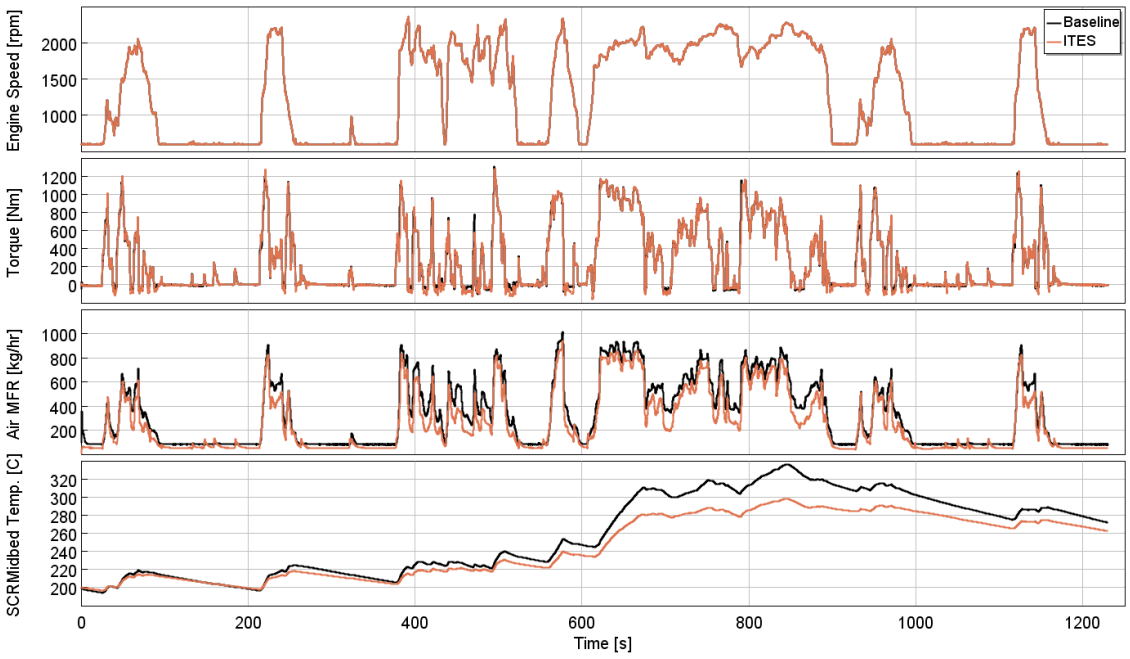

Figure 54 Comparison of engine speed, engine torque, air mass flowrate and SCR mid-bed temperature between baseline engine and downsized engine with ITES system on Hot-start HDFTP cycle.

Figure 55 shows the instantaneous and cumulative engine out NOx emissions and fuel consumption on the hot-start FTP cycle. In comparison to the baseline engine, the downsized engine with the ITES system showed a very similar engine out NOx emission. While the NOx emissions typically increase due to increase in combustion temperature and pressure from engine downsizing, the slight reduction in air-fuel ratio and retarded combustion phasing for maintaining peak cylinder pressure limit, helped bring the overall NOx emissions close to that of the baseline engine. On the other hand, the cumulative fuel consumption for the downsized engine with ITES system reduced by >8% in comparison to the baseline engine. As shown in the instantaneous fuel consumption plot, the primary reduction in fuel flow was observed in the 600-900s range, wherein the engine was operated at higher speeds. This was consistent with **Figure 40**, wherein due to lower friction on the downsized engine with ITES system, the highest benefit in fuel consumption was observed at higher engine speeds and low loads.

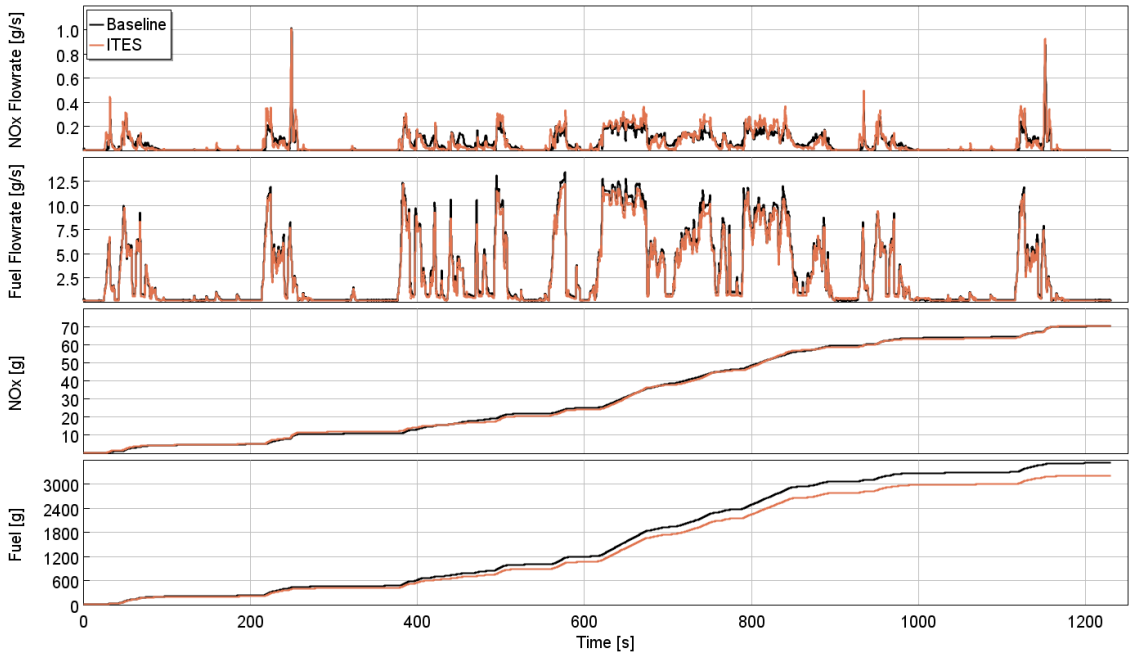

Figure 55 Comparison of engine out NOx and fuel consumption between baseline engine and downsized engine with ITES system on Hot-start HDFTP cycle.

The key performance variables for the ITES system were also evaluated on the HDFTP cycle and are shown in **Figure 56**. The ITES system control strategy described in chapter 4 worked well in sustaining battery state of charge at around 0.5. During the highway portion of the HDFTP cycle (600-800s), the ITES motor-generator provided torque assist to the engine (during pedal tip-ins), which led to the reduction in SOC down to 0.47. However, the control strategy responded to the lower SOC and brought it back up to 0.5 towards the end of the cycle, with energy recuperation at lower engine loads. The figure also shows the TC turbine, secondary compressor and motor-generator power, and their operating speed over the cycle. The TC turbine was able to produce up to 20kW of power during the cycle with majority of power generated during the higher engine speed operation between 600-800s. The secondary compressor consumed up to 5kW of power and was engaged when the engine transitioned through the lower engine speeds and high load operating points on the HDFTP cycle. The ITES motor-generator operation was closely coupled to the overall ITES control strategy and ITES operation in different modes. The positive power spikes on the motor-generator were due to the secondary compressor activation at lower engine speeds and due to torque assist events at higher engine speeds. On the other hand, the negative power on the motor-generator was due to electrical turbogeneration at higher engine speeds and due to energy recuperation at lower engine loads. In accordance with the ECMS-based control algorithm, the energy recuperation was done at lower engine speed and loads to achieve load-shift on the engine and reduce cycle-averaged BSFC.

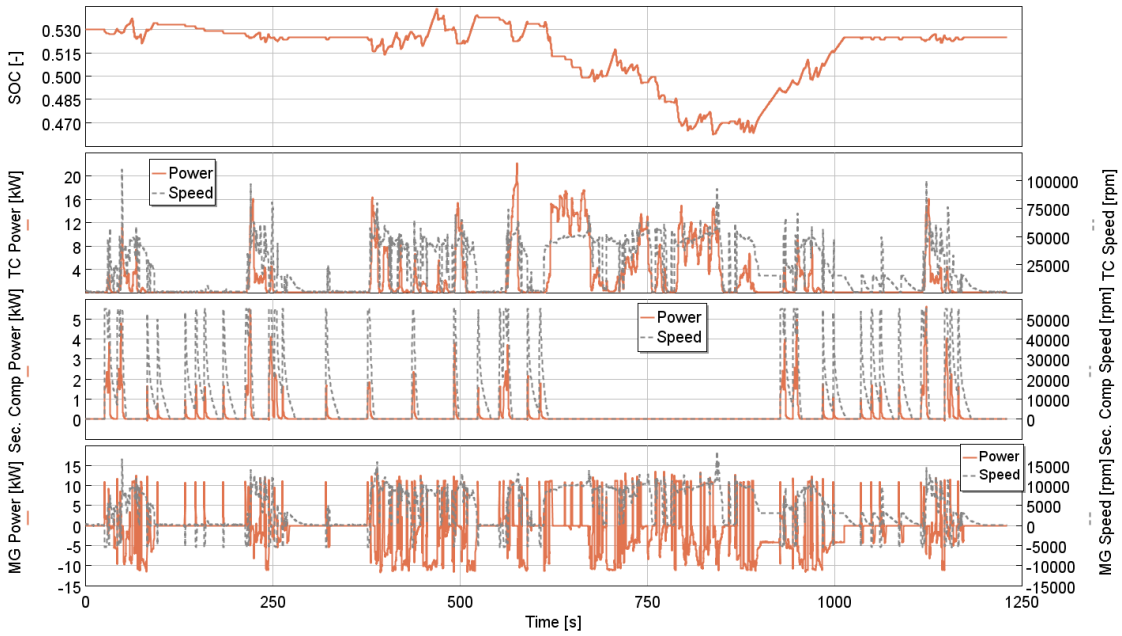

Figure 56 ITES system and battery performance variables on the HDFTP cycle.

Finally, the cycle averaged BSFC and BSNOx were compared between the baseline engine and the downsized engine with ITES system. As shown in **Figure 57**, the downsized engine with the ITES system was predicted to achieve 8.45% reduction in fuel consumption in comparison to baseline engine. The BSFC benefit was predicted with engine-out BSNOx within 1.1% between the two architectures. To quantify the load following capability of the downsized engine with ITES system, torque regression analysis was conducted to determine the coefficient of correlation between the target torque command and the actual engine torque in simulation. As shown in the figure, while there was some reduction in Torque Rsq on the downsized engine with the ITES system, the difference was within 0.04%. To conclude, the downsized engine with ITES system was predicted to achieve 8.45% reduction in engine fuel consumption on the HDFTP cycle with similar engine-out NOx and load following capability.

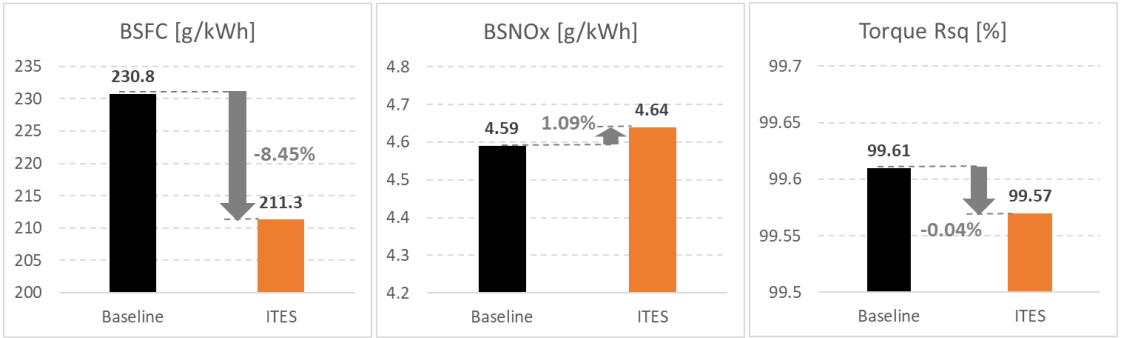

Figure 57 Comparison of cycle averaged BSFC, cycle averaged BSNOx and engine torque regression on the HDFTP cycle between the baseline engine and the downsized engine with the ITES system.

To investigate the potential of the ITES system in aftertreatment warmup, cold-start HDFTP cycle was run on the downsized engine with ITES system model in standard mode and in warmup mode. The engine coolant and oil temperature profiles were directly imposed from measured data collected on baseline engine. The pipe wall temperatures, catalyst temperature and in-cylinder temperatures in the model were initialized at 25°C to capture the impact of higher heat-transfer from the engine during a cold-start event. As shown in **Figure 58**, the warmup mode calibration on the ITES system was able to achieve up to 25°C higher SCR mid-bed temperature which led to a faster SCR light-off. As described in section 5.2, the increase in engine-out exhaust temperature was achieved through engine load shift by the ITES motor-generator and through the modulation of TC turbine speed in electrical turbogeneration mode.

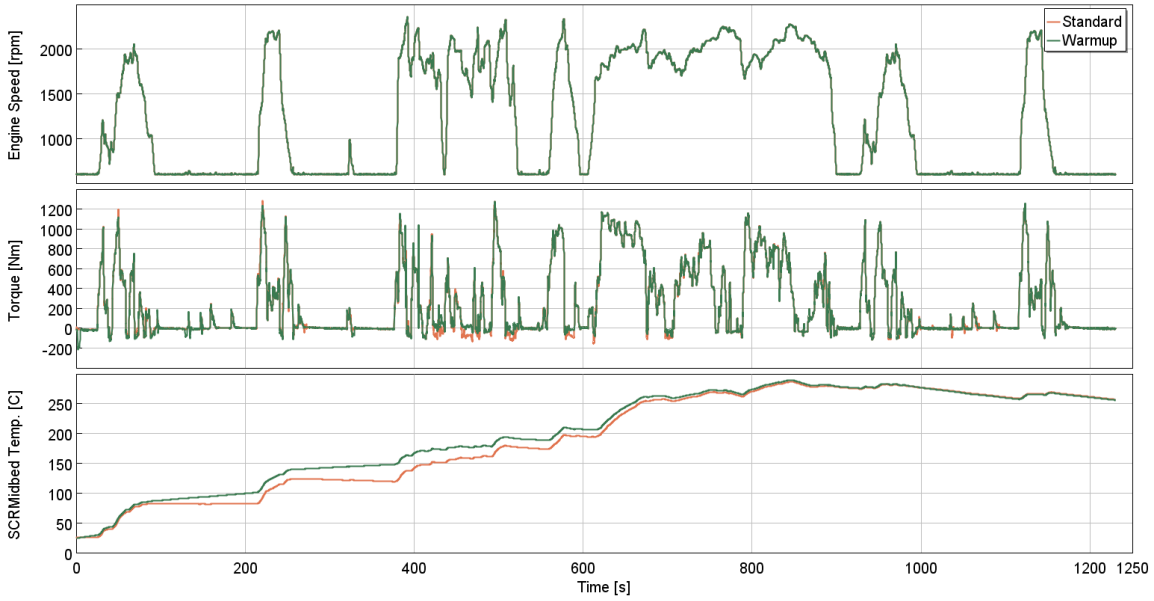

Figure 58 Comparison of engine speed, engine torque and SCR mid-bed temperature on the HDFTP cycle for the downsized engine with ITES system in standard operating mode and in SCR warmup mode.

Due to higher engine load-shift and TC turbine power in the warmup mode, the battery SOC increased during the initial SCR warmup phase, as shown in **Figure 59**. Correspondingly, the ITES motor-generator showed a higher generation power during the first 400 seconds of the HDFTP cycle in the warmup mode. Furthermore, the engine load shift also increased the engine fuel flowrate which contributed towards the faster rise in SCR mid-bed temperature. However, once the SOC increased beyond 0.8 and/or the SCR mid-bed temperature reached light-off temperature, the ECMS-based steady state control strategy reacted and reduced SOC down to the target level of 0.5. This was achieved through engine torque assist by the ITES motor-generator after 400 seconds in the HDFTP cycle. Towards the end of the cycle, the final SOC converged to the same value of 0.525 for both the standard mode and warmup mode cases.

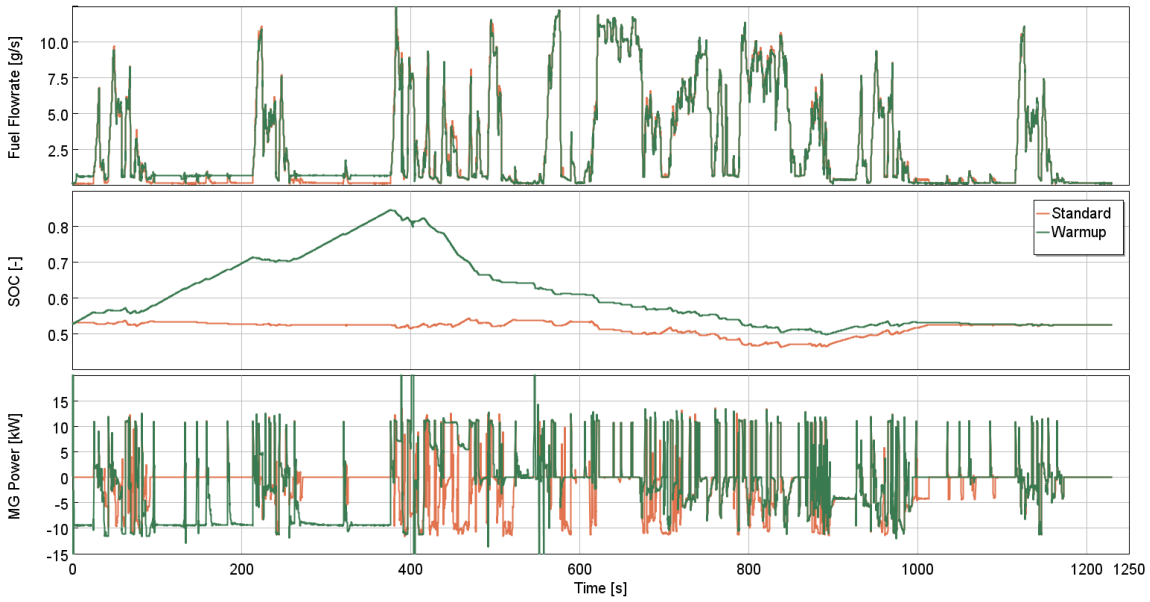

Figure 59 Comparison of fuel flowrate, battery SOC and ITES motor-generator power on the HDFTP cycle for the downsized engine with ITES system in standard operating mode and in SCR warmup mode.

Overall, a 73 second faster SCR light-off (>180°C mid-bed) could be achieved with the warmup mode calibration applied on the ITES system. Further reduction in SCR warm up time could have been achieved with injection timing retard, post injection and increased EGR rates. However, to quantify the aftertreatment warmup benefit with the ITES system only, these engine calibration changes were not investigated. As shown in **Figure 60**, the benefit in aftertreatment warmup time of 73 seconds was achieved with a 2.44% penalty in cycle-averaged fuel consumption and a 3.06% lower cycle-averaged engine out NOx emissions.

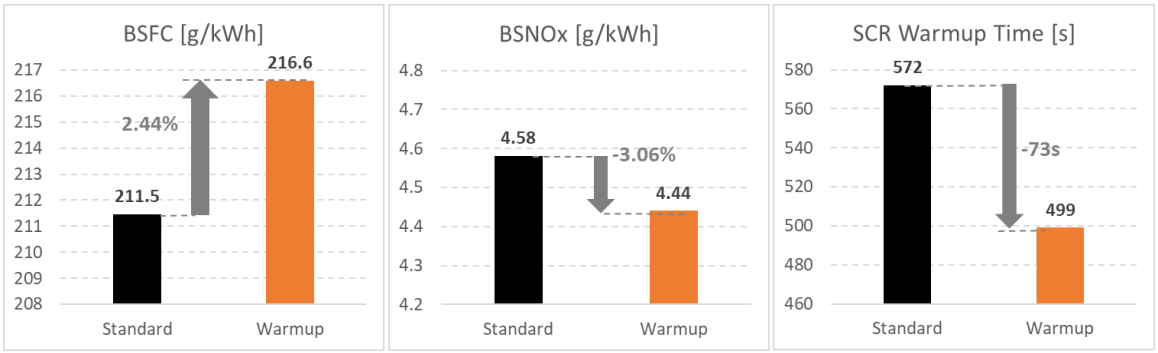

Figure 60 Comparison of cycle averaged BSFC, cycle averaged BSNOx and SCR warmup time on the downsized engine with ITES system in standard operating mode and in SCR warmup mode.

6 Vehicle Simulation Assessment

This chapter describes the vehicle simulations that were conducted to understand the potential benefits of the ITES technology in a medium-duty urban vocational application. Apart from reduction in vehicle fuel consumption, the performance and emissions impact of ITES technology were also assessed. As described in chapter 3, the FRM engine models of the baseline engine and the downsized engine with ITES system were integrated into a validated vehicle propulsion model (Appendix B) of the Freightliner M2 106 vehicle. The baseline engine model integration in the vehicle model was relatively straight-forward with simple integration of engine pedal and ignition control from vehicle ECU. However, for the downsized engine model with ITES system, the vehicle ECU model was expanded to include hybrid functions of start-stop, e-creep and regeneration, as described in section 4.4. The key specifications of the vehicle models applied in this simulation assessment have been shown in **Table 5**.

Table 5 Summary of vehicle and engine specifications applied in the simulation assessment.

Parameter	Validated Vehicle Model	Vehicle with Baseline Engine	Vehicle with Downsized Engine + ITES
Vehicle Type	Class 6-7 Urban	Class 6-7 Urban	Class 6-7 Urban
Chassis Weight	15,695 lbs	15,695 lbs	**15,530 lbs***
Payload	9,305 lbs	9,305 lbs	9,305 lbs
Engine Displacement	6.7 L	7.7 L	**5.1 L**
Rated Power	224 kW @ 2600 rpm	228 kW @ 2400 rpm	228 kW @ 2400 rpm
System Voltage	12 V	12 V	48 V
Transmission Type	Allison2000 (5 Spd)	Allison2000 (5 Spd)	Allison2000 (5 Spd)
Rolling Resistance Coefficient	0.009	0.009	0.009
Vehicle Aero-drag CdA	6.06 m^2	6.06 m^2	6.06 m^2
Final Drive Ratio	5.22	5.22	5.22
Tire Size	275/80 R22.5	275/80 R22.5	275/80 R22.5
Aux Load	2.35 kW	2.35 kW	2.35 kW

*75kg weight reduction due to downsizing (includes weight increase from ITES components)

First, the acceleration and top speed performance of the vehicle with the downsized engine was compared against that of the vehicle with the baseline engine. This was done to assess the impact of ITES system enabled engine downsizing on vehicle drivability. Thereafter, the vehicle models were simulated on ARB Transient cycle [3] to evaluate the fuel economy benefit of the downsized engine with ITES system, in comparison to baseline engine. The fuel economy benefit was broken down into contributions from engine

efficiency increase, engine start-stop and mild-hybrid functions (regen and e-creep). In the next step, the sensitivity of ITES system 48V battery capacity to fuel economy and battery life predictions was evaluated to determine the optimum battery size. Lastly, vehicle simulations were conducted on a real-world drive cycle to predict the fuel economy benefit of the downsized engine with the ITES system, and to verify the intended operation of ITES system control strategy.

6.1 Vehicle Performance

One of the primary challenges of engine downsizing is load response performance. With the ITES system enabled secondary compressor on the downsized engine, the load response of the downsized engine was expected to be similar to that of the baseline engine. Based on the simulation results shown in section 4.2 and 5.3, it could be concluded that the engine load response performance was very similar between the baseline and downsized engine. However, the final model-based assessment of this performance metric was done through vehicle acceleration simulation. As shown in **Figure 61**, the acceleration performance of the vehicle with downsized engine and ITES system was compared against that of the vehicle with the baseline engine.

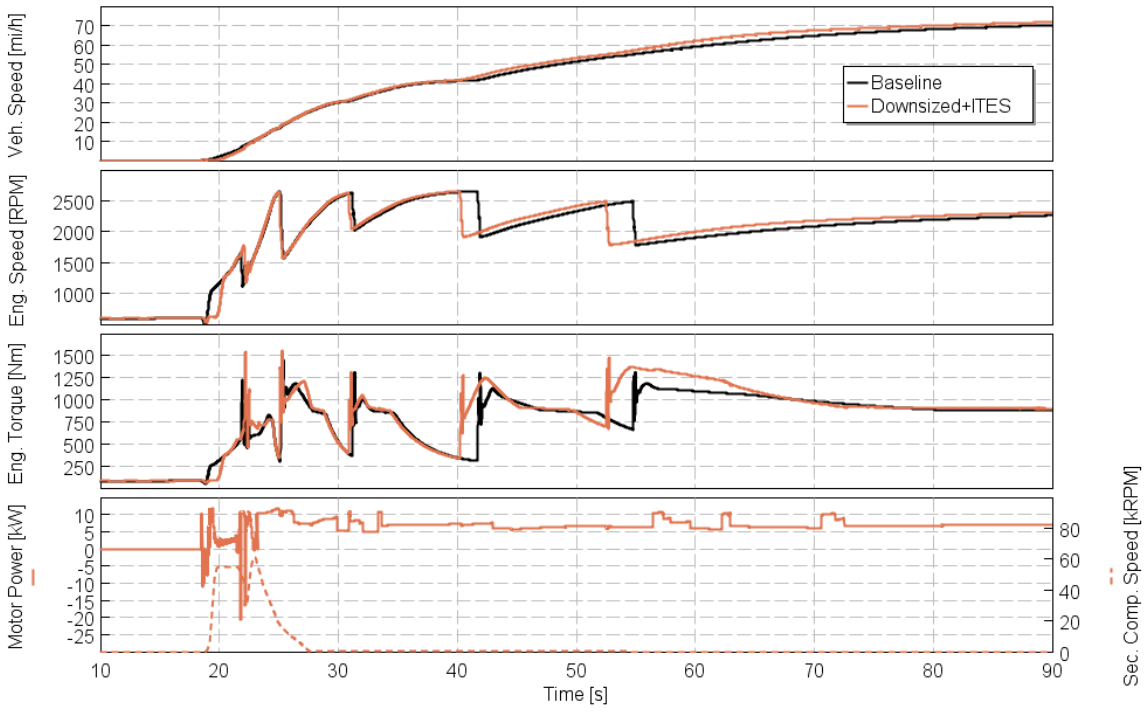

Figure 61 Acceleration performance comparison between vehicle with baseline engine and vehicle with downsized engine+ITES system.

The step change in accelerator pedal was applied at t=20s for both vehicles. As observed in engine speed and torque response plots, the baseline engine responded faster in the first 2 seconds due to higher engine displacement (higher charge air). However, as the ITES system ramped up the secondary compressor speed, the downsized engine was able to catch

up and eventually exceed the torque response of the baseline engine at around 25s. Once the engine transitioned above 1500rpm speed, wherein the secondary compressor was not needed, the ITES system switched to mode B and the ITES motor directly assisted the vehicle in acceleration. Overall, the vehicle with the downsized engine and ITES system was able to achieve a 0-60mph timing of 38.8s which was 3.7s faster than the vehicle with baseline engine. As shown in **Table 6**, while the acceleration performance was predicted to be better on the vehicle with downsized engine and ITES system, no noticeable difference was observed between the two vehicles on the maximum vehicle speed.

Table 6 Comparison of vehicle acceleration and top-speed performance between baseline engine and downsized engine with ITES system.

Performance Metric	M2 106 Vehicle with Baseline Engine	M2 106 Vehicle with Downsized Engine + ITES
Acceleration (0-60mph)	42.5	38.8
Top Speed	75.0	75.2

6.2 ARB Transient Cycle

The ARB transient cycle is a regulatory vehicle drive cycle that carries up to 92% weightage on vehicle greenhouse emissions for class 6-7 urban vocational applications [2, 3]. The cycle represents typical city driving at low speeds with frequent start-stop, acceleration and braking events, which makes it well suited for evaluation of potential fuel savings with electrified powertrains [8, 37, 45]. Both the models were simulated on this cycle and key performance metrics were compared. Since the vehicle with the downsized engine and ITES system enabled multiple ICE and mild-hybrid technologies, it was important to evaluate the contribution of each in the overall fuel economy benefit against vehicle with baseline engine. Furthermore, the breakdown of losses in each vehicle propulsion system component model were correlated to the predicted fuel economy benefit. Lastly, the impact of battery capacity variation on battery life and fuel economy was quantified and a method for selection of optimum battery capacity was proposed.

6.2.1 Fuel Economy Benefit Breakdown

In this section, a detailed analysis of the fuel economy benefit of the vehicle with the downsized engine and the ITES system has been presented. The vehicle model was first setup without any start-stop, e-creep or regenerative braking functions and simulated on the ARB transient cycle. The idea was to only quantify the fuel economy benefit from engine downsizing without any hybrid functionality. Thereafter, start-stop function was enabled in the control strategy and the ARB transient cycle simulation was run again. Lastly, the e-creep and regenerative braking functions were also enabled in the control strategy before running a final drive cycle simulation. The results from these three simulations on the vehicle model with the downsized engine and ITES system were

compared against those from the vehicle with the baseline engine. The four cases including baseline have been compared in **Figure 62** to **Figure 66**.

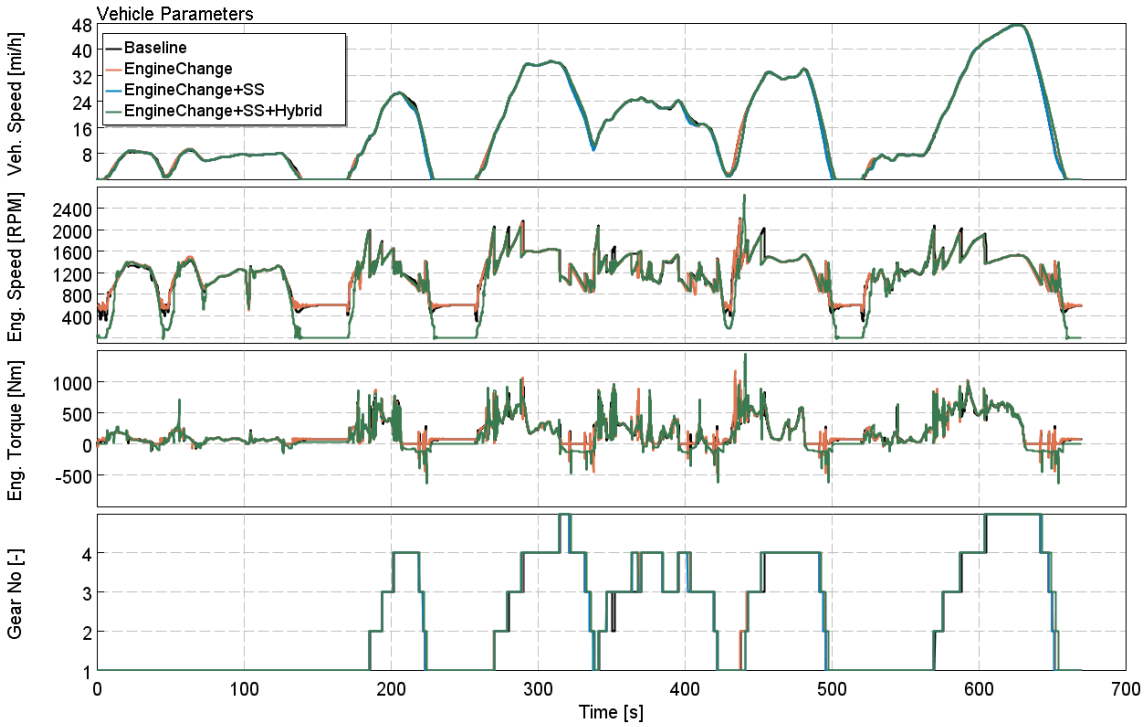

Figure 62 Comparison of vehicle speed, engine speed, engine torque and transmission gear number between vehicle with baseline engine and vehicle with downsized engine+ITES system run in multiple operating modes; EngineChange – engine downsizing with ITES system only, EngineChange +SS – engine downsizing and start-stop technology, EngineChange+SS+Hybrid – engine downsizing, start-stop, regeneration and e-creep.

Starting with **Figure 62**, vehicle speed comparison showed minor differences during vehicle launch, due to the lag from engine start-stop. Since the transmission and final drive ratio were kept consistent among the different cases, no significant differences were observed on the engine speed trace apart from portions with engine start-stop. With regards to engine torque at flywheel, the case with regeneration (hybrid) showed a lower torque during braking due to generation torque applied on the ITES motor-generator. Lastly, the gear shift strategy did not show much difference among the various configurations.

As shown in **Figure 63**, the cumulative CO2 emissions showed the expected trend of reduction with engine downsizing and hybrid system functionality. Similar trend was also observed for NOx emissions, except in the case with the addition of start-stop, wherein NOx emissions showed slight increase. This was due to the NOx spike resulting from high engine power demand right after engine start-up. Due to the delay from the engine startup event, higher engine torque was requested to catch up to the vehicle speed target profile. The SCR mid-bed temperature predictions showed an advantage on the downsized engine with ITES system (EngineChange) due to lower lambda values at lower loads. However, with the addition of engine start-stop functionality, the SCR mid-bed temperature reduced

due to engine stop events. Furthermore, with e-creep and regeneration functions, more torque assist was provided by the ITES motor which reduced engine load and hence exhaust temperature. Overall, the SCR mid-bed temperature could be maintained above activation temperature (~200°C) for all the configurations with downsized engine and ITES system.

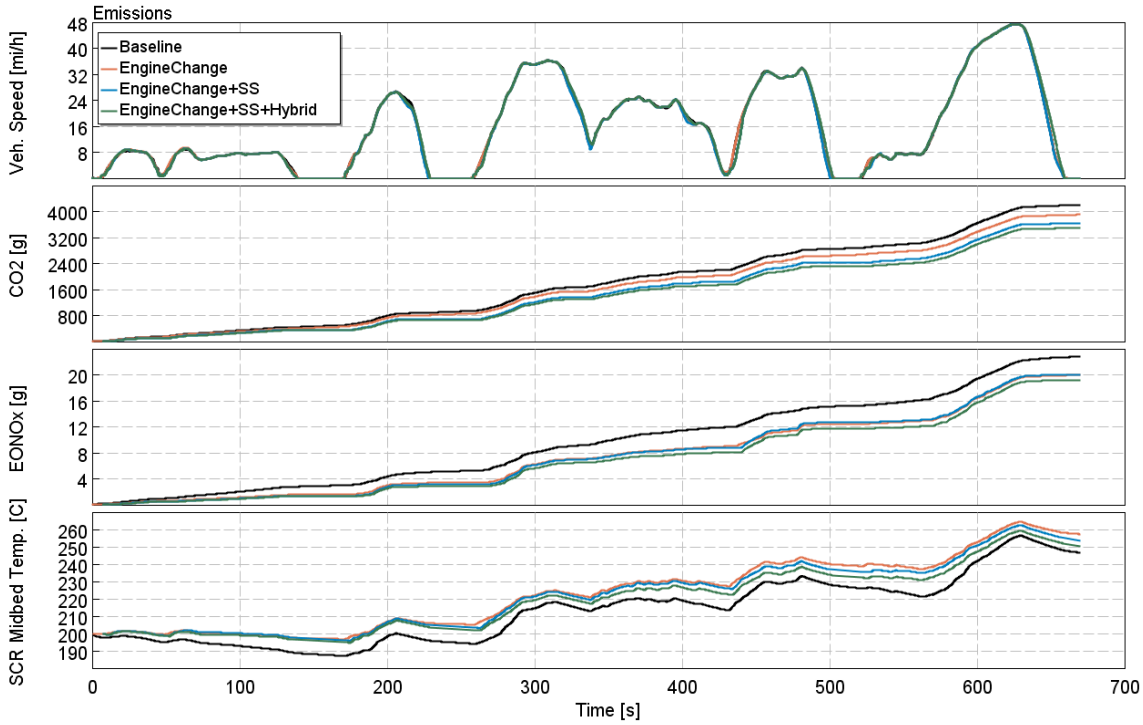

Figure 63 Comparison of vehicle speed, engine-out CO2 emission, engine-out NOx emission and SCR mid-bed temperature between vehicle with baseline engine and vehicle with downsized engine+ITES system run in multiple operating modes; EngineChange – engine downsizing with ITES system only, EngineChange +SS – engine downsizing and start-stop technology, EngineChange+SS+Hybrid – engine downsizing, start-stop, regeneration and e-creep.

Battery SOC was sustained in all the cases for the downsized engine with the ITES system. The target SOC was set at 55% while initial SOC was adjusted to make sure that SOC at end of the cycle was within 0.5% of initial SOC. As shown in **Figure 64**, minimal SOC variation was observed for the case with just the engine change wherein the ITES system was only operated to maximize engine efficiency and meet engine torque demands. With addition of engine start-stop function, electrical energy was consumed by ITES motor-generator during engine startup which led to a reduction in final SOC and hence in initial SOC. Lastly, for the case with full hybrid functionality of the ITES system, regeneration added energy into the battery leading to higher final SOC and hence higher initial SOC.

ITES motor-generator power showed the expected trend of increased regeneration and torque assist for the case with complete hybrid functionality. For the case with just start-stop function, SOC based regenerations were triggered by the ECMS strategy after an engine startup or a vehicle acceleration event. The ITES motor-generator was least used

for the case with just the engine change. For all the cases, the battery current followed the same trend as ITES motor-generator power and was maintained within operating limits calculated by the BMS. Similarly, the ITES motor-generator speed was within operating limits for all the cases. The ITES motor-generator operating speed was very similar between the different cases except during vehicle stops.

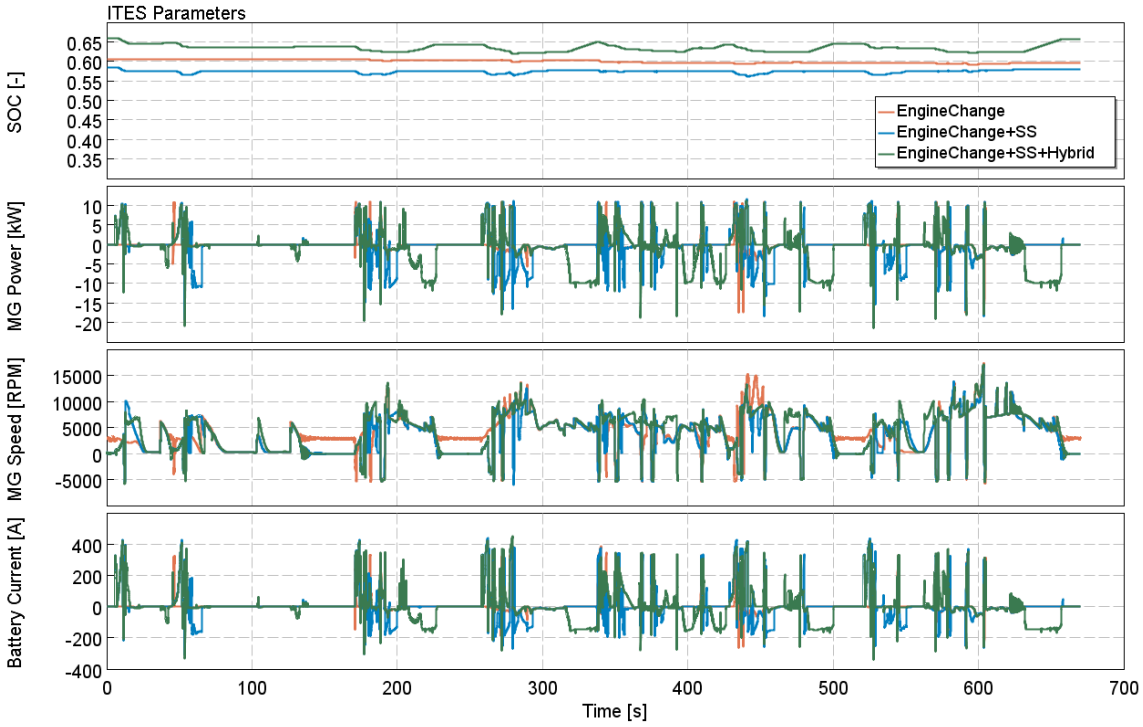

Figure 64 Comparison of 48V battery SOC, ITES motor-generator power, ITES motor-generator speed and 48V battery terminal current between different operating modes on the vehicle with downsized engine+ITES system; EngineChange – engine downsizing with ITES system only, EngineChange +SS – engine downsizing and start-stop technology, EngineChange+SS+Hybrid – engine downsizing, start-stop, regeneration and e-creep.

The cycle-averaged fuel economy and emission results from the analysis are shown in **Figure 65**. As indicated in **Figure 63**, incremental gains in vehicle fuel economy and CO2 emissions were observed with increase in ITES system hybrid functions. Fuel economy was calculated on miles-per-gallon equivalent (MPGe) basis with correction applied for initial and final SOC difference [37]. In comparison to the baseline vehicle, 6.7% increase in vehicle fuel economy was observed from engine downsizing, enabled by the ITES system. With engine start-stop, a further increase of 5.2% was observed in vehicle fuel economy which was similar to that observed by Lerin et al. [46]. Finally, with the full hybrid functionality of e-creep and regeneration, another 6.2% increase in fuel economy was observed. Overall, the vehicle model with the downsized engine and ITES system predicted a 19.3% increase in vehicle fuel economy and a 17.6% reduction in CO2 emissions over the vehicle model with the baseline engine.

With regards to engine out NOx emissions, a 12.2% reduction was observed from engine downsizing enabled by the ITES system, as shown in **Figure 65**. A slight increase in NOx emissions was observed with engine start-stop function due to rapid acceleration request by the driver model after delay from engine startup. The NOx spike from these transient events offset the benefits of zero idle-NOx emission. Lastly, the stored energy from regenerative braking was used to provide torque assist to the engine which led to reduced NOx emissions. Overall, a 16.2% reduction in engine out NOx emissions was predicted on the vehicle with downsized engine and ITES system in comparison to vehicle with baseline engine.

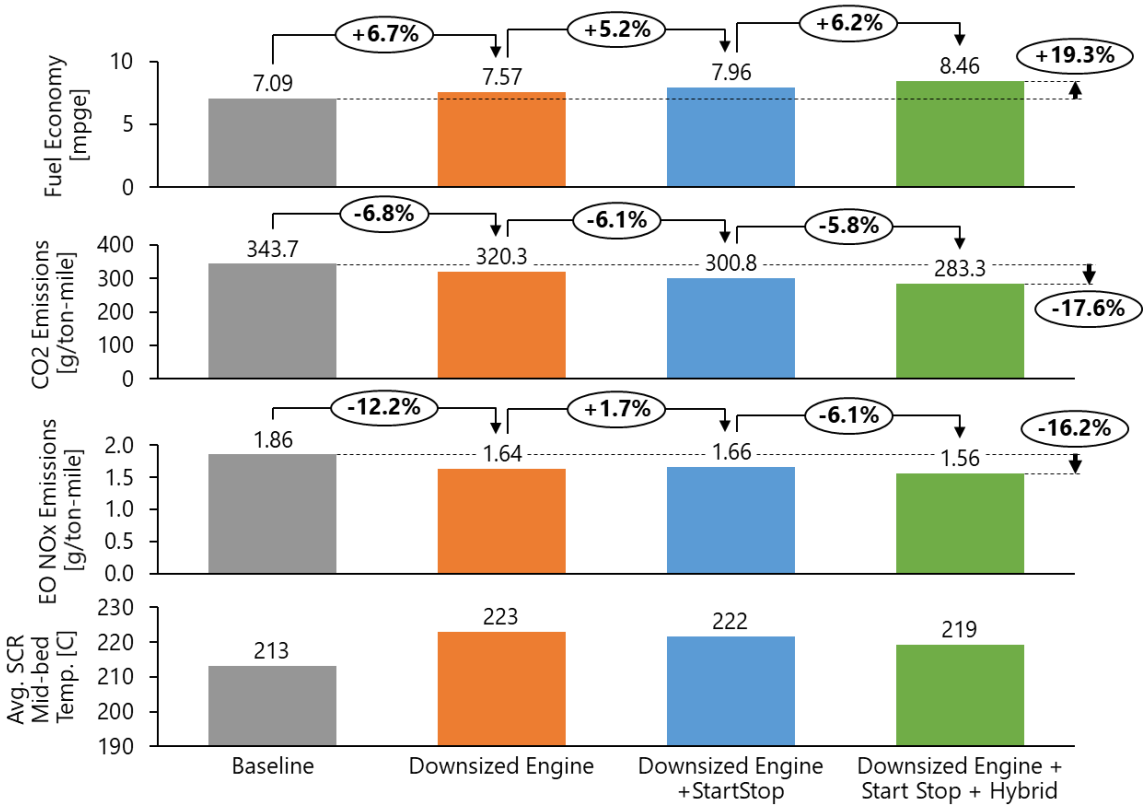

Figure 65 Comparison of cycle fuel economy, engine-out cumulative CO2 emission, engine-out cumulative NOx emission and average SCR mid-bed temperature between vehicle with baseline engine and vehicle with downsized engine+ITES system run in multiple operating modes; EngineChange – engine downsizing with ITES system only, EngineChange +SS – engine downsizing and start-stop technology, EngineChange+SS+Hybrid – engine downsizing, start-stop, regeneration and e-creep.

Since no detailed reaction-based aftertreatment models were developed as part of this research, tailpipe NOx emissions were not predicted. However, an empirical SCR mid-bed temperature model was implemented to predict the impact of different ITES system functions on aftertreatment thermal management. An increase in cycle-averaged SCR mid-bed temperature was predicted with engine downsizing due to reduction in engine displacement/air-fuel ratios. As expected with the engine start-stop and other hybrid functions, the cycle-averaged SCR mid-bed temperature reduced with increase in level of

hybridization. However, for all the cases with the downsized engine and ITES system, the cycle-averaged SCR mid-bed temperature stayed above that of the baseline engine.

To further analyze the overall fuel economy benefit of the vehicle with downsized engine and ITES system, the time distribution plots of engine operating maps were compared in **Figure 66**. The figure showed the three main effects of ITES system enabled mild-hybridization.

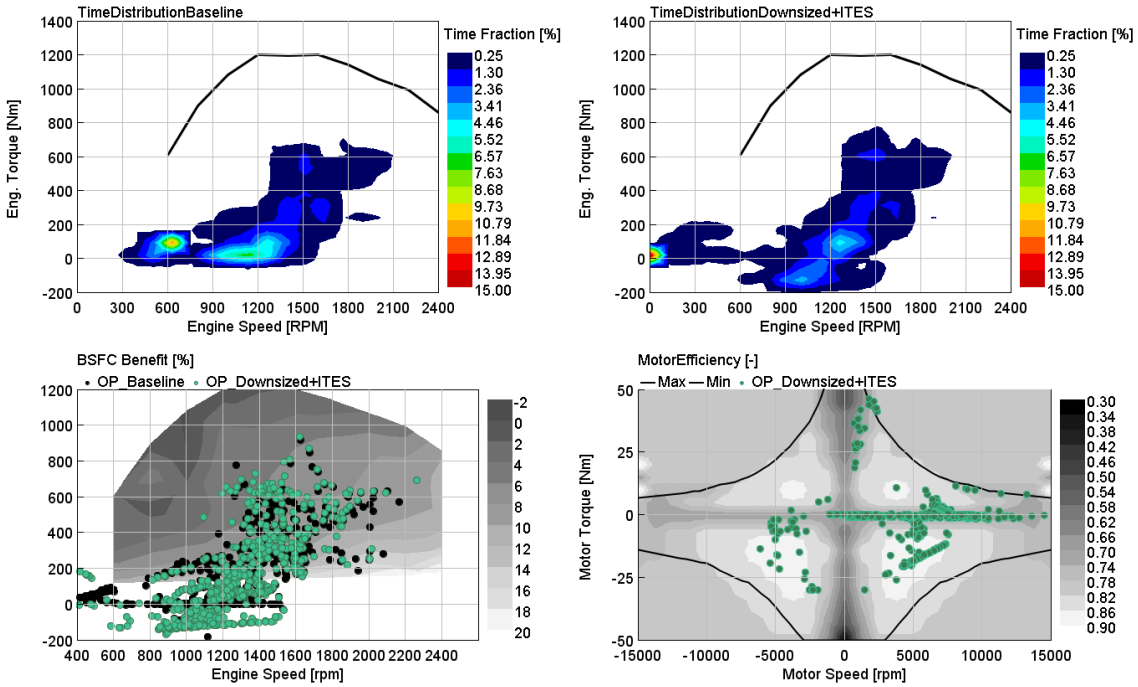

Figure 66 Time distribution and location of engine operating points on the baseline and the downsized engine with the ITES system (EngineChange+SS+Hybrid) for ARB transient cycle. ITES motor-generator operating points also shown on the motor-generator efficiency map.

First, due to engine start-stop operation, the operating region around engine idle was almost eliminated and moved to zero engine speed and load. This effect helped reduce fuel consumption due to reduced engine idle time when vehicle was not in motion. Secondly, engine operation around 900-1200rpm and 0-200Nm load on the baseline engine was redistributed on the downsized engine to higher engine loads, wherein the engine BSFC was much lower. This could also be observed on the BSFC benefit map which shows the operating point comparison between baseline engine and downsized engine with ITES system. This engine load-shift effect helped reduce cycle-averaged BSFC by operating engine at higher loads and storing the excess energy in the battery for later use during torque assist. Lastly, more negative torque operation on the engine was observed due to regenerative braking and e-creep. This could also be observed on the motor-generator operating points shown in the figure. With most operating points running in high efficiency region, the operating point spread confirmed that the ITES motor-generator and geartrain were well matched for the application. Overall, in addition to the existing benefit from

engine downsizing, mild-hybridization further reduced cycle-averaged BSFC through optimized engine operation with high motor-generator efficiency.

While the above analysis helped understand the efficiency gains from engine operation, a more detailed breakdown of vehicle losses in all the cases has been shown in **Figure 67**. As expected, the engine related losses such as exhaust energy, in-cylinder heat transfer and friction losses reduced from the baseline engine to downsized engine with all hybrid functions. The highest reduction was observed in friction and in-cylinder heat transfer losses for the downsized engine in comparison to the baseline engine. This was due to higher BMEP/mechanical efficiency and lower surface-to-volume ratio on the downsized engine. With the start-stop function, engine losses reduced due to lesser engine idling during vehicle stop events. Lastly, with e-creep and regeneration hybrid functions, energy recovered from vehicle braking could be utilized to provide torque assist to the engine, which led to reduced engine work/losses.

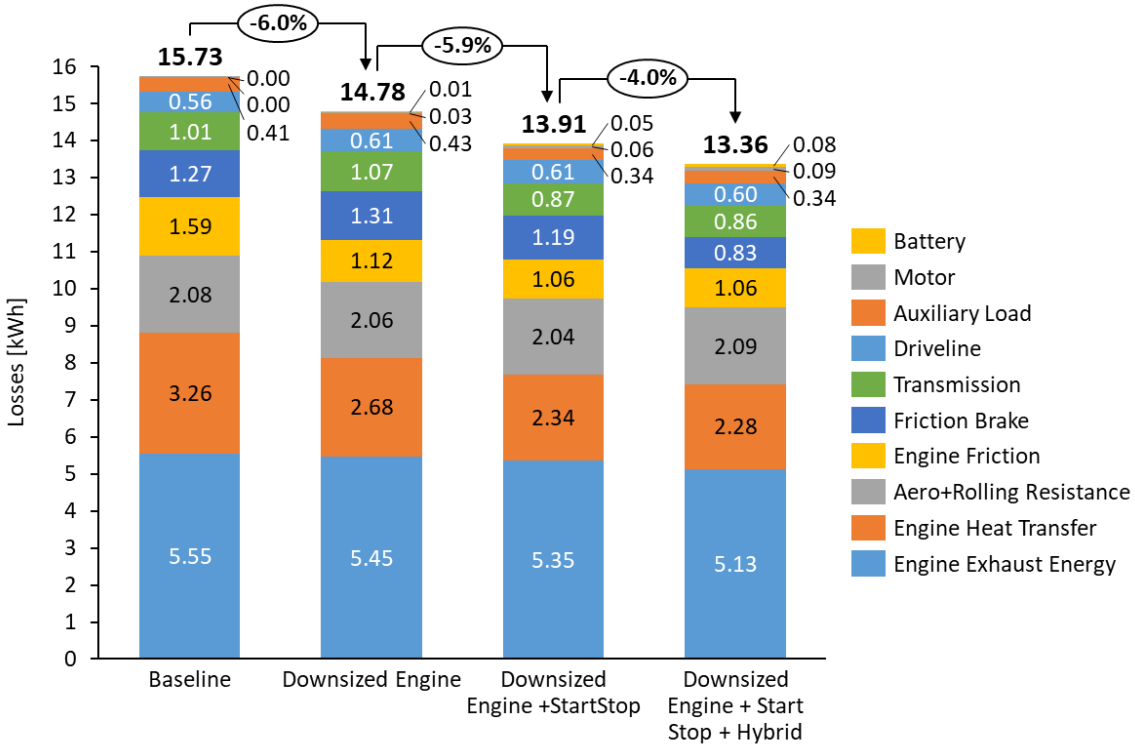

Figure 67 Comparison of energy losses between vehicle with baseline engine and vehicle with downsized engine+ITES system run in multiple operating modes; EngineChange – engine downsizing with ITES system only, EngineChange +SS – engine downsizing and start-stop technology, EngineChange+SS+Hybrid – engine downsizing, start-stop, regeneration and e-creep.

Other loss categories with significant variation amongst the different cases were friction brake, transmission and auxiliary load. Friction brake losses reduced with the addition of engine start-stop functionality as it triggered SOC based regeneration events. A considerable amount of electrical energy was consumed by the ITES motor-generator

during engine starting which led to a battery SOC reduction. The ECMS-based control strategy then reacted to the lower SOC and led to regeneration during idle/motoring thereby reducing friction brake losses. For the last case, with the addition of regenerative braking, the vehicle kinetic energy was recuperated by the ITES motor-generator and hence the friction brake losses were reduced. With regards to the transmission losses, a step change was observed with engine start-stop function, wherein the losses from torque converter during engine idle were reduced. A similar impact was observed on the losses due to engine auxiliary load. These losses also reduced due to reduction in engine idle duration over the cycle. Overall, 15.9% reduction in losses were observed on the vehicle with the downsized engine and ITES system in comparison to the vehicle with the baseline engine. The analysis showed the significant opportunity ITES system presents in improving vehicle fuel economy without an adverse impact on emissions and aftertreatment system temperature.

6.2.2 Battery Size Optimization on Drive Cycle

In all previous analysis in this study, 48V LFP battery pack size of 32Ah (14s4p) was selected to match the ITES motor-generator power capabilities. However, a battery optimization method has been proposed to best balance battery size/cost/weight, battery life, vehicle performance and fuel economy. Since the ARB transient cycle is the most representative vehicle drive cycle for this application, battery capacity of the vehicle with the downsized engine and ITES system was swept from 24Ah to 48Ah (14s3p to 14s6p). As shown in **Figure 68**, the vehicle speed following was very similar for all battery capacities equal to or greater than 32Ah. However, for 24Ah battery capacity, slower vehicle speed response was observed after vehicle start from standstill. The engine speed traces were very similar for the different battery pack sizes except during the phases with the lower vehicle speed response for 24Ah battery pack. The key difference among the different battery pack sizes was observed on the ITES motor-generator power during vehicle braking events. While the peak motoring power of the ITES motor-generator was very similar between the different battery pack sizes, much higher continuous generation power could be achieved with larger battery size. This was due to higher continuous charging current limit with larger battery capacity (10C charge/discharge).

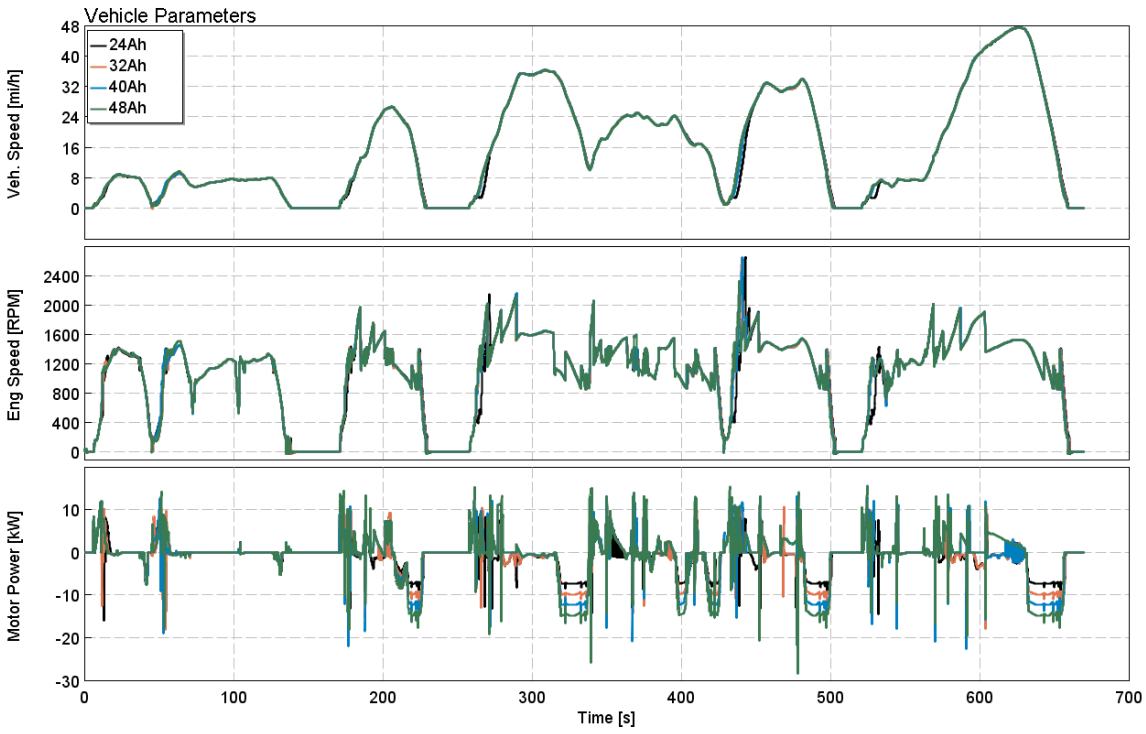

Figure 68 Comparison of vehicle speed, engine speed and ITES motor-generator power between multiple battery capacities on the ARB transient cycle for the vehicle with downsized engine and ITES system.

Initial battery SOC was adjusted in the simulation to match final SOC within 0.5%. As shown in **Figure 69**, initial SOC was lower for lower battery capacity due to lower level of brake regeneration/energy storage over the cycle. Furthermore, lower battery capacities also saw larger SOC variation over the cycle. Consistent with the observations made on ITES motor-generator power, higher charging current was observed on the larger battery packs, as shown in **Figure 69**. The figure also showed reduced voltage variation over the cycle for larger battery packs due to lower pack resistance. Overall, with increase in battery pack size, higher charging current and regeneration energy could be achieved, with a reduction in battery voltage and SOC variation over the drive cycle.

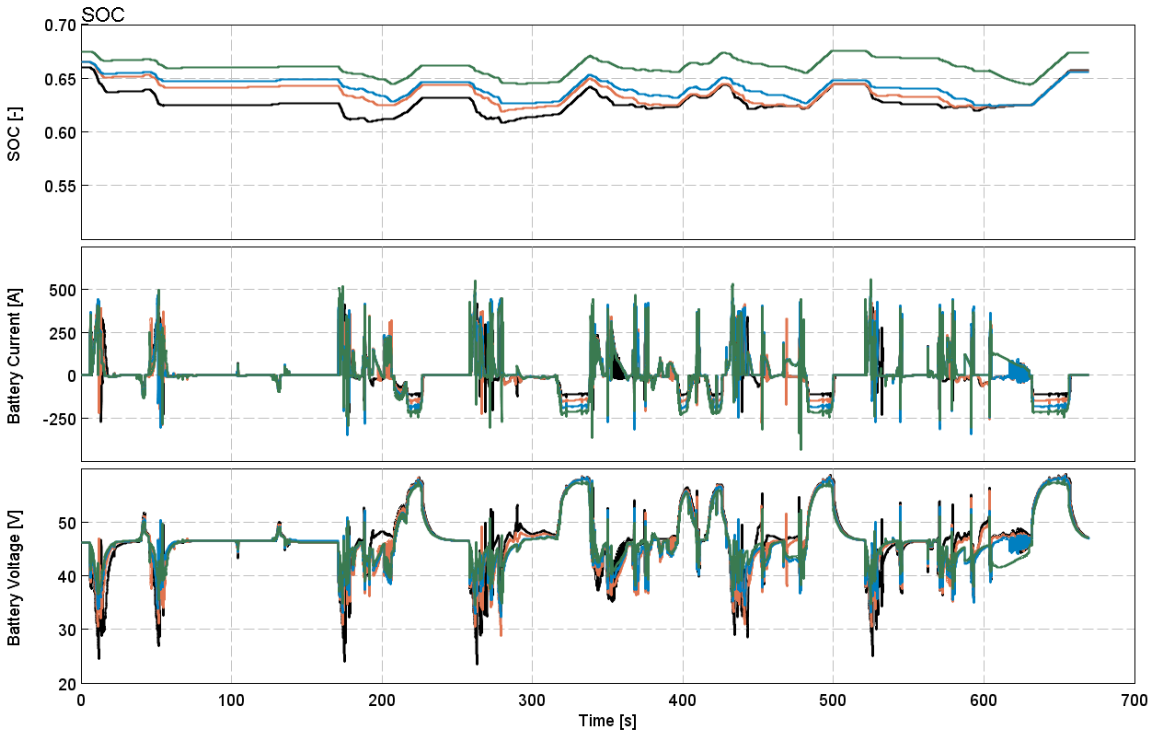

Figure 69 Comparison of SOC, battery current and battery voltage between multiple battery capacities on the ARB transient cycle for the vehicle with downsized engine and ITES system.

Based on the assessments above, it would be desirable to use the largest battery size to maximize performance, minimize battery voltage variation and minimize battery SOC variation. However, due to battery cost, weight and packaging, an optimum size needs to be determined that meets the vehicle requirements of battery life, fuel economy and performance. While fuel economy and performance predictions are relatively straight-forward, battery life was predicted using empirical correlation developed by Wang et al. [39] as shown below. This aging model was implemented to predict irrecoverable battery capacity loss after 8 years or 192,000 miles of operation (24,0000 miles/year). Since ARB transient cycle is considered representative of 90% of vehicle driving [2], the aging calculation was made with the assumption that this drive cycle was run repeatedly until end of useful life.

$$Q_{loss} = B \times e^{\left(\frac{-31700+370.3\times Crate}{RT}\right)} \times {A_h}^{0.55} \text{ [39]}$$

Where:

Q_{loss} is irrecoverable battery capacity loss after specified cycles

$A_h = cycles \times DOD \times 2$

B = [31,630 21,681 12,934 15,512] corresponding to Crate of [C/2 2C 6C 10C]

R is Universal gas constant

T is Battery operating temperature

DOD is depth of discharge (maxSOC-minSOC during drive cycle)

The battery cycles and C-rate calculations were implemented in the model using the following equations.

$$Cycles = \frac{Useful\_Life\_Dist.\,[miles]}{ARB\_Transient\_Cycle\_Dist.\,[miles]} \times \frac{Cycle\_Charge\_Throughput\ [Ah]}{2 \times Battery\_Capacity\ [Ah] \times 0.8}$$

$$Crate = \frac{abs(Battery\_Current)}{Battery\_Capacity}$$

Except for the 24Ah pack, the cycle-following performance of the different battery pack sizes was very similar. To narrow down the battery size selection, fuel economy and battery life were compared amongst the different battery packs, as shown in **Figure 70**.

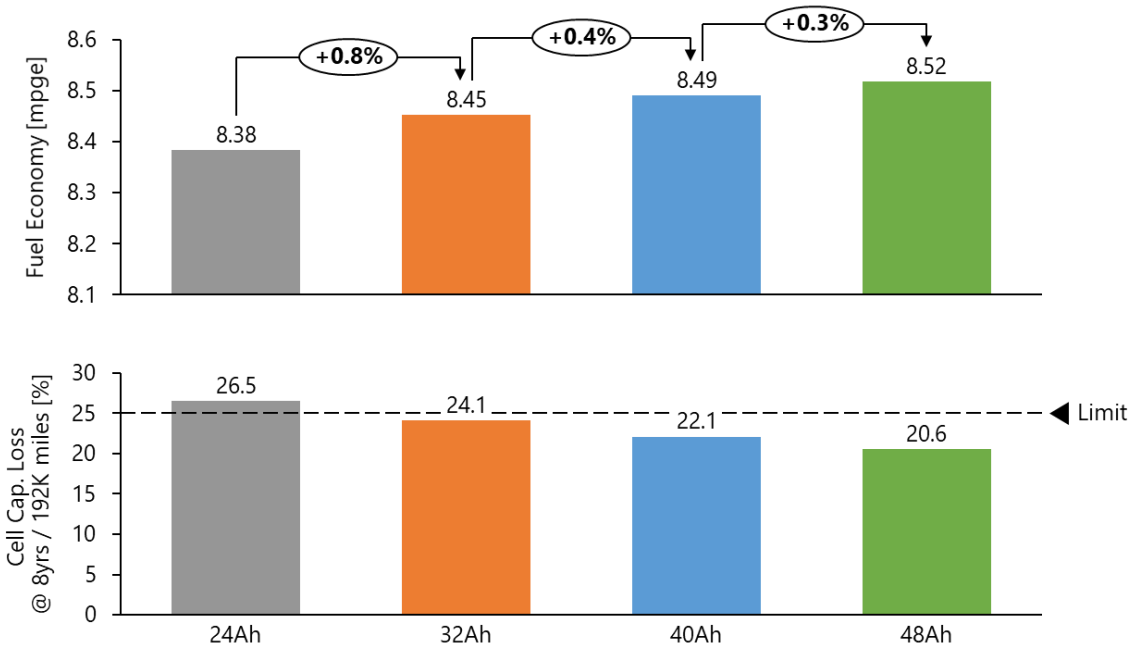

Figure 70 Comparison of fuel economy and battery life between multiple battery capacities on the ARB transient cycle for the vehicle with downsized engine and ITES system.

As expected, fuel economy increased with increase in battery pack size due to increase in total energy captured from regeneration. However, the incremental gains reduced with every step increase in battery capacity. It was observed that marginal gains in fuel economy were observed above 40Ah capacity and it could be estimated that above 60Ah capacity, no further increase in fuel economy would be observed. In terms of battery life, the irrecoverable battery capacity loss reduced linearly with increase in battery pack size. This was due to reduction in C-rate, battery depth of discharge and battery cycles with increase in battery capacity. While no strict threshold has been defined in the heavy-duty industry, typical criteria for battery life is considered to be >75% recoverable battery capacity at end of useful life [47]. Although the battery pack capacity of 32Ah showed an acceptable

battery capacity degradation at the end of useful life, 40Ah pack capacity was finally selected to account for modeling error, battery temperature variation throughout useful life and uncertainty in prediction of real-world usage. Overall, the 40Ah battery pack size was selected as the optimum to maximize performance, fuel economy and battery life while minimizing battery cost, weight and packaging volume.

6.3 Real-World Drive Cycle

In the last step of this research, a final assessment of the benefits and functionality of ITES system was done on a real-world drive cycle. To develop a representative drive cycle for class 6-7 urban vocational application, a driving route for a Fedex distribution center truck around Ann Arbor area in Michigan, USA was selected. The vehicle speed and grade profiles for the route were generated using GT-RealDrive tool as shown in **Figure 71**. The speed profile shows the expected drive cycle dynamics of low-speed driving with frequent start-stops. The total length of the drive cycle was 23.6 miles with an average speed of 14.7 miles per hour.

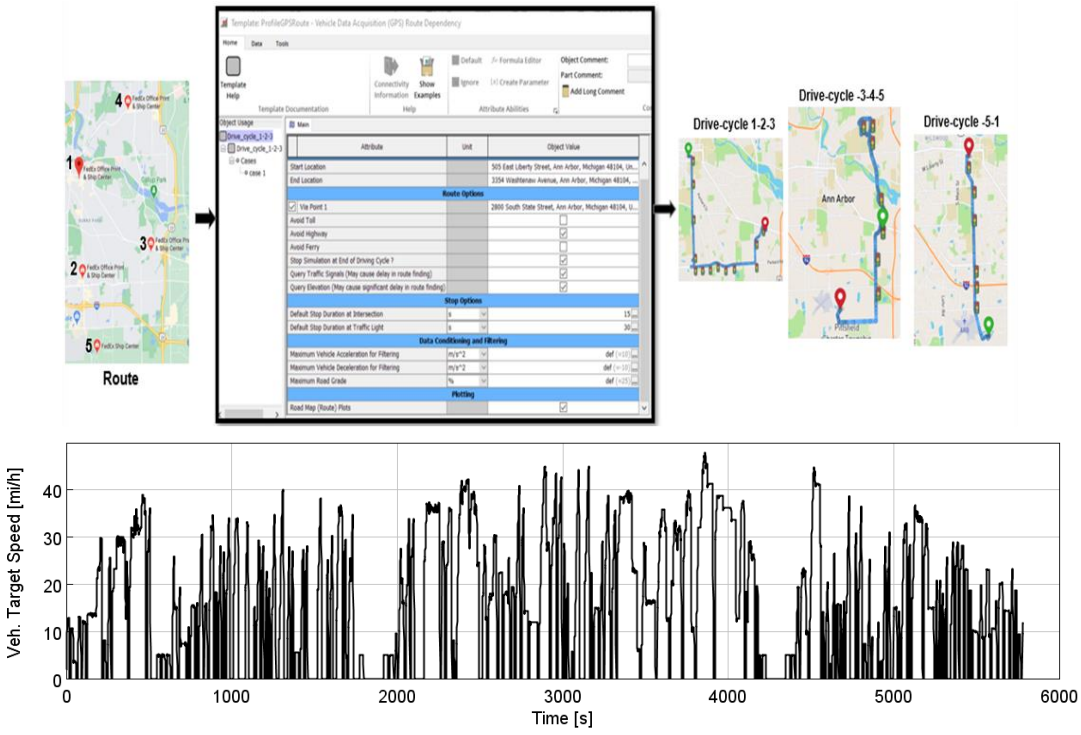

Figure 71 Vehicle drive cycle generation using GT-RealDrive tool for a facility-to-facility Fedex distribution truck operated around Ann-Arbor Michigan USA.

Once the drive cycle was developed, both the baseline vehicle and the vehicle with downsized engine and ITES system were simulated on this real-world drive cycle. The drive cycles were setup as a function of distance and subjected to same acceleration and deceleration constraints. As shown in **Figure 72**, both the vehicles were able to follow the drive cycle and meet mission time. Based on findings in section 6.2, the vehicle with downsized engine and ITES system was simulated with a 40Ah battery capacity. As shown

in the figure, the battery SOC was sustained well during the drive cycle which helped verify the feasibility of ECMS-based supervisory control algorithm for ITES system. Figure 73 Control mode distribution over the real-world drive cycle.The trend in SOC could be further confirmed by the ITES motor-generator operation, wherein similar motoring and generating power was observed on the drive cycle. Furthermore**,** the ECMS-based optimal hybrid strategy was active for 42.2% of the drive-cycle time, as shown in **Figure 73.** The transient override of this optimal control algorithm occurred for 14.3% (=7.0% / (42.2%+7.0%)) of the time when the hybrid mode (**Table 4**) was active during the real-world drive cycle.

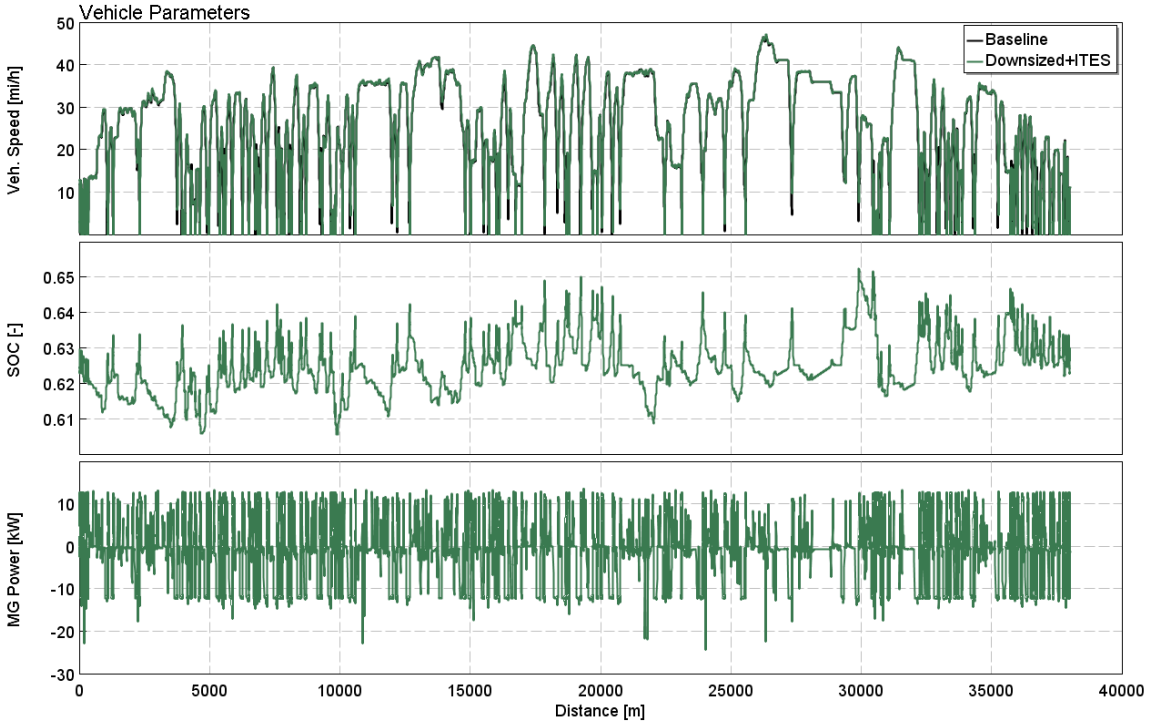

Figure 72 Comparison of vehicle speed between the baseline vehicle and the vehicle with the downsized engine and ITES system on the real-world drive cycle. 48V battery SOC and ITES motor-generator power also shown for the vehicle with downsized engine and ITES system.

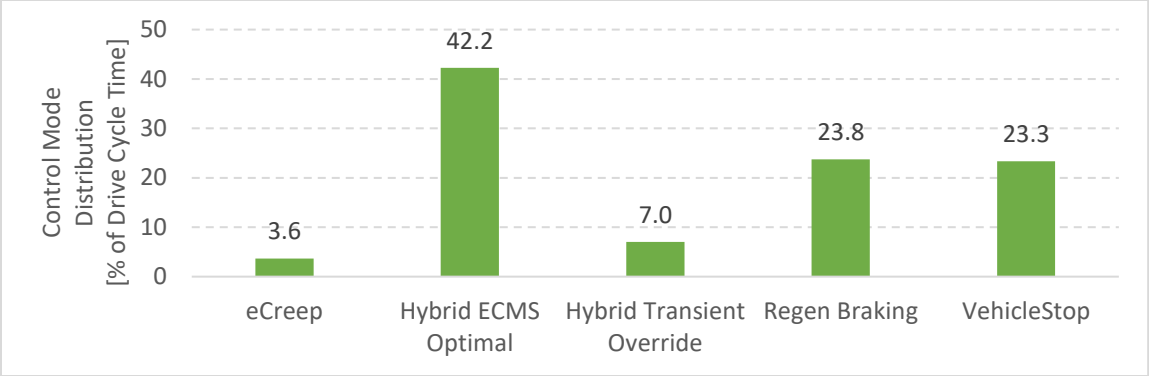

Figure 73 Control mode distribution over the real-world drive cycle.

The cumulative fuel consumption and NOx emissions are shown in **Figure 74**. The reduction in fuel consumption on the vehicle with the downsized engine and ITES system was primarily observed during stop-go sections of the drive cycle. The engine out NOx emissions also reduced during stop-go sections of the drive cycle. However, due to higher engine out NOx emissions at higher engine speed and loads, the overall NOx emission reduction on the downsized engine with ITES system was relatively lower. **Figure 74** also shows that no significant difference was observed on the SCR mid-bed temperature between the two cases. Even during stop-go operation, the SCR mid-bed temperature could be maintained above 220°C on the downsized engine with the ITES system.

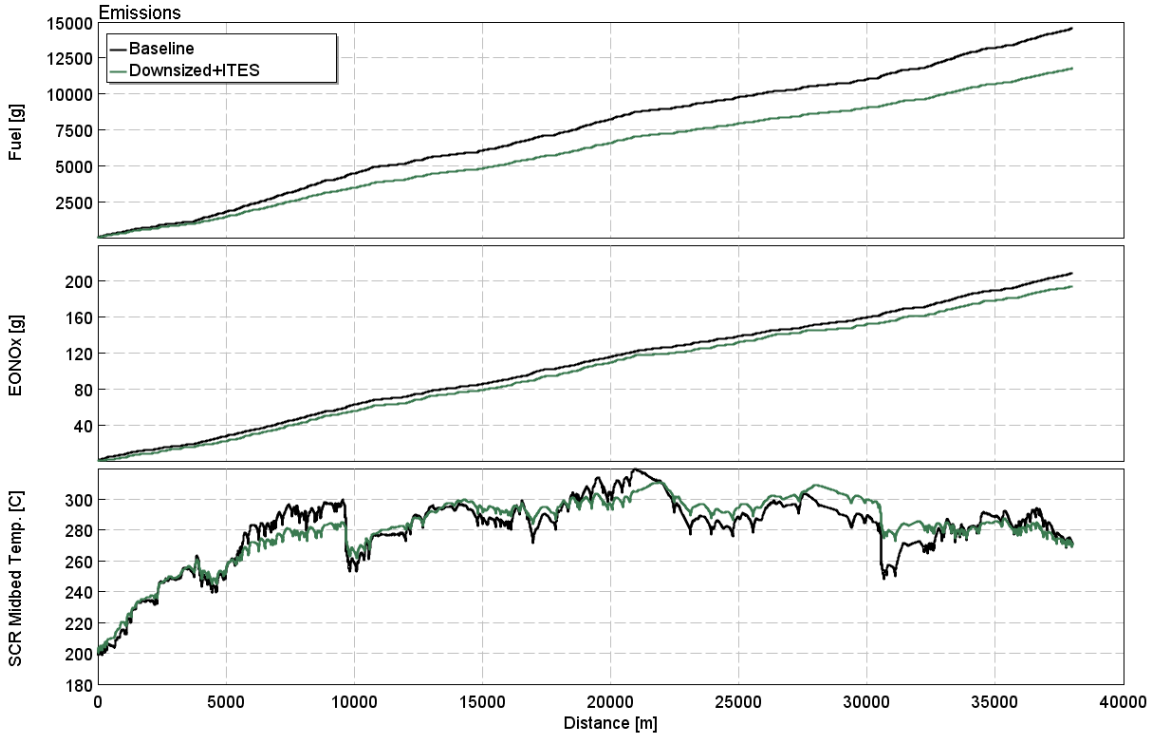

Figure 74 Comparison of fuel consumed, engine out NOx and SCR mid-bed temperature between the baseline vehicle and the vehicle with the downsized engine and ITES system, on the real-world drive cycle.

The cycle-averaged performance metrics have been compared between the baseline vehicle and the vehicle with downsized engine and ITES system in **Figure 75**. In comparison to the ARB transient cycle, a higher fuel economy benefit of 23.7% was observed on the real-world drive cycle, due to more frequent stop-go operation. A marginal reduction of 7.3% in engine-out NOx emissions with higher SCR mid-bed temperature was observed on the vehicle with the downsized engine and ITES system. Hence, it could be concluded that no increase in tailpipe emissions was predicted for the downsized engine with the ITES system. Lastly, since the drive cycle was run as a distance vs speed target profile, it was verified that no reduction in mission time was observed on the vehicle with the downsized engine and ITES system in comparison to baseline.

Overall, the assessment showed that the ITES system could enable engine downsizing and mild hybridization to significantly reduce vehicle fuel consumption on real-world drive cycle, while maintaining baseline performance and emissions.

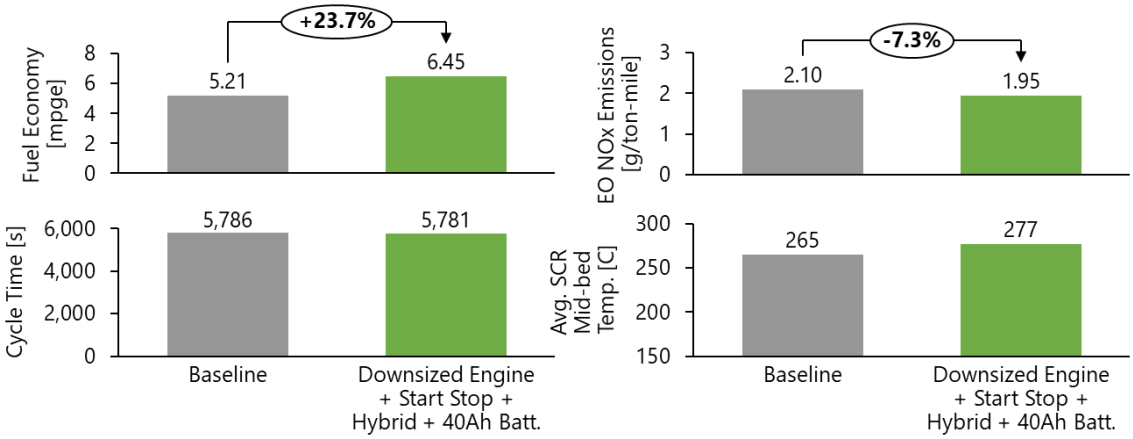

Figure 75 Comparison of fuel economy, cycle duration, engine out NOx emissions and average SCR mid-bed temperature between the baseline vehicle and the vehicle with the downsized engine and ITES system, on the real-world drive cycle.

7 Conclusions and Future Work

To summarize this research, multiple concepts for integration of turbogeneration, supercharging and mild hybridization technologies on an internal combustion engine were first explored through a qualitative analysis. Thereafter, the leading concept (ITES system) was down-selected and further developed through model-based assessment. A baseline 1D multi-physics engine model for a 7.7L 6-cylinder medium heavy-duty diesel engine, applied in Class 6-7 vocational truck, was developed and validated against test data in GT-SUITE. Using the same modeling method, a multi-physics model of the ITES system was developed and integrated into a downsized 5.1L 4-cylinder version of the medium heavy-duty diesel engine model.

Once a system level model of the concept was developed, a model-based method for sizing and optimization of geartrain, secondary compressor, turbogeneration turbine, motor-generator and battery was proposed. The methodology was then applied to size the ITES system components for the 5.1L downsized 4-cylinder engine and verified through steady state engine simulation.

In parallel, a control strategy based on equivalent fuel consumption (battery + fuel) minimization was developed to determine optimal ITES system operating mode and motor torque. While the strategy worked well in steady state operation, slow engine torque response and mode-switch related torque spikes were observed during transient engine operation. The control strategy was expanded to include transient and mode-switch control functions to address these concerns. The methods applied were verified through transient engine simulation. Lastly, the control strategy was expanded to include mild-hybrid functions such as start-stop, regeneration, e-creep and torque assist for vehicle integration.

With the ITES component sizes optimized and robust control strategy developed, the performance and emissions benefit of the integration technology was evaluated through engine and vehicle simulation. Steady state engine simulation assessment showed that, in comparison to the baseline 7.7L engine, the downsized 5.1L engine with the ITES system could achieve 6.3% reduction in fuel consumption and 0.32g/kWh reduction in engine out NOx emissions. Furthermore, the downsized engine with ITES system was able to meet the baseline engine air-fuel ratio and full load torque targets. The assessment also showed that, in comparison to independent integration of technologies, the ITES system could achieve similar or better (up to 2%) benefit in engine fuel consumption during steady state operation.

As the future tailpipe emission regulations continue to get more stringent, the impact of ITES system on aftertreatment temperature and its capability in aftertreatment warmup was also assessed through steady state simulation. The downsized engine with ITES system consistently showed lower exhaust temperatures at higher engine speed and loads due to higher engine efficiency and two stage turbocharging. However, at lower loads, the ITES system enabled an efficient control authority over air/fuel flow to enable faster aftertreatment warmup and temperature-hold. At higher engine speed and low loads, the ITES system was able to control turbocompound turbine speed to reduce airflow, increase

fuelflow and increase exhaust temperature. At lower engine speed and loads, the ITES system was able to load-shift the engine to increase fuelflow, exhaust temperature and exhaust massflow rate. The assessment showed that at lower engine loads, the ITES system could achieve 50-100°C increase in aftertreatment inlet temperature, at a lower fuel penalty than that incurred with exhaust flap and exhaust VVT technologies.

Next, transient HDFTP cycle engine simulations were conducted to verify ITES system functionality, predict cycle-averaged fuel consumption, predict cycle-averaged NOx emissions, and aftertreatment warmup performance. With the robust control strategy, no concerns were identified in ITES system operation over transient cycle. The control strategy also resulted in a battery charge sustain over the HDFTP cycle. Overall, the downsized engine with the ITES system showed a 8.45% benefit in fuel consumption over the baseline engine, while maintaining engine-out NOx emissions and cycle regression within 1%. In terms of aftertreatment temperature, the downsized engine with ITES system did show lower SCR mid-bed temperatures during high speed and load operation on the HDFTP cycle. However, the SCR mid-bed temperature was still predicted to be above SCR light-off temperature throughout the hot-start HDFTP cycle. A separate assessment was made to understand the potential benefit of ITES system-based aftertreatment thermal management during cold-start FTP cycle. The simulation results showed that with the ITES system enabled aftertreatment thermal management functions, the SCR light-off time and engine-out NOx could be reduced by 73s and 3% respectively, at a moderate fuel consumption penalty of 2.44%.

To continue the model-based verification process, vehicle simulations were conducted to further evaluate ITES system control strategy, fuel economy benefit, emissions impact and vehicle performance with the downsized engine and ITES system. A baseline dynamic 1D vehicle propulsion system model of a Freightliner M2 106 truck was developed and validated against test data. Thereafter, the sub-models for the baseline engine and the downsized engine with ITES system were integrated into the vehicle model. The two vehicle models were then simulated on acceleration performance cycle, regulatory ARB transient cycle and a real-world drive cycle for Class 6-7 vocational application truck. The simulation results showed that the downsized engine with ITES system was able to achieve a 3.7s faster 0-60mph time of 38.8s in comparison to the vehicle with baseline engine. This was enabled by the higher boosting capability of the ITES system as well as torque assist from the ITES motor.

Once the vehicle performance was predicted to be acceptable, dynamic vehicle drive cycle simulation was run on the ARB's transient cycle which carried up to 90% weightage in GEM fuel economy calculations for vocational trucks. The ARB transient cycle simulation results showed that the vehicle with the downsized engine and ITES system could achieve a 19.3% increase in vehicle fuel economy in comparison to baseline vehicle. The breakdown of fuel economy benefit showed 6.7% increase from engine downsizing, 5.2% from engine start-stop and 6.2% from mild-hybrid functions. Due to engine start-stop and load-shift, engine out NOx emissions was also predicted to be reduced by 16.2% without any reduction in cycle averaged SCR mid-bed temperature.

While the ITES components had been sized much earlier in the research study, a final battery sizing methodology was proposed and applied during ARB transient cycle assessment. Since the drive cycle represented 90% of all expected driving scenarios (GEM tool weightage), the cycle could be used as a target cycle to determine cycle energy needs and predict battery life. Initially, a battery size of 32Ah was selected to meet the power demand of the 15kW ITES motor-generator unit. However, the vehicle drive cycle-based sizing analysis showed that a battery capacity of atleast 40Ah was needed to achieve 8 years of battery life with a target recoverable capacity of 80%. Furthermore, the fuel economy benefit increased with increase in battery capacity however beyond 40Ah no significant increase in fuel economy was predicted. Overall, after the battery re-sizing, the vehicle with downsized engine and ITES system predicted a 19.7% increase in fuel economy over baseline vehicle on the ARB transient cycle.

Lastly, a real-world drive cycle was developed using GT-RealDrive tool by extracting vehicle speed profile as a function of distance for a Fed-ex delivery truck operating in Ann Arbor city area in Michigan, USA. Both the vehicle models were then simulated on the real-world drive cycle for performance comparison. Due to higher kinetic intensity and start-stop nature of the real-world cycle, an even higher benefit of 23.7% in fuel economy was predicted on the vehicle with the downsized engine and ITES system, in comparison to baseline vehicle. Along with the significant fuel economy benefit, a 7.3% reduction in engine out NOx emissions was also predicted for the vehicle with the downsized engine and the ITES system. With regards to cycle following, both vehicles were able to follow the speed targets well and achieve an overall mission time within 5 seconds of each other. Overall, the simulation results verified the successful operation of ITES system and the robustness of control strategy in sustaining charge on real-world cycle.

Future work would include further development of the ITES system through hardware development, engine testing and build-up of a demonstrator vehicle. With the development of high efficiency fuel agnostic powertrains (especially H2 ICE) in the future, the ITES system can prove to be highly instrumental in achieving low-cost mild-hybridization, higher engine power density, fast transient engine response, lower GHG emissions and ultra-low NOx emissions.

8 Reference List

[1] Federal Register / Vol. 77, No. 199 / Monday, October 15, 2012 / Rules and Regulations 49 CFR Parts 523, 531, 533. et al. and 600 2017 and Later Model Year Light-Duty Vehicle Greenhouse Gas Emissions and Corporate Average Fuel Economy Standards; Final Rule

[2] Federal Register / Vol. 81, No. 206 / Tuesday, October 25, 2016 / Rules and Regulations Greenhouse Gas Emissions and Fuel Efficiency Standards for Medium- and Heavy-Duty Engines and Vehicles— Phase 2

[3] Greenhouse Gas Emissions and Fuel Efficiency Standards for Medium- and Heavy-Duty Engines and Vehicles - Phase 2, Regulatory Impact Analysis, EPA, NHTSA, EPA-420-R-16-900, August 2016

[4] Yoon, K., Hong, J., and Shim, J.Y., "A Study on Front End Auxiliary Drive(FEAD) System of 48V Mild Hybrid Engine," SAE Technical Paper 2018-01-0414, 2018, doi:10.4271/2018-01-0414.

[5] Drury, W., Patel, C., Atkins, A., and Wearing, A., "High Power Density, 48V Electrified Drivetrain Technology for Future Hybrid and Electric Vehicles," SSAE Int. J. Advances & Curr. Prac. in Mobility 1(1):55-60, 2019, doi:10.4271/2019-26-0034.

[6] De Cesare, M., Cavina, N., and Brugnoni, E., "Conceptual Design and Analytic Assessment of 48V Electric Hybrid Powertrain Architectures for Passenger Cars," SAE Technical Paper 2019-01-0353, 2019, doi:10.4271/2019-01-0353.

[7] Liu, Z., Ivanco, A., and Filipi, Z., "Impacts of Real-World Driving and Driver Aggressiveness on Fuel Consumption of 48V Mild Hybrid Vehicle," SAE Int. J. Alt. Power. 5(2):2016, doi:10.4271/2016-01-1166.

[8] Dahodwala, M., Joshi, S., Dhanraj, F., Ahuja, N. et al., "Evaluation of 48V and High Voltage Parallel Hybrid Diesel Powertrain Architectures for Class 6-7 Medium Heavy-Duty Vehicles," SAE Technical Paper 2021-01-0720, 2021, doi:10.4271/2021-01-0720.

[9] Dahodwala, M., Joshi, S., Krishnamoorthy, H., Koehler, E. et al., "Evaluation of System Configurations for Downsizing a Heavy-Duty Diesel Engine for Non-Road Applications," SAE Int. J. Engines 9(4):2016, doi:10.4271/2016-01-8058.

[10] Joshi, S, Dahodwala, M, Koehler, E, & Franke, M. "Engine Strategies to Meet Phase-2 Greenhouse Gas Emission Legislation for Heavy-Duty Diesel Engines." Proceedings of the ASME 2017 Internal Combustion Engine Division Fall Technical Conference. Volume 2: Emissions Control Systems; Instrumentation, Controls, and Hybrids; Numerical Simulation; Engine Design and Mechanical Development. Seattle, Washington, USA. October 15–18, 2017. V002T06A007. ASME.

[11] King, J., Barker, L., Turner, J., and Martin, J., "SuperGen - A Novel Low Costs Electro-Mechanical Mild Hybrid and Boosting System for Engine Efficiency Enhancements," SAE Technical Paper 2016-01-0682, 2016, doi:10.4271/2016-01-0682.

[12] Keidel, S., Wetzel, P., Biller, B., Bevan, K. et al., "Diesel Engine Fuel Economy Improvement Enabled by Supercharging and Downspeeding," SAE Int. J. Commer. Veh. 5(2):483-493, 2012, https://doi.org/10.4271/2012-01-1941.

[13] Smith, E.M., "Electrified Heavy-Duty 4-cylinder Engine Concept for Class 8 Trucks," SAE Technical Paper 2021-01-0719, 2021, doi:10.4271/2021-01-0719.

[14] Eichler, K., Jeihouni, Y., and Ritterskamp, C., "Fuel Economy Benefits for Commercial Diesel Engines with Waste Heat Recovery," SAE Int. J. Commer. Veh. 8(2):491-505, 2015, https://doi.org/10.4271/2015-01-2807.

[15] Xu, Bin et al. "A Comprehensive Review of Organic Rankine Cycle Waste Heat Recovery Systems in Heavy-Duty Diesel Engine Applications." Renewable & sustainable energy reviews 107 (2019): 145–170. Web.

[16] "Reducing Fuel Consumption With Exhaust –TurboCompound", https://voith.com/corp-en/drives-transmissions/turbocompound.html, Last accessed on 11/08/2021.

[17] "Volvo Trucks Introduces Enhanced Turbo Compound Engine in VNL Models", https://www.volvotrucks.us/news-and-stories/press-releases/2019/august/volvo-trucks-introduces-enhanced-turbo-compound-engine-in-vnl-models/, Last accessed on 11/08/2021.

[18] International Journal of Automotive Engineering Vol. 3 (2012) No. 2 p. 69-73 'Effectiveness of Mechanical Turbo Compounding in a Modern Heavy-Duty Diesel Engine' Callahan Timothy J., Branyon David P., Forster Ana C., Ross Michael G., Simpson Dean J. http://doi.org/10.20485/jsaeijae .3.2_69.

[19] Sharp, C., Webb, C., Neely, G., Carter, M. et al., "Achieving Ultra Low NOX Emissions Levels with a 2017 Heavy-Duty On-Highway TC Diesel Engine and an Advanced Technology Emissions System - Thermal Management Strategies," SAE Int. J. Engines 10(4):2017, doi:10.4271/2017-01-0954.
[20] "Volvo D13 Turbo Compound Engine Powers New Volvo VNL Series to 7.5 Percent Improvement in Fuel Efficiency", https://www.volvogroup.com/en/news-and-media/news/2017/jul/volvo-d13-turbo-compound-engine-powers.html, Last Accessed on 11/09/2021.
[21] Bin Xu, Dhruvang Rathod, Adamu Yebi, Zoran Filipi, Simona Onori, Mark Hoffman, "A comprehensive review of organic rankine cycle waste heat recovery systems in heavy-duty diesel engine applications", Renewable and Sustainable Energy Reviews, Volume 107, 2019, Pages 145-170, ISSN 1364-0321, https://doi.org/10.1016/j.rser.2019.03.012 .
[22] Turner, J., Popplewell, A., Marshall, D., Johnson, T. et al., "SuperGen on Ultraboost: Variable-Speed Centrifugal Supercharging as an Enabling Technology for Extreme Engine Downsizing," SAE Int. J. Engines 8(4):2015, doi:10.4271/2015-01-1282.
[23] Suelter, B., Itou, T., Waldron, T., and Brin, J., "Optimizing Steady State Diesel Efficiency and Emissions Using a SuperTurboTM on an Isuzu 7.8L Engine," SAE Technical Paper 2019-01-0318, 2019, doi:10.4271/2019-01-0318.
[24] Neely, G.D., Sharp, C., and Rao, S., "CARB Low NOx Stage 3 Program - Modified Engine Calibration and Hardware Evaluations," SAE Technical Paper 2020-01-0318, 2020, doi:10.4271/2020-01-0318.
[25] Koci, C., Steffen, J., Kruiswyk, R., Guo, F. et al., "A Hybrid Heavy-Duty Diesel Power System for Off-Road Applications - Concept Definition," SAE Technical Paper 2021-01-0449, 2021, doi:10.4271/2021-01-0449.
[26] Cooper, A., Bassett, M., Hall, J., Harrington, A. et al., "HyPACE - Hybrid Petrol Advance Combustion Engine - Advanced Boosting System for Extended Stoichiometric Operation and Improved Dynamic Response," SAE Technical Paper 2019-01-0325, 2019, doi:10.4271/2019-01-0325.
[27] Eggimann, F., Frigo, S., Lutzemberger, G., Pasini, G. et al., "Numerical Analysis of Electrically Assisted Turbocharger Application on Hybrid Vehicle," SAE Technical Paper 2021-01-5090, 2021, doi:10.4271/2021-01-5090.
[28] Song K, Upadhyay D, Xie H. An assessment of performance trade-offs in diesel engines equipped with regenerative electrically assisted turbochargers. International Journal of Engine Research. 2019;20(5):510-526. doi:10.1177/1468087418762170.
[29] MOELLER et al. (2006). Automotive supercharger, Patent, GB2398108 (B).
[30] BRINKS et al. (2017) Super-Turbocharger Having a High Speed Traction Drive and a Continuously Variable Transmission, Patent, US9581078 (B2).
[31] DIEMER et al. (2016) Electrically Assisted Turbocharger, Patent, US9470231 (B2).
[32] JOHNSON (2016) Turbocharger with Electrically Coupled Fully Variable Turbo-Compound Capability and Method of Controlling the same, Patent Application, US20160017793 (A1).
[33] JOSHI et al. (2019), Systems for power integration of turbines, compressors and hybrid energy devices with internal combustion engines, Patent, US10384525 (B2).
[34] Giakoumis, Evangelos. (2016). Review of Some Methods for Improving Transient Response in Automotive Diesel Engines through Various Turbocharging Configurations. Frontiers in Mechanical Engineering. 2. 10.3389/fmech.2016.00004
[35] GT-SUITE Overview, https://www.gtisoft.com/gt-suite/gt-suite-overview/ , Accessed on 12/05/2021.
[36] J. B. Heywood, "Internal Combustion Engine Fundamentals," McGraw-Hill Education 2E, New York, 2018.
[37] Joshi, S., Dahodwala, M., Koehler, E., Franke, M. et al., "Trade-Off Analysis and Systematic Optimization of a Heavy-Duty Diesel Hybrid Powertrain," SAE Technical Paper 2020-01-0847, 2020, https://doi.org/10.4271/2020-01-0847.
[38] Lee, S., Cherry, J., Safoutin, M., McDonald, J. et al., "Modeling and Validation of 48V Mild Hybrid Lithium-Ion Battery Pack," SAE Int. J. Alt. Power. 7(3):273–287, 2018, doi:10.4271/2018-01-0433.
[39] John Wang, Ping Liu, Jocelyn Hicks-Garner, Elena Sherman, Souren Soukiazian, Mark Verbrugge, Harshad Tataria, James Musser, Peter Finamore, Cycle-life model for graphite-LiFePO4 cells, Journal of Power Sources, Volume 196, Issue 8, 2011, Pages 3942-3948, ISSN 0378-7753, https://doi.org/10.1016/j.jpowsour.2010.11.134.

[40] D. Smith, R. Graves, J. Lustbader, K Kelly et al, “Medium- and Heavy-Duty Vehicle Electrification, An Assessment of Technology and Knowledge Gaps”, ORNL, NREL, US Department of Energy, Office of Energy Efficiency & Renewable Energy, December 2019, https://info.ornl.gov/sites/publications/Files/Pub136575.pdf, Accessed on 12/05/2021.
[41] N. Kim, S. Cha and H. Peng, "Optimal Control of Hybrid Electric Vehicles Based on Pontryagin's Minimum Principle," in IEEE Transactions on Control Systems Technology, vol. 19, no. 5, pp. 1279-1287, Sept. 2011, doi: 10.1109/TCST.2010.2061232.
[42] https://www.ecfr.gov/current/title-40/chapter-I/subchapter-C/part-86/subpart-N/section-86.1370 , Accessed on 03/20/2022.
[43] Sappok, A., Govani, I., Kamp, C., Wang, Y. et al., "In-Situ Optical Analysis of Ash Formation and Transport in Diesel Particulate Filters During Active and Passive DPF Regeneration Processes," SAE Int. J. Fuels Lubr. 6(2):336-349, 2013, https://doi.org/10.4271/2013-01-0519.
[44] Dhanraj, F., Dahodwala, M., Joshi, S., Koehler, E. et al., "Evaluation of 48V Technologies to Meet Future CO2 and Low NOx Emission Regulations for Medium Heavy-Duty Diesel Engines," SAE Technical Paper 2022-01-0555, 2022, https://doi.org/10.4271/2022-01-0555.
[45] Joshi, S., Dahodwala, M., Ahuja, N., Dhanraj, F. et al., "Evaluation of Hybrid, Electric and Fuel Cell Powertrain Solutions for Class 6-7 Medium Heavy-Duty Vehicles," *SAE Int. J. Adv. & Curr. Prac. in Mobility* 3(6):2955-2971, 2021, https://doi.org/10.4271/2021-01-0723.
[46] Lerin, C, Curran, S, Moses-DeBusk, M, Cook, A, Boronat Colomer, V, Kaul, B, & Deter, D. "Hardware-in-the-Loop Investigation of Emissions Challenges in Hybrid Medium- and Heavy-Duty Powertrains Using a Pre-Production Diesel-Electric Parallel Hybrid System With and Without Stop-Start Operation." Proceedings of the ASME 2021 Internal Combustion Engine Division Fall Technical Conference. ASME 2021 Internal Combustion Engine Division Fall Technical Conference. Virtual, Online. October 13–15, 2021. V001T07A009. ASME.
[47] Samveg Saxena, Caroline Le Floch, Jason MacDonald, Scott Moura, Quantifying EV battery end-of-life through analysis of travel needs with vehicle powertrain models, Journal of Power Sources, Volume 282, 2015, Pages 265-276, ISSN 0378-7753, https://doi.org/10.1016/j.jpowsour.2015.01.072.
[48] Dahodwala, Mufaddel, et al. “Strategies for Meeting Phase 2 GHG and Ultra-Low NOx Emission Standards for Heavy-Duty Diesel Engines.” SAE International Journal of Engines, vol. 11, no. 6, SAE International, 2018, pp. 1109–22, https://www.jstor.org/stable/26649151.

APPENDIX

A Baseline Engine Model Validation

As outlined in section 3, a GT-SUITE model of the baseline 6 cylinder 7.7L medium heavy-duty diesel engine was developed and validated against test data. The engine specifications have been shown in **Figure 10** while the engine layout has been shown in **Figure A.1**. The modeling methodology in GT-SUITE has also been described in section 3 and hence this section will only discuss model validation results.

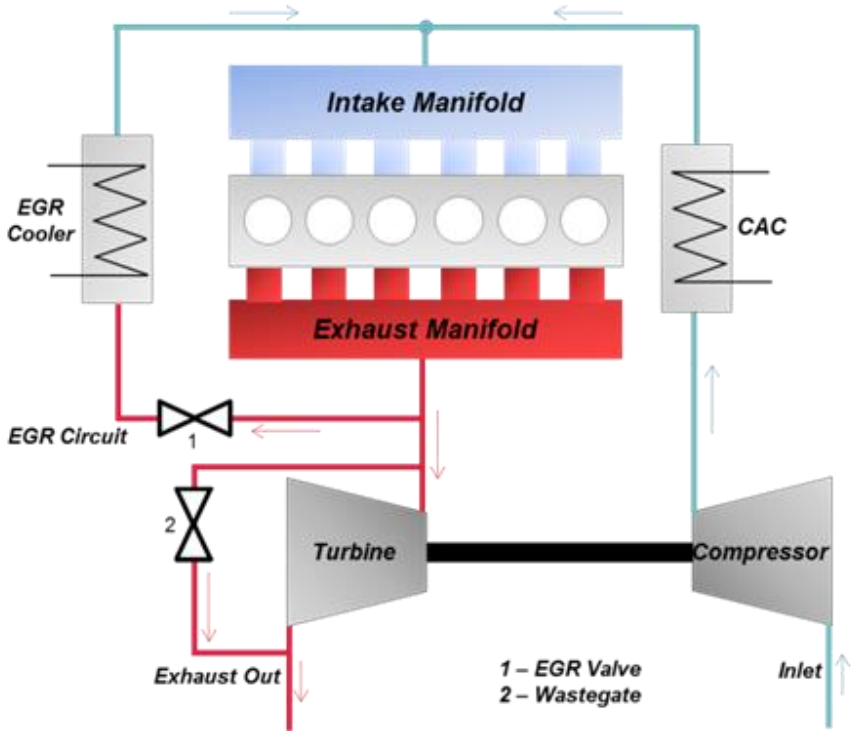

Figure A.1. Baseline 6 cylinder 7.7L medium heavy-duty diesel engine air system layout

The DI-Pulse combustion model was calibrated against the available cylinder pressure dataset collected on engine dynamometer. The injector rate profile data and injector geometry were obtained from supplier and implemented in the model. The standard Woshni GT heat transfer model was applied to model heat transfer between combustion gas and in-cylinder surfaces. The seven key combustion model parameters were calibrated using genetic algorithm optimization technique to minimize burn rate error over 20 engine operating points. The resultant match for the key operating points has been shown in **Figure A.2**. Overall, good correlation was observed with IMEP error within 3% and peak cylinder pressure error within 6%. Further improvement could have been possible in peak cylinder pressure correlation by allowing for higher error in IMEP, however since the focus of the analysis was fuel consumption, IMEP correlation was prioritized.

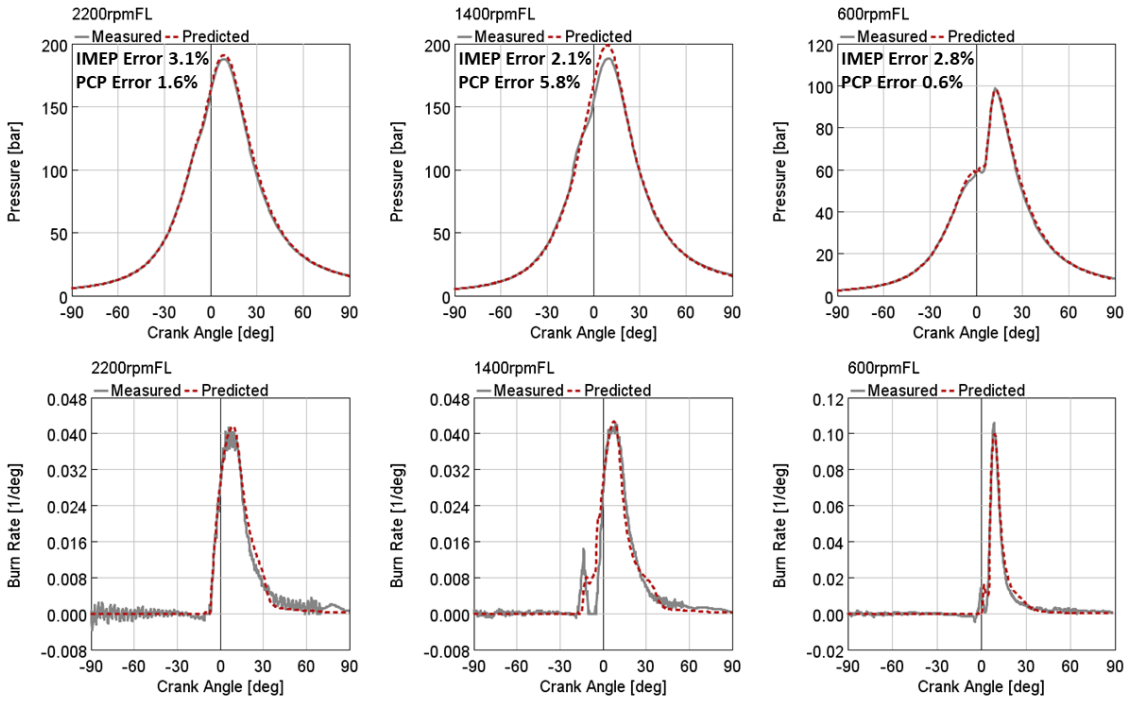

Figure A.2. Baseline engine combustion model correlation between experimental data and simulation.

Once the combustion model was calibrated, another genetic-algorithm based optimization was run to calibrate the six Zeldowich mechanism coefficients for the NOx model. In order to achieve acceptable model accuracy for engine test cycle simulation, the 'NOx calibration multiplier' coefficient was setup to have engine speed and BMEP dependency [48]. **Table A.1** shows the final combustion and NOx model parameters used in the models.

Table A.1. Final calibrated combustion and NOx model parameters for baseline engine.

DI Pulse Parameters	Values
Entrainment Rate Multiplier	1.51
Ignition Delay Multiplier	0.75
Premixed Combustion Rate Multiplier	0.013
Diffusion Combustion Rate Multiplier	1.84
Diffusion Combustion Rate Transition Timing	0.563
Diffusion Combustion Rate Final Value	0.141
Diffusion Combustion Rate Transition Rate	10.5

NOx Model Parameters	Values
NOx Calibration Multiplier	Speed/Load Dependency (25% max deviation)
N2 Oxidation Rate Multiplier	3.63
N2 Oxidation Activation Energy Multiplier	0.934
N Oxidation Rate Multiplier	1.671
N Oxidation Activation Energy Multiplier	0.969
OH Reduction Rate Multiplier	0.258

Next, the Chen-Flynn engine friction model was calibrated against available engine friction data. The coefficients were fitted to engine friction data from more than 50 engine

operating points with varying engine speed and load. The final coefficients are shown in equation below:

$$FMEP = 0.1888 + 0.0028.P_{cylmax} + 0.1118.c_{p,m} + 0.0022.c_{p.m}^{2}$$

Where P_{cylmax} is peak cylinder pressure in bar and $c_{p,m}$ is mean piston speed in m/s. The correlation between the predicted friction mean effective pressure (FMEP) and calculated FMEP is shown in **Figure A.3**. Overall, the friction model correlated within 10% of measured data for majority of the operating points. Excursions were observed at lower engine speed, possibly due to constant thermodynamic loss angle assumption in measured data, and/or absence of combustion phasing dependence in FMEP model. While further improvements could be made in friction model, the correlation was deemed sufficient for this analysis.

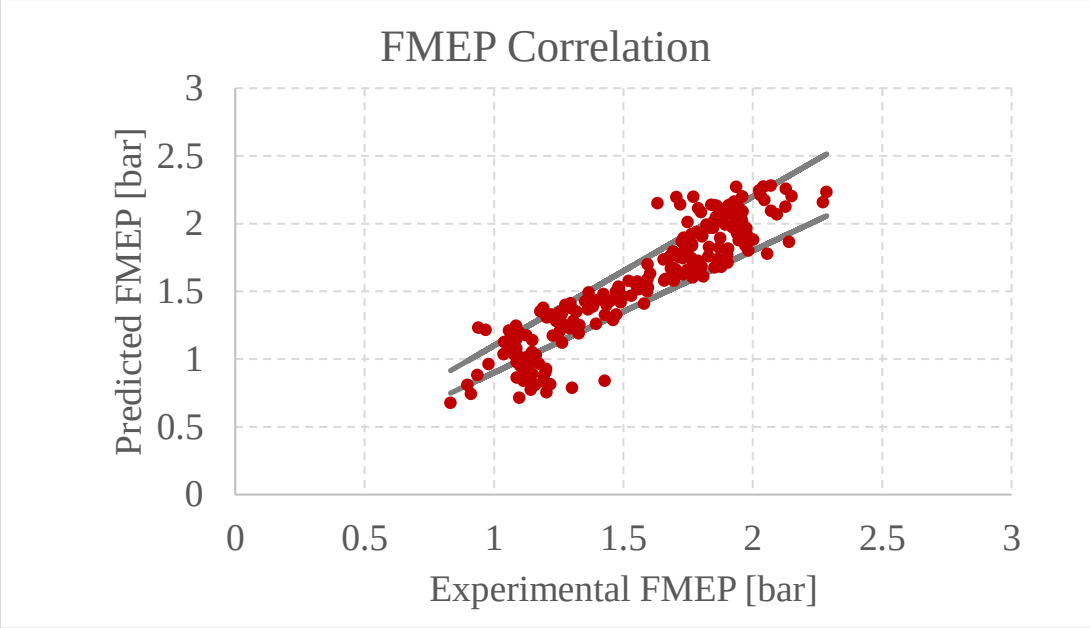

Figure A.3. FMEP correlation between predicted and experimental dataset.

The engine air and exhaust path internal geometries were extracted from available CAD data and setup as 1D flow components within GT-SUITE. Valve lift curves were directly measured on the engine with lash and updated in the model. Turbomachinery maps were directly obtained from suppliers and populated in the model while the aftertreatment unit was modeled as a simple pressure drop orifice element. Charge air and EGR cooler were modeled using a semi-predictive effectiveness map developed from experimental data. Lastly, all parameters for fuel injection, EGR valve and wastegate were obtained from ECU base calibration maps. **Figure A.4** shows the complete GT-SUITE model of the baseline engine air system, combustion system and cranktrain. The model was developed as an FRM by combining flow volumes, using large discretization lengths and using cylinder slaving to achieve fast run time for engine test cycle simulation.

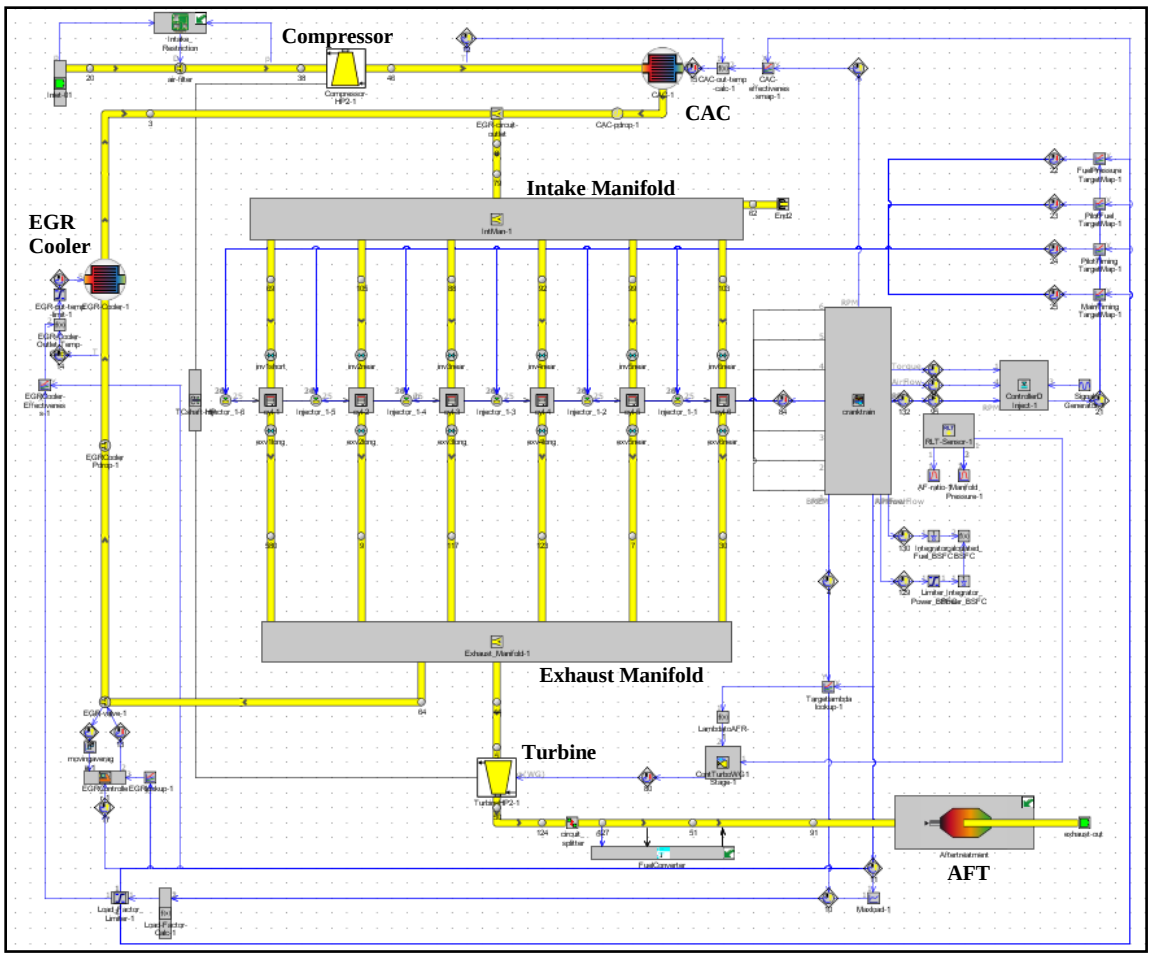

Figure A.4. GT-SUITE FRM model for the baseline 6 cylinder 7.7L medium heavy-duty diesel engine.

Once the model was developed, the next step was to validate the model on engine full load curve, engine operating map and HDFTP cycle. **Table A.2** shows the experimental data boundary conditions that were maintained for all engine simulations. To target these boundary conditions, the intake restriction orifice, exhaust restriction orifice, CAC restriction orifice, CAC effectiveness map multiplier and EGR cooler effectiveness map multiplier were all calibrated at rated power operating point. Once the parameters were calibrated, they were fixed for all other engine simulations.

Table A.2. Boundary conditions for all engine simulations.

Rated Power Boundary Conditions	Values
Ambient Pressure	1.013 bar
Ambient Temperature	25 C
Intake Restriction	2.3 kPa
Coolant Temperature	86 C
CAC Outlet Temperature	44 C
CAC Pressure Drop	8.1 kPa
Exhaust Restriction	21.8 kPa

Figure A.5 shows the correlation between experimental data and simulation for the full load curve. Since engine fueling was controlled to target engine torque from experimental data, the key performance metrics of interest were BSFC, BSNOx and lambda. BSFC and BSNOx correlated within 2% of experimental data while lambda deviations were as high as 0.1 units at lower engine speeds. This was possibly due to error in airflow measurements at lower flowrates as well as due to the large discretization lengths in the model that were necessary for model run time. Temperature and pressure predictions in intake manifold, exhaust manifold and near turbomachinery correlated well against experimental data which provided the necessary confidence in engine air path model.

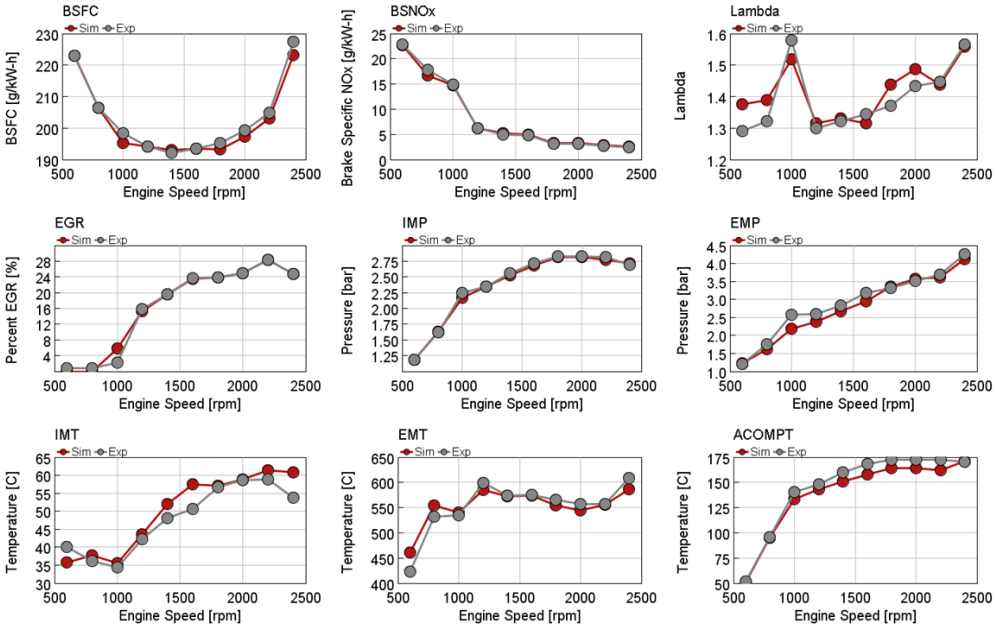

Figure A.5. Baseline model correlation on full load curve for multiple engine performance parameters.

After the model predictions on engine full load curve were verified, complete engine map prediction for 50 operating points was compared against experimental data. **Figure A.6** shows the comparison of key performance metrics between simulation results and experimental data. For majority of the engine operating region, fuel consumption correlated within 2%. At lower engine loads, the error increased up to 5%, possibly due to fuel flow measurement accuracy, as well as friction modeling error. Overall, the fuel consumption correlation was considered acceptable as the lower load region of the engine operating map does not contribute significantly to cycle averaged fuel consumption. Similarly, NOx model correlated within 5% for majority of engine operating region however at lower engine loads, the error in NOx model increased up to 15%. Overall, NOx predictions were also considered acceptable due to lower NOx contribution from lower load region of the engine operating map, in cycle averaged NOx emission calculation.

Lastly, the HDFTP cycle was run on the baseline model and the simulations results were compared against experimental data as shown in **Figure A.7**. The model predictions were within 1% for BSFC and within 2% for cycle averaged NOx emissions.

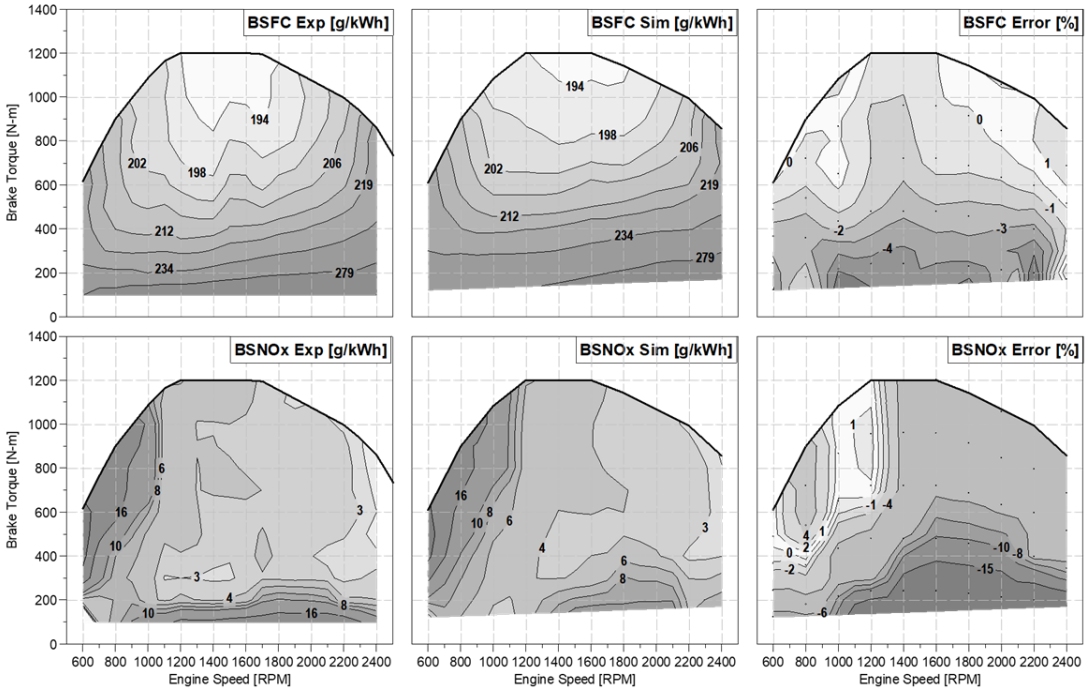

Figure A.6. Baseline model correlation on engine map for BSFC and BSNOx.

The simulation results also followed the trends in transient NOx and fuel flow rate predictions over the cycle, when compared against experimental data. Since fuel flow was controlled to target engine torque over the drive cycle, >98% coefficient of correlation was achieved in cycle quality.

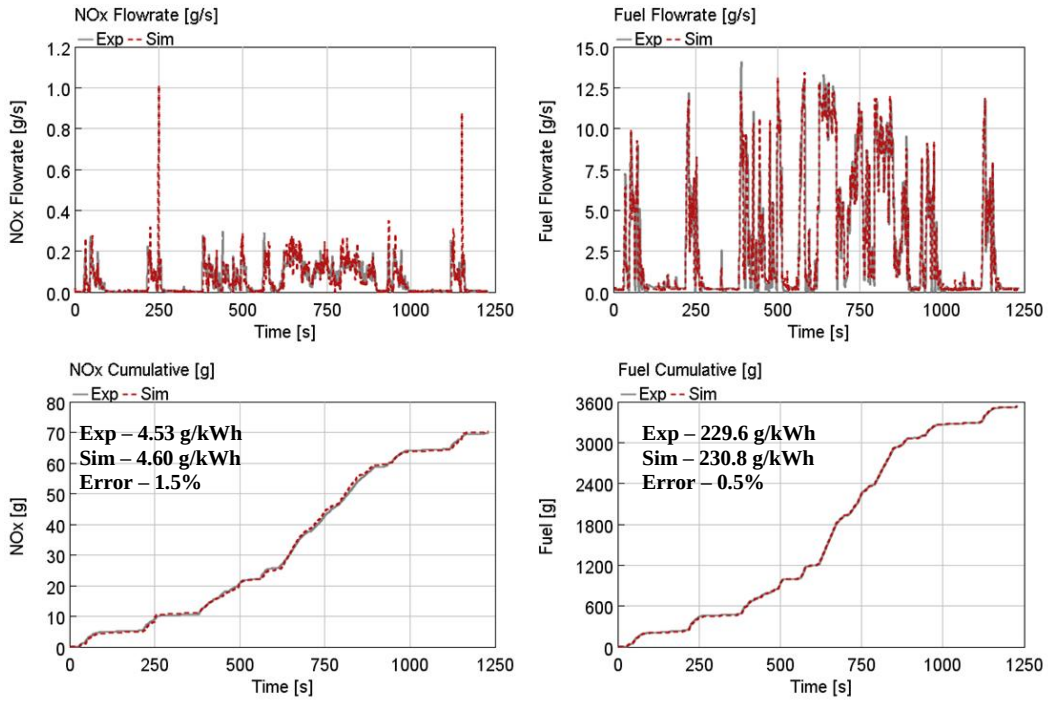

Figure A.7. Baseline model correlation on HDFTP cycle for BSFC and BSNOx.

B Baseline Vehicle Model Validation

The baseline vehicle model used in this study was adapted from a validated GT-SUITE vehicle model developed for an M2 106 freightliner truck, installed with a Cummins 6.7L diesel engine [37]. **Figure B.1** shows the specification of this vehicle, its powertrain components and its longitudinal dynamics parameters. The vehicle model was initially developed with the 6.7L map-based engine sub-model and validated against vehicle test data collected through CAN measurements. Later on, the 6 cylinder 6.7L map-based engine sub-model was replaced with a higher fidelity fast running engine model of the 7.7L baseline engine, for the purpose of this research as described in section 6.1. The reason behind not using the 6.7L Cummins engine as the baseline engine was lack of available data for engine modeling.

Parameter	Specification
Vehicle Type	Class 6-7 Urban
Chassis Weight	15,695 lbs
Engine Displacement	6.7 L
Advertised Rated Power	300 hp @ 2600 rpm
System Voltage	12 V
Transmission Type	Allison2000 (5 Spd)
Rolling Resistance Coefficient	0.009
Vehicle Aero-drag CdA	6.06 m^2
Final Drive Ratio	5.22
Tire Size	275/80 R22.5
Aux Load	2.35 kW

Figure B.1. Vehicle specifications of the M2 106 freightliner truck applied in urban vocational application.

The methodology of vehicle modeling has been described in detail in section 3.1 and was followed in this model development process. **Figure B.2** shows the GT-SUITE model of the Freightliner M2 106 truck representing longitudinal vehicle dynamics, driver and propulsion system. The engine was modeled as a map-based object with BMEP, friction and fuel consumption defined as a function of pedal request and engine speed. The complete engine cranktrain assembly was modeled as a lumped inertia object and connected to the transmission. The input to the driver model was a target vehicle speed profile which was converted by the model into accelerator and brake pedal positions for the propulsion model. The accelerator pedal position was then converted to engine BMEP request by engine controller. The torque input to the engine lumped inertia object was then transmitted through the torque converter, the transmission gear and finally the axle to predict vehicle motion. The transmission gear and lockup clutch actuation was controlled by transmission control unit based on predefined strategies. The brake pedal input was directly translated to a retarding torque input and evenly distributed to all vehicle wheels.

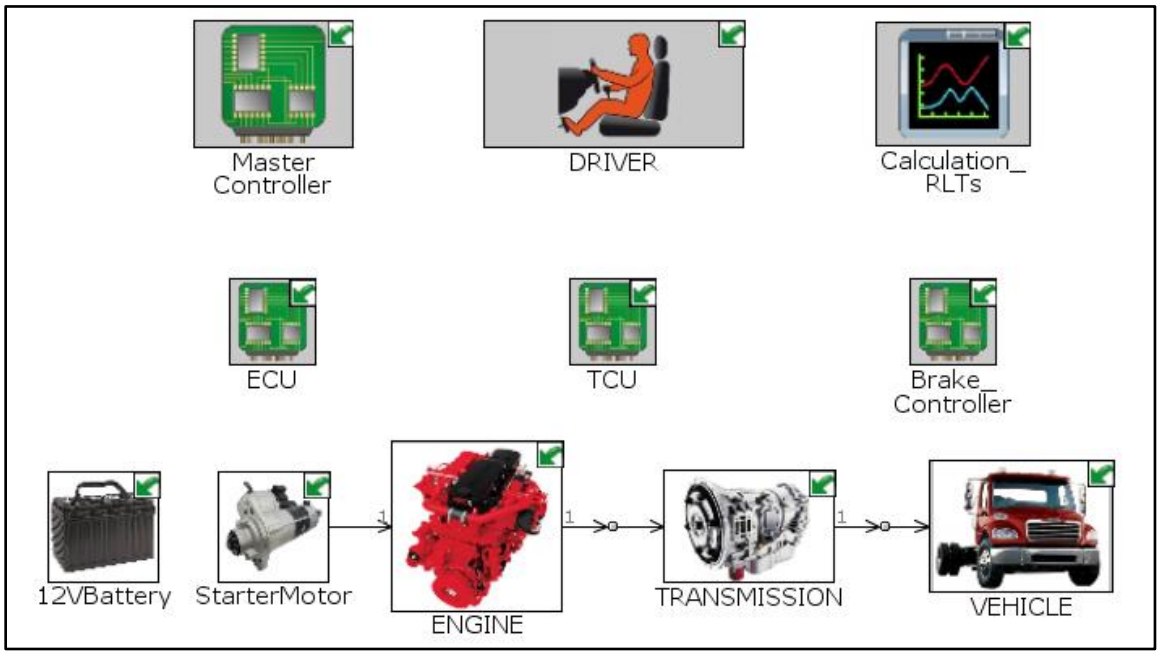

Figure B.2. GT-SUITE 1D model of the M2 106 freightliner truck with the Cummins 6.7L engine and Allison 2000 series transmission

The vehicle was run on a custom route without payload and data was collected for engine, transmission and vehicle CAN channels available through standard J1939 protocol. The route was selected to represent urban driving with fast acceleration, fast deceleration and start-stop operation. The model was then subjected to the same vehicle speed profile and the performance was compared. **Figure B.3** shows the model correlation against test data collected for the custom drive cycle. Most variables achieved coefficient of correlation above 95% except engine speed and fuel flow. For these two variables, a maximum regression of only 89% could be achieved with significant calibration effort on engine inertia, torque converter performance, gear shift strategy and vehicle dynamics parameters. This was possibly due to slower update rate of CAN data as well as the use of map-based engine model which did not capture internal engine dynamics. Overall, the predicted fuel economy from simulation was within 1% of measured fuel economy, which was considered acceptable for the application of the model in this research. As described in section 6.1, the map-based Cummins 6.7L engine model in this vehicle model was replaced with a higher fidelity FRM engine model of the baseline 7.7L engine. This was possible as the manufacturer sells this vehicle with both engine options.

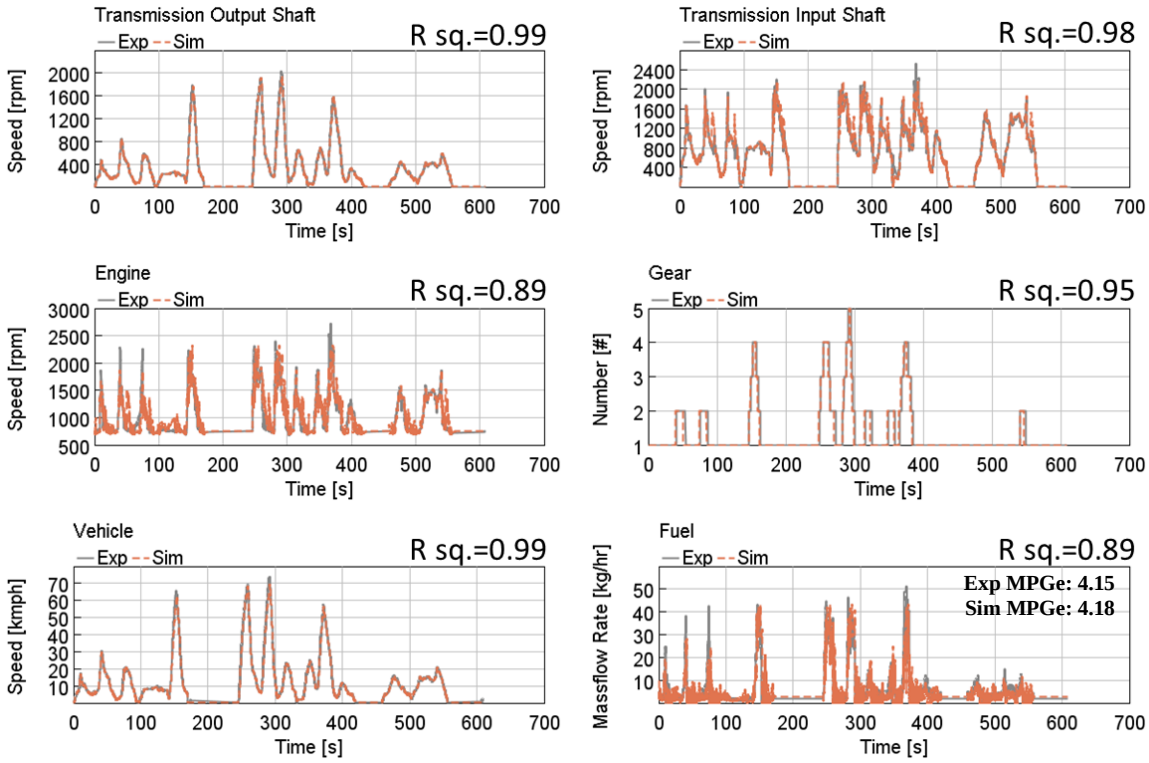

Figure B.3. Correlation between experimental data and simulation results from the GT-SUITE vehicle model of the Freightliner M2 106 truck.

C Copyright documentation

CCC Marketplace™

This is a License Agreement between Satyum Joshi / Michigan Technological University ("User") and Copyright Clearance Center, Inc. ("CCC") on behalf of the Rightsholder identified in the order details below. The license consists of the order details, the Marketplace Order General Terms and Conditions below, and any Rightsholder Terms and Conditions which are included below.

All payments must be made in full to CCC in accordance with the Marketplace Order General Terms and Conditions below.

Order Date	25-Aug-2022	Type of Use	Republish in a thesis/dissertation
Order License ID	1261934-1	Portion	Chapter/article
System ID	2018-01-0887		

LICENSED CONTENT

Publication Title	Novel Approach to Integration of Turbocompounding, Electrification and Supercharging Through Use of Planetary Gear System	Rightsholder	SAE International
		Publication Type	Report
Author/Editor	Joshi, Satyum		
Date	01/01/2018		

REQUEST DETAILS

Portion Type	Chapter/article	Rights Requested	Main product
Page range(s)	1-12	Distribution	Worldwide
Total number of pages	12	Translation	Original language of publication
Format (select all that apply)	Print, Electronic	Copies for the disabled?	No
Who will republish the content?	Author of requested content	Minor editing privileges?	No
Duration of Use	Life of current edition	Incidental promotional use?	No
Lifetime Unit Quantity	Up to 499	Currency	USD

NEW WORK DETAILS

Title	CONCEPT EVALUATION AND DEVELOPMENT OF A NOVEL APPROACH FOR INTEGRATION OF TURBOGENERATION, ELECTRIFICATION AND SUPERCHARGING ON HEAVY DUTY ENGINES	**Institution name**	Michigan Technological University
		Expected presentation date	2022-12-12
Instructor name	Jeffrey D. Naber		

ADDITIONAL DETAILS

Order reference number	N/A	**The requesting person / organization to appear on the license**	Satyum Joshi / Michigan Technological University

REUSE CONTENT DETAILS

Title, description or numeric reference of the portion(s)	Multiple portions including text and images	**Title of the article/chapter the portion is from**	N/A
Editor of portion(s)	N/A	**Author of portion(s)**	Joshi, Satyum
Volume of serial or monograph	N/A	**Issue, if republishing an article from a serial**	N/A
Page or page range of portion	1-12	**Publication date of portion**	2022-12-12

CCC | Marketplace™

This is a License Agreement between Satyum Joshi / Michigan Technological University ("User") and Copyright Clearance Center, Inc. ("CCC") on behalf of the Rightsholder identified in the order details below. The license consists of the order details, the Marketplace Order General Terms and Conditions below, and any Rightsholder Terms and Conditions which are included below.

All payments must be made in full to CCC in accordance with the Marketplace Order General Terms and Conditions below.

Order Date	10-Sep-2022	**Type of Use**	Republish in a thesis/dissertation
Order License ID	1267183-1	**Publisher**	SAE International
System ID	2020-01-0847	**Portion**	Chapter/article

LICENSED CONTENT

Publication Title	Trade-Off Analysis and Systematic Optimization of a Heavy-Duty Diesel Hybrid Powertrain : 2020-01-0847	**Rightsholder**	SAE International
		Publication Type	Report
Author/Editor	Dahodwala, Mufaddel, Joshi, Satyum		
Date	01/01/2020		

REQUEST DETAILS

Portion Type	Chapter/article	**Rights Requested**	Main product
Page range(s)	1-12	**Distribution**	Worldwide
Total number of pages	12	**Translation**	Original language of publication
Format (select all that apply)	Print	**Copies for the disabled?**	No
Who will republish the content?	Author of requested content	**Minor editing privileges?**	No
Duration of Use	Life of current edition	**Incidental promotional use?**	No
Lifetime Unit Quantity	Up to 499	**Currency**	USD

NEW WORK DETAILS

Title	CONCEPT EVALUATION AND DEVELOPMENT OF A NOVEL APPROACH FOR INTEGRATION OF TURBOGENERATION, ELECTRIFICATION AND SUPERCHARGING ON HEAVY DUTY ENGINES	**Institution name**	Michigan Technological University
		Expected presentation date	2022-12-12
Instructor name	Dr. Jeffrey D. Naber		

ADDITIONAL DETAILS

Order reference number	N/A	**The requesting person / organization to appear on the license**	Satyum Joshi / Michigan Technological University

REUSE CONTENT DETAILS

Title, description or numeric reference of the portion(s)	Multiple portions including text and images	**Title of the article/chapter the portion is from**	N/A
Editor of portion(s)	N/A	**Author of portion(s)**	Joshi, Satyum
Volume of serial or monograph	N/A	**Issue, if republishing an article from a serial**	N/A
Page or page range of portion	1-12	**Publication date of portion**	2020-01-01

https://marketplace.copyright.com/rs-ui-web/mp/products-terms_and_conditions